THE EQUATIONS OF STATE OF HYDROGEN AND ARGON; APPLICATIONS TO THE JOVIAN INTERIOR

Thesis by

Peter Leonard Lagus

In Partial Fulfillment of the Requirements

For the Degree of

Doctor of Philosophy

California Institute of Technology

Pasadena, California

1974

(Submitted June 29, 1973)

Οὐ ποτε ἀμαθίαν νικήσει διδασκαλία

Λαγυσ

ACKNOWLEDGMENTS

It is a pleasure to acknowledge the active guidance, support, and inspiration of Dr. Thomas J. Ahrens throughout this study, and the many hours of patient explanation, encouragement, and advice received from Professor James A. Westphal.

I have been involved in many fruitful discussions with Dr. Charles Archambeau, Dr. Peter Goldreich, Dr. Duane Muhlman, and Dr. Don Anderson regarding aspects of this thesis and am deeply in their debt. Dr. Hugh Kieffer kindly provided a copy of his program to integrate the equations of hydrostatic equilibrium.

To Sol Giles I owe a special debt, for it was he who taught me the distinction between a machinist and an instrument maker; without his expertise and enthusiasm the experiment described in this thesis might never have come to fruition.

My colleagues Rex Gibbons, Dr. Ed Gaffney, and Dr. Geoffrey Davies have provided many helpful comments and stimulating discussions.

Messrs. Harold Richeson, John Lower, and David Johnson assisted in the execution of the experiments described herein, and I thank them for their "good shooting".

To Dr. and Mrs. Milton Goldstein, formerly of Chicago, Illinois, who provided a teenage boy with a direction and a dream, this thesis is humbly and gratefully dedicated.

Special thanks to Laszlo Lenches and Joe Galvan for drafting the many figures in this thesis.

The author was supported during part of this research by a NASA traineeship and a California State Fellowship.

ABSTRACT

Hugoniot data for solid argon (initially at 77°K and 1 bar) and solid hydrogen (initially at 5°K and 1 bar) have been obtained to 143 kbar and 6.4 kbar respectively utilizing a propellant gun. The argon data (at volumes of 15.28, 14.84 and 14.64 cc/mole) are in fair agreement with previous shock data, and in excellent agreement with recent theoretically predicted Hugoniots. The hydrogen data (at volumes of 17.10, 15.32, 15.27, 15.11 cc/mole) are compared with Hugoniots calculated from published isothermal compression data. For both argon and hydrogen, the present data are consistent with the assumption that γ/V is constant. Furthermore, to compressions of $V/V_0 \simeq 0.65$, no gross inconsistencies exist between shock-wave and isothermal compression measurements in solid hydrogen.

A simple equation of state (EOS) for molecular hydrogen based on a spherically averaged De Boer-type repulsion potential which explicitly includes the zero point energy reproduces experimental pressure-volume data between 5 kbar and 370 kbar. This molecular equation of state when combined with recent metallic equations of state implies a molecular to metallic phase transition pressure of 1.9 ± 0.4 Mbar at 0°K.

A thermally expanded model of Jupiter which incorporates this molecular equation of state, recent metallic hydrogen and helium equations of state, and a van der Waals-type atmosphere yields a model with a hydrogen abundance of $x = 0.57$. However, the interior temperatures are everywhere above the melting temperature of metallic hydrogen.

CONTENTS

I. INTRODUCTION

Investigation and discussion of the properties of the largest planet in the solar system, Jupiter, ultimately devolves to a discussion regarding knowledge of the properties of hydrogen under extreme pressure and high temperature.

Isothermal compression data for the gas phase of hydrogen are generally limited to pressures less than approximately 2000 atm (see, for instance, Landolt-Bornstein 1971). The sole exception to this is the data of Bridgman (1924) to 13,000 atm at 65°C and 30°C. However, there appears to be a systematic error in these measurements and therefore they are generally discounted (De Marcus 1958).

For liquid hydrogen, isotherms are available to pressures of less than 1000 atm (see, for instance, Roder 1963). There does exist one shock datum at 39.5 kbar (van Thiel and Alder 1966a).

The isothermal compression measurements (to 20 kbar) of Stewart (1956) at 4°K represent the sole isothermal compression data extant for the solid phase of molecular hydrogen.

As this thesis is being written, two sets of experiments (Grigoriev et al. 1972 on solid hydrogen and Hawke et al. 1973 on liquid hydrogen) have appeared in print. Both measurements utilize a magnetic flux compression technique to isentropically compress hydrogen to pressures approaching 10 Mbars (compressions of $V_o/V \simeq 15$). However, the technique used is new and unproven and has rather large uncertainties attendant to it (± 50% in volume at a given volume and

$\sim$100% in pressure at a given pressure). Such data auger well for the future, but cannot stand by themselves at present.

Theoretical investigations are complicated by two factors: 1) a transition in hydrogen from the molecular to a metallic phase first investigated by Wigner and Huntington (1935), and 2) a large zero point energy due to low mass and weak binding in both the molecular and metallic phases. Properties of the metallic phase are thought to be well known (Neece et al. 1971, Trubitsyn 1966, Dynin 1972) although it should be stressed that no direct evidence has been published to date demonstrating the existence of this phase. Grigoriev et al. (1972) find a break in the slope of their experimental pressure-volume curve at 2.6 Mbar and attribute this to the molecular to metallic phase transition.

The theoretical situation regarding molecular hydrogen is less satisfactory than for metallic hydrogen. Kronig et al. (1946) attempted to calculate an equation of state for molecular hydrogen using a Lennard-Jones 6-12 interaction potential. Their calculation is of little value since 1) they neglected zero point energy entirely, and 2) the 6-12 potential is known to be too "stiff" at large compressions (van Thiel and Alder 1966b, Zubarev and Telegin 1962).

Recently attention has focused on calculation of the pressure-volume properties of solid molecular hydrogen using a quantum crystal formalism which has been used to successfully predict these properties for solid helium (Wu 1967, Krumhansl and Wu 1972, Bruce 1972, Pollack et al. 1972, Ebner and Sung 1970,1971,1972). However, all of these attempts to theoretically reproduce the 4^{o}K isotherm of Stewart have

failed at isothermal pressures greater than ∿5 kbar. These discrepancies have prompted some theoretical investigators to question the validity of the experimental isotherm.

Due primarily to this incomplete theoretical and experimental understanding of the pressure-volume properties of molecular hydrogen, various investigators (De Marcus 1958, Hubbard 1968,1969,1970) have adopted essentially ad hoc procedures when incorporating a solid molecular hydrogen layer into models of the Jovian interior.

The paucity of experimental data regarding the properties of solid molecular hydrogen coupled with the far-from-satisfactory theoretical situation led to the research detailed in this thesis.

Chapter II and Appendices detail the experimental technique and apparatus which was developed and used in conjunction with a propellant gun to conduct the first shock wave studies on solid molecular hydrogen. Solid argon was also studied since it could be compared with previously published data (Dick et al. 1970). The shock wave data for hydrogen and the Stewart $4^{o}K$ isotherm are found to be consistent to compressions of $V/V_{o} \simeq 0.65$.

In Chapter III and Appendices, a $0^{o}K$ pressure-volume relation, derived from a De Boer (1942) repulsion potential which is spherically averaged in the manner of Trubitsyn (1966), is developed. The contribution of zero point motion to the total internal energy and pressure is explicitly included using several different methods. The resultant theoretical $0^{o}K$ compression curve is compared with the $4^{o}K$ Stewart (1956) isotherm as well as a datum point at 370 kb due to

Grigoriev et al. (1972). The physical origin of zero point energy is discussed, and the "quantum crystal" formalism which works well for solid helium but not solid hydrogen is also briefly described.

In Chapter IV and Appendix, an attempt has been made to calculate a thermally expanded model of the interior of Jupiter using the improved hydrogen equation of state of Chapter III and a van der Waals type atmosphere. The resulting model is compared with previously proposed thermally expanded Jovian models. In the Appendix the equations (Peebles 1964) used to calculate model planets are explicitly derived as their derivation is tedious and is not fully outlined elsewhere.

Chapter V briefly recapitulates the major conclusions of this thesis.

References for Chapter I

1. Bridgman, P. W., Proc. Amer. Acad. 59, 173 (1924).

2. Bruce, T. A., Phys. Rev. B5, 4170 (1972).

3. De Boer, J., Physica 9, 363 (1942).

4. De Marcus, W. C., A.J. 63, 2 (1958).

5. Dick, R. D., R. H. Warnes and J. Skalyo, J. Chem. Phys. 53, 1648 (1970).

6. Dynin, E. A., Sov. Phys. Sol. St. 13, 2089 (1972).

7. Ebner, C. and C. C. Sung, Sol. St. Comm. 8, 1903 (1970).

8. Ebner, C. and C. C. Sung, Phys. Rev. B4, 2638 (1971).

9. Ebner, C. and C. C. Sung, Sol. St. Comm. 11, 489 (1972).

10. Grigoriev, F. V., S. B. Kormer, O. L. Mikhailova, A. P. Tolachka, and V. D. Urlin, JETP 5, 288 (1972).

11. Hawke, R. S., D. E. Duerre, J. G. Huebel, R. N. Keeler, and H. Klapper, PEPI 6, 44 (1973).

12. Hubbard, W. B., Ap. J. 152,745 (1968).

13. Hubbard, W. B., Ap. J. 155, 333 (1969).

14. Hubbard, W. B., Ap. J. 162, 687 (1970).

15. Kronig, R., J. De Boer, and J. Korringa, Physica 12, 245 (1946).

16. Krumhansl, J. A. and S. Wu, Phys. Rev. B5, 4155 (1972).

17. Landolt-Bornstein, II Band, 1 Teil "Mechanisch Thermische Zustandgrössen, Springer-Verlag, Berlin (1971).

18. Neece, G. A., F. J. Rogers and W. G. Hoover, J. Comp. Phys. 7, 621 (1971).

19. Peebles, P.J.E., Ap. J. 140, 328 (1964).

20. Pollack, E. L., T. A. Bruce, G. V. Chester, J. A. Krumhansl, Phys. Rev. B5, 4180 (1972).

21. Roder, H. M., Cryogenics 3, 16 (1963).

22. Stewart, J. W., J. Phys. Chem. Solids 1, 146 (1956).

23. Trubitsyn, V. P., Sov. Phys. Sol. St. 7, 2708 (1966).

24. van Thiel, M. and B. J. Alder, Mol. Phys. 10, 428 (1966a).

25. van Thiel, M. and B. J. Alder, J. Chem. Phys. 44, 1056 (1966b).

26. Wigner, E. and H. B. Huntington, J. Chem. Phys. 3, 764 (1935).

27. Wu, S., "A Quantum Theory of Equation of State for Solid Hydrogen", Ph.D. Dissertation, Cornell University (1967).

28. Zubarev, V. N. and G. S. Telegin, Dok. Sov. Phys. 7, 34 (1962).

CHAPTER II

SHOCK WAVE MEASUREMENTS ON SOLID HYDROGEN AND ARGON

A. Introduction

Although shock wave experiments on a large class of ordinary solids and liquids have been obtained in the last 25 years (summarized in Keeler 1973), relatively few shock data have been reported for solidified gases initially at cryogenic temperatures. Previous work on both liquid and solid gases has been limited to experiments using explosive lens techniques to generate shocks in the material under study. Dick et al. (1970) report Hugoniot data to 640 kbar in solid argon. Zubarev and Telegin (1962) have measured pressure-volume properties under shock for liquid nitrogen and solid carbon dioxide. van Thiel and Alder (1966a,1966b) have studied the liquid argon Hugoniot extensively and also report a single measurement on liquid hydrogen. Keeler et al. (1965) provide several Hugoniot points for liquid xenon. The various experiments utilize a container whose Hugoniot is known in which samples are grown. Shorting pins are placed within the sample chamber at accurately measured positions, and samples are grown around them. Measurement of the time interval between closing of the various shorting pins then gives a measure of the shock velocity. The explosive lens/flyer plate assembly is generally shielded from the sample container by some type of insulation until a short time before detonation, generally on the order of a few seconds. It is assumed that appreciable warming of the sample does not occur in this time. This configuration has the drawback that it

is not possible to inspect the condition of the solid gas sample prior to shock arrival. The assumption is made that the specimen is 100% dense. Experience at this laboratory shows that freeze-out of the sample gas feed or freezing over of a partially liquid region can easily lead to flawed samples and thus the assumption of a 100% dense solid is not necessarily justified.

This chapter describes experimental apparatus and technique which, when used in conjunction with a propellant or light gas gun, can be used to obtain Hugoniot data for solid gases. The major advantages of the methods proposed here are:

1) Continuous visual monitoring of the condition of the sample,
2) Exposure of the sample container to a warm environment for times less than 0.1 milliseconds,
3) Ability to obtain pressure-volume data for condensed gases directly in the pressure range 0-2 kbar (static dilatometric experiments cannot obtain reliable p-v data due to the large ram friction at cryogenic temperatures (Stewart 1956,1968),
4) Control of sample pressure in a shock-wave experiment with a gun is superior to that attainable with explosives.

B. Experimental Design and Operation

Equation of state data, or, more specifically, pressure-volume-energy relations, can be obtained in a series of experiments in which plane shocks of differing amplitudes are driven into a series of samples. Well defined mechanical shock waves are usually generated in a fluid or solid sample by impacting it with a carefully machined and

accurately aligned solid striker plate. The striker plate is accelerated to a high velocity using either a gun or chemical explosives.

The experiments described in this chapter utilize a high performance propellant gun (Ahrens, et al. 1973) to launch 40 mm diameter projectiles to speeds in excess of 2.5 km/sec into an evacuated expansion and impact chamber. Targets of the material being studied possessing a suitable geometry are placed within the impact chamber and aligned with the muzzle of the gun. Measurements of the projectile and shock velocities are carried out optically and electronically in the impact chamber. Projectile velocities are measured to better than 0.3%. A TRW image converter streaking camera and a synchronized xenon flash system are used to measure shock velocities in the sample targets. Streak camera time calibration is obtained to better than 0.5% using a specially designed intensity-modulated laser system.

The pressure, volume or density, and internal energy associated with a dynamically produced high pressure shock state may be calculated using the Rankine-Hugoniot equations (Rice 1958). The parameters which are required in these equations and which are usually measured are the shock velocity, particle velocity, and the initial density of the target material. In practice, it is difficult to measure the particle velocity in the sample directly, and instead, the velocity of the striker plate is measured prior to impact. An impedance matching solution is then employed to determine the particle velocity in the sample. A series of such experiments, each with a different shock pressure, are required to generate the locus of shock states which represents the Hugoniot curve.

In order to ascertain the feasibility of carrying out detailed shock wave measurements on solid molecular hydrogen, several years ago experiments were undertaken on the solidification of various gases. Samples of solidified argon and hydrogen of dimensions suitable for shock wave experimentation were prepared. These samples were found to be quite clear, transparent, and apparently free of cracks, inclusions and voids. Examination of specimens under 10X magnification failed to reveal imperfections. These results suggested that an appropriate experimental technique for measuring shock velocities directly within the solidified sample would utilize an immersed foil similar to that used by Ahrens and Ruderman (1966).

Basically the design utilized an expendable high-vacuum shroud within which the sample target was suspended. The target itself was connected to an external sample gas manifold by means of Swagelok fittings mounted on a stainless steel flange. Samples of the appropriate gas were grown in situ after alignment of the target. To impact the target, a projectile entered the high-vacuum shroud by penetrating a thin stainless steel foil. A lucite window in the shroud allowed visual inspection of the target and also enabled a xenon flash/streak camera system to record the passage of a shock wave through the sample.

Considerable experimentation was required before an appropriate sample target configuration was perfected (see Fig. 1a). The target consisted of an open faced disc approximately 1 cm deep by 3 cm in diameter machined from type 304 stainless steel. Wall thicknesses were nominally 1.5 mm. The bottom surfaces of the sample container were machined flat and parallel to 0.001". A copper flange was silver

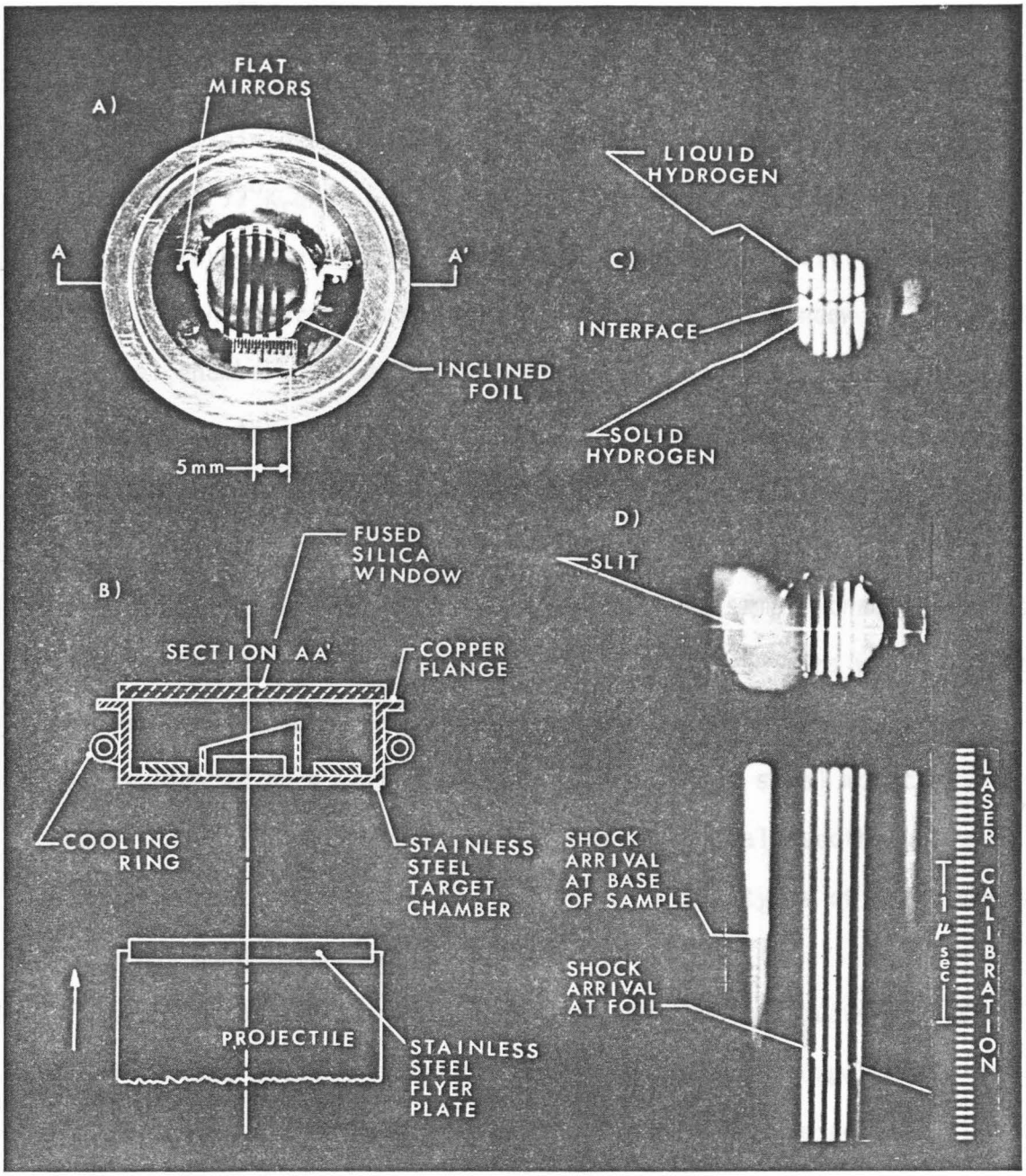

Figure 1. a) Solid hydrogen target. b) Cross-section of target showing position of foil and mirrors. c) Half-grown solid hydrogen crystal, showing liquid-solid interface. d) Target prior to experiment, with a typical streak camera record below. Next to the record is the time calibration.

soldered to the open lip of the target. Initially this flange was constructed of stainless steel, but this often resulted in destruction of the window at 77°K. At 5°K, targets with a stainless steel flange always destroyed the window. Since the thermal conductivity of the copper is much greater than either the fused silica window or the stainless steel chamber, it uniformly distributed the thermal stresses experienced by the window during cooling. Shorting pins (E.G. & G. type CA-1038) were mounted on the outside circumference of the target slightly ahead of the back surface. The closure of these pins by the striker plate immediately prior to impact of the sample chamber was used to trigger the image converter streak camera. These pins were connected to the external camera trigger circuits via vacuum electrical feedthroughs located on a vacuum port in the stainless steel mounting flange. An additional 3 connector vacuum electrical feedthrough was incorporated into the design to facilitate future types of experiments but was not used in these experiments.

Cooling of the target was accomplished by continuously passing the appropriate cryogen (liquid nitrogen in the argon experiments and liquid nitrogen followed by liquid helium in hydrogen experiments) through a 5/16" diameter copper coil. This coil was attached with pure tin to the lower 2/3 of the circumference of the stainless steel sample chamber. Two thin wall (0.020") stainless steel tubes were attached to the copper coil. The other end of these tubes was concentrically silver soldered to a 3/4" diameter by 5-1/2" long, 0.035" thick stainless steel tube. These 3/4" diameter tubes were connected to a stainless steel flange at the top of the gun chamber by Swagelok fittings. These

input lines act as standoff tubes, and minimize thermal transport from the warm exterior environment to the target. A 1/4" diameter type 304 stainless steel tube (which provided sample gas to the target chamber) was heliarc welded to the top center of the chamber. In the argon experiments this tube was connected to the exterior gas supply by means of a stainless steel standoff tube. For the hydrogen experiments it was found that the entrance of warm (room temperature) hydrogen gas into the liquid helium cooled target resulted in the formation of radial tension cracks in the fused silica window. This cracking generally degraded the vacuum in the shroud to the point where the particular experimental run had to be abandoned. To minimize the thermal stresses which induced this window failure, a liquid nitrogen heat exchanger was placed between the 1/4" diameter stainless steel tube and the standoff tube. The heat exchanger consisted of approximately 6 feet of 1/4" copper tubing wound in a helix which was mounted in a 2-1/2" diameter by 9" long brass dewar. This dewar was connected to the mounting flange by means of a standoff tube and a copper vent tube held fast by Swagelok fittings.

Misalignment of the target chamber by rotation upon cooling was substantial during initial experimentation. By fully annealing the copper cooling ring, rotational movement could be reduced to $1/2^{o}$ or less for the actual experiments.

Measurement of shock velocity directly within a solid gas sample was accomplished by a thin reflecting foil placed within a transparent target at a known angle with respect to the shock propagation direction (see Fig. 1b). The arrival of a shock wave at the foil provides a

redundant set of measurements of the shock transit time through the substance. This method is the optical analog of the shorting pin technique discussed previously. Initially a thin (0.001") mylar film was bonded to a stainless steel ring of known dimensions with epoxy adhesive (Resinbond 907). Reflecting aluminum bands 1 mm wide, spaced 1 mm apart were vacuum deposited on the mylar film. In later experiments, a microscope slide cover glass (0.007" thick) with gold bands was used in place of the mylar film. The dimensions of the ring foil assembly were chosen by first calculating expected shock transit times in slabs of stainless steel and mylar or glass having infinite lateral extent (no edge rarefactions). Dimensions for the ring/foil assembly which implied longer shock transit times through the stainless steel plus foil than through the sample were then adopted. The ring/foil assembly was bonded to the inside bottom surface of the target using RTV adhesive. Two flat, 1 mm thick, half-silvered mirrors were also bonded to the bottom surface, one on each side of the ring, with epoxy adhesive (Resinbond 907). Adhesive was filleted around the perimeter of the mirrors, thereby insuring that the mirrored surface was in physical contact with the bottom surface of the sample chamber. In preliminary experiments, extinction of the reflecting mirrors by the entering shock wave proved to be erratic. This problem was overcome by severely abrading the surface immediately beneath the mirrors; subsequently only sharp extinctions occurred. In addition to providing the time of arrival of the shock wave at the base of the solid gas sample, extinction of these mirrors provides a measure of the tilt of the shock wave entering the sample.

The bond between the silica window and the copper flange proved to be surprisingly strong. Overpressures of two atmospheres at liquid helium temperatures produced no measurable leakage at the interface. Diffusion of hydrogen through the bond was negligible.

When using liquid helium coolant, temperatures within the target varying little from $5^{o}K$ were measured by means of liquid helium vapor pressure, and $5^{o}K$ was therefore adopted for the initial temperature of the solid hydrogen target. The heat influx to the argon targets as indicated by the boil-off rate of liquid nitrogen, was very small (5 mℓ/sec) and thus the boiling point of liquid nitrogen ($77^{o}K$) was adopted for the temperature of the solid argon targets.

In the event of an equipment, target, or window failure, a target could not be reliably reused without first being dismantled and reassembled, since it was found that thermal cycling noticeably degraded the epoxy adhesive bond strength. Such cycling did not appear to affect the silicone rubber adhesive bond strength at all.

Alignment of the target required that the axis of the target disc be coincident with the axis of the muzzle. Hence, a vacuum-tight spherical bowl flange (labeled A in Fig. 2) was employed to allow three-dimensional and rotatory adjustments of the target. A 1" thick stainless steel plate (B) possessing appropriate vacuum ports and Swagelok fittings was mounted on the spherical bowl flange. A 6" diameter by 1/2" wall stainless steel tube (C) was heliarc welded to the bottom of plate B with its axis coincident with the axis of the plate. This tube acted as a receiver for an expendable 2024 aluminum high-vacuum shroud (D) which encompassed the sample target. An O-ring

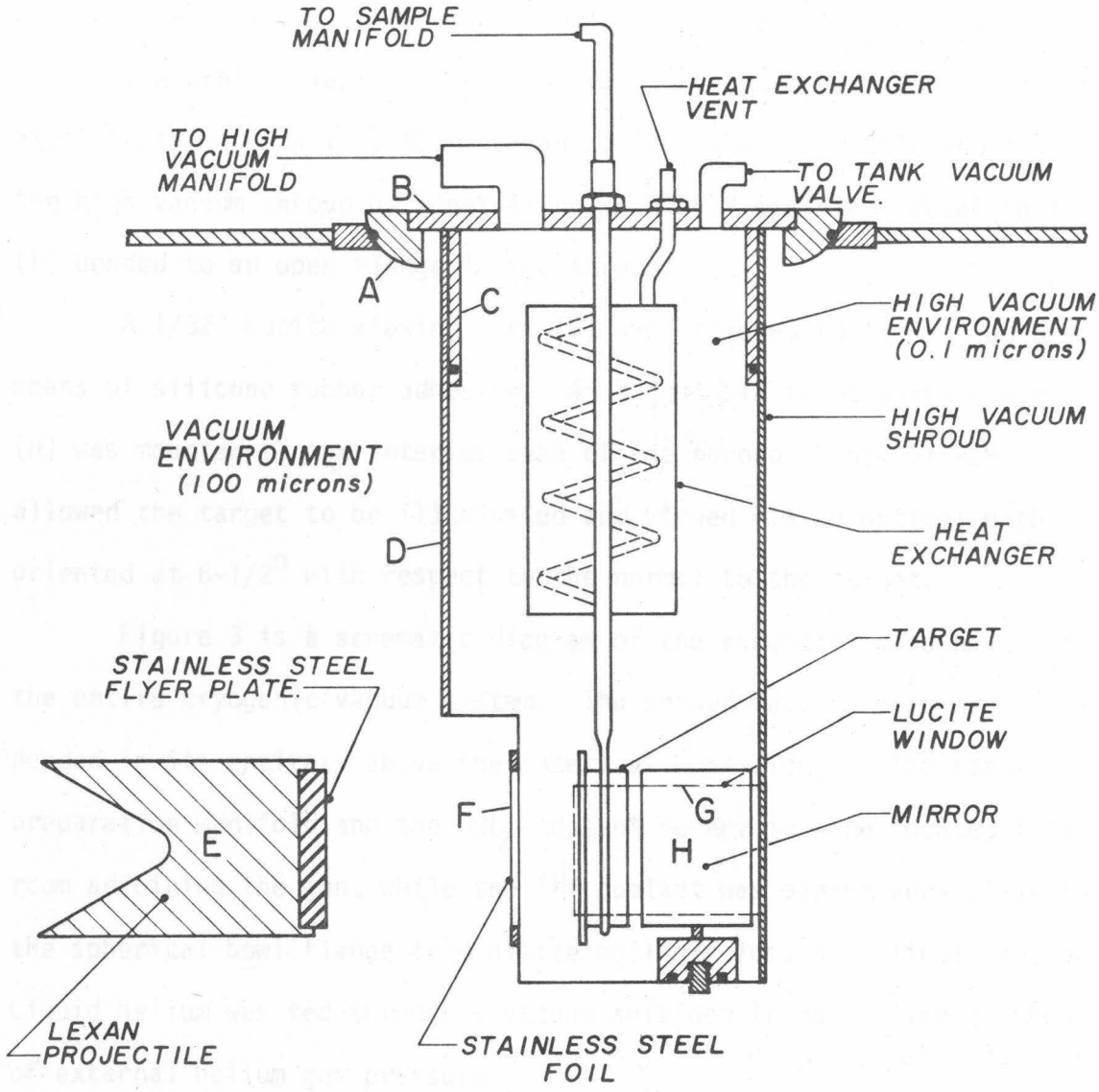

Figure 2. Experimental configuration (cross-section) showing target position and vacuum shroud.

was mounted on the circumference of the receiver tube; slight compression of the O-ring by the shroud provided an excellent vacuum seal.

The projectile (E) was a 1/2" thick by 30 mm diameter stainless steel plate mounted in a 40 mm Lexan sabot. The projectile entered the high vacuum shroud by penetrating an 0.001" stainless steel foil (F) bonded to an open flange in the shroud.

A 1/32" Lucite viewing port (G) was attached to the shroud by means of silicone rubber adhesive. An adjustable front surface mirror (H) was mounted to the interior base of the shroud. This mirror allowed the target to be illuminated and viewed via an optical path oriented at $6\text{-}1/2^{o}$ with respect to the normal to the target.

Figure 3 is a schematic diagram of the essential components of the entire cryogenic vacuum system. The shroud vacuum system was suspended in its entirety above the spherical bowl flange. The sample preparation manifold and the ℓN_2 coolant reservoir were located in a room adjoining the gun, while the ℓHe coolant was placed very close to the spherical bowl flange to minimize boil-off losses of liquid helium. Liquid helium was fed through a vacuum shielded transfer line by means of external helium gas pressure.

Initial pumpdown of the high vacuum shroud was accomplished in conjunction with the pumpdown of the impact chamber of the gun. At pressures of $\sim$500 microns, the shroud was closed off from the impact chamber vacuum and the shroud vacuum system was used to evacuate the shroud to pressures between 10^{-4} and 10^{-5}torr. Pressures in the shroud were monitored by a CVC Model VG 1A/3 ionization and a CVC Model GTC004 thermocouple vacuum gauge.

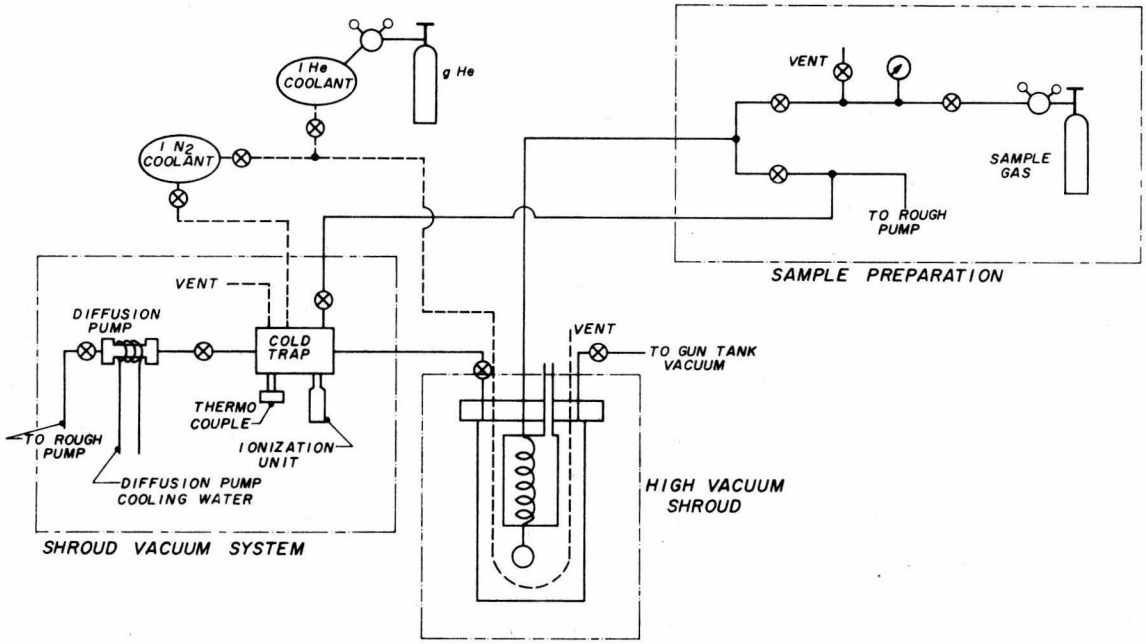

Figure 3. Schematic diagram of Cryogenic vacuum system for shock wave experiments on solidified gases.

Sample preparation was accomplished with the aid of an external manifold. A Wallace and Tiernan pressure gauge was used to monitor sample feed pressure. The sample target chamber was first evacuated and then flushed with the appropriate sample gas. Pressure in the target was then brought up to slightly above atmospheric pressure (usually 32" Hg) after which target cooling commenced. For argon, liquid nitrogen was gradually passed through the copper cooling ring until the sample gas pressure began to drop, indicating the onset of liquification (usually required 45 min to 1 hr). Additional sample gas (sufficient to maintain a pressure of 32" Hg) was then valved into the chamber as more liquid formed. Approximately 30 min was required to fill the chamber with liquid and an additional 90 min was necessary for growth of the polycrystalline solid. For hydrogen, the cooling procedure was similar to that for argon except that following the initial cooling with liquid nitrogen, the heat exchanger in the target was filled with liquid nitrogen after which liquid helium was passed through the target cooling coil. Condensation occurred in approximately the same total time as for argon, but solidification required an average of only 45 min.

All samples which were shocked were visually free of cracks, voids, and inclusions. The condition of the sample was visually monitored until 1 min before impact (see Fig. 1c). Sample gases were obtained from the Linde Corporation and had stated purities of 99.996% for argon and 99.999% for hydrogen.

Cryogen consumption was moderate. Typically 120 liters of liquid nitrogen were used in a 3 hour argon experiment. A hydrogen

experiment required 10 liters/hr of liquid helium in addition to 100 liters of liquid nitrogen. During initial experimentation, substantial leaks developed in the high vacuum system after several hours of cooling with liquid nitrogen. These leaks were attributed to the freezing out of the Teflon ferrules used to hold the standoff tubes in the Swagelok fittings. Extruded aluminum heat sink material was firmly clamped to the circumference of the standoff tubes immediately above the Swagelok fittings. A small squirrel cage blower was used to circulate room temperature air over the heat sink. This effectively eliminated the "freeze-out" of the Teflon ferrules.

Figure 1d shows a typical streak camera record of a hydrogen shot. The mirror positions can be correlated with the streak lines in the target picture. The bright line crossing the diameter of the target corresponds to the slit position used in obtaining the streak record. The extinction of the two outermost lines corresponds to the arrival of the shock at the base of the solid gas sample. The angled break apparent in the five streaked images of the reflecting bands corresponds to the arrival of the shock at the foil. The interval between extinction of the outside mirrors and the interruption of the grid lines gives five measures of the shock velocity within the sample. All usable data for these experiments were chosen on the basis of sharp extinction of the outside mirrors, and a definite break in the grid lines on the foil.

Particle velocities in the sample were obtained by an impedance match solution (Rice 1958). The Hugoniot for stainless steel was taken from McQueen et al. (1970).

$$U_s = 4.569 + 1.490\ U_p \qquad (1)$$

using a density of $\rho_o = 7.896$ gm/cc. This Hugoniot was corrected to 77^oK and 5^oK using the thermal expansion data of Coruccini and Gniewek (1961) and a Gruneisen parameter of 2.170[17] (see Appendix I).

The low temperature Hugoniot is insensitive to the exact value of the Gruneisen parameter; in fact the 77^oK and 5^oK Hugoniot curves were indistinguishable in the pressure-particle velocity plane. In light of the uncertainty in the measured projectile velocity (0.3%) as well as the uncertainties in the room temperature and cold Hugoniots of stainless steel which are propagated in an impedance match solution, the uncertainty in the particle velocity in the solidified gas sample is $\sim$0.5%.

The density of normal hydrogen has been determined by Megaw (1939) to be 0.089 ± 0.004 gm/cc at 4^oK. Assuming that Ahlers' thermal expansion data (1963) are valid, the density would be $\sim$0.1% or 0.00009 gm/cm^3 less at 5^oK. For argon, the technique used to produce a solid sample and the cooling time required are similar to those reported by Pollack and Farabaugh (1965). They report obtaining transparent, 100% dense polycrystalline solids. Therefore, the assumption is made that the solid argon samples had a density of $\rho_o = 1.65$ gm/cm^3 corresponding to a molar volume of 24.21 cm^3/mole (Lawrence and Neal, 1965). The major uncertainty in shock transit time (and thus shock velocity) is due to the somewhat arbitrary nature of picking the exact time of extinction of the outside mirrors, and the exact time of arrival of the

shock at the foil. The largest contribution to this uncertainty is the finite width of the slit used in obtaining the streak record (typically 1.5-3% uncertainty in extinction position). Uncertainties in physical dimensions of target and rings, nonlinearities in camera writing rate, and the uncertainty in the exact extinction point of mirrors and foil, lead to a total uncertainty in shock velocity of 4-5%. This uncertainty could be substantially reduced by examining the negatives obtained with the streak camera with a microdensitometer and assigning an arbitrary (say 1/e) diminution of light as the extinction point.

Three of the data points in solid hydrogen were closely grouped in projectile velocity. The measured shock velocities also cluster quite closely implying excellent reproducibility and indicating that an uncertainty in shock velocity of 5% is probably an overestimate.

C. Results

A series of four shots in solid argon and ten shots in solid hydrogen was undertaken resulting in three acceptable argon data points and four acceptable hydrogen data points. The shots which did not produce usable data did not do so for a variety of reasons including streak camera/xenon flash malfunction, lack of definite breaks in resultant streak pictures, and target failure.

In Table I, Hugoniot data is presented for solid argon and solid hydrogen. Figure 4 shows the present argon data plotted along with the data of Dick et al. (1970). Note that at a given compression, these data lie at a slightly higher pressure than do those of Dick et al.

Table 1

Hugoniot Data for Solid Argon and Solid Hydrogen

SHOT NUMBER	u_p (mm/μsec)	U_s (mm/μsec)	P(kbar)	V(cc/mole)	T(^oK)
		ARGON			
Initially at 77^oK and 1 Bar		V_o = 24.21 cc/mole	ρ_o = 1.65 gm/cm^3	Lawrence and Neal (1965)	
246	1.425 ± 0.009	3.86 ± 0.17	90.8 ± 4.5	15.28 ± 0.75	1367
248	1.650 ± 0.010	4.27 ± 0.18	116.1 ± 5.8	14.84 ± 0.74	1883
249	1.850 ± 0.011	4.68 ± 0.20	143.0 ± 7.2	14.64 ± 0.73	2444
		HYDROGEN			
Initially at 5^oK and 1 Bar		V_o = 22.65 cc/mole	ρ_o = 0.089 gm/cm^3	Megaw (1939)	
275	0.801 ± 0.005	3.31 ± 0.13	2.36 ± 0.11	17.10 ± 0.60	38
254	1.496 ± 0.010	4.63 ± 0.21	6.16 ± 0.32	15.27 ± 0.79	71
282	1.515 ± 0.011	4.71 ± 0.20	6.36 ± 0.32	15.32 ± 0.76	73
283	1.525 ± 0.008	4.62 ± 0.16	6.27 ± 0.27	15.11 ± 0.79	72

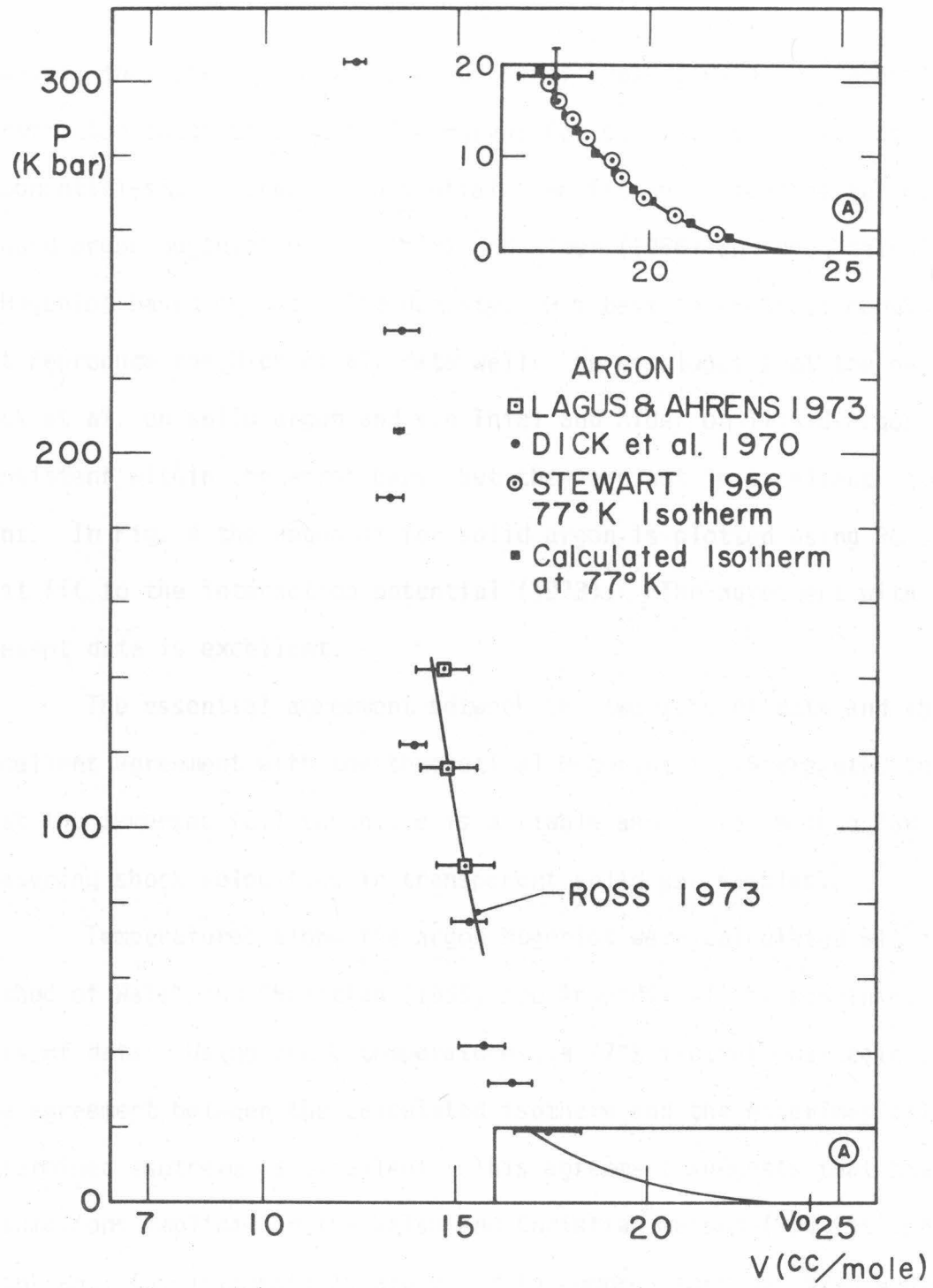

Figure 4. Solid argon Hugoniot data. The insert displays the calculated and experimentally determined 77°K isotherm at an expanded pressure scale.

However, they agree within the error bars. Ross (1973) has recently constructed theoretical Hugoniot curves for solid argon utilizing an exponential-six interaction potential. He fit the potential to the liquid argon Hugoniot of van Thiel and Alder (1966) and then calculated a Hugoniot based on the solid density. His best theoretical model does not reproduce the Dick et al. data well. He concludes that the data of Dick et al. on solid argon and van Thiel and Alder on liquid argon are consistent within the error bars, but they are not in excellent agreement. In Fig. 4 the Hugoniot for solid argon is plotted using Ross' best fit to the interaction potential (1973). The agreement with the present data is excellent.

The essential agreement between the two sets of data and the excellent agreement with the theoretical Hugoniot is interpreted to mean that the immersed foil technique is a viable and useful method for measuring shock velocities in transparent solid gas samples.

Temperatures along the argon Hugoniot were calculated with the method of Walsh and Christian (1955, see Appendix II) by combining both sets of data. Using these temperatures, a $77^{o}K$ isotherm was calculated. The agreement between the calculated isotherm and the experimentally determined isotherm is excellent. This agreement suggests that the assumptions implicit in the Walsh and Christian method (γ/V is constant and C_V is constant) are valid to compressions of $V/V_o \simeq 0.6$ for solid argon. The values for the specific heat, $C_V = 5.76$ cal/mole ^{o}K, and for the Gruneisen parameter, $\gamma = 2.50$ at a volume of 24.2 cc/mole were taken from the data of Lawrence and Neal (1965). In

the U_s-U_p plane, the zero particle velocity intercept for the present data is 1.10 ± 0.07 km/sec (for the combined sets it is 1.05 km/sec). This is consistent with the bulk sound speed of 1.05 km/sec calculated from the data of Lawrence and Neal (1965). Dick et al. (1970) calculated that the Hugoniot crossed the melting line at 250 kb with a temperature of 5900°K. Using the Walsh and Christian method a calculated temperature of ~4900°K is found at this pressure. On this basis it appears that the present Hugoniot data lie within the solid phase.

However, in the previously mentioned paper of Ross, a melting point of 50 kbar at 700°K is calculated for the solid argon Hugoniot. This would imply that the present Hugoniot points are in the liquid phase. Resolution of this dilemma awaits the direct experimental measurement of temperatures on the Hugoniot.

Calculation of temperature in hydrogen is not as straightforward as in the case of argon, since it is initially at a temperature where the specific heat changes rapidly as a function of temperature. Therefore a theoretical Hugoniot for hydrogen was first calculated from the Stewart data utilizing a Gruneisen parameter which varied as

$$\gamma = \gamma_0 (V/V_0)^A \qquad (2)$$

In Fig. 5 the present Hugoniot data is plotted along with Stewart's 4°K isotherm, and theoretical Hugoniots calculated using values of A equal to 1.0, 1.25, and 1.50 in equation 2. A value of γ_0 equal to 2.34 at a reference volume of 21.19 cc/mole (Ahlers 1963) was used. Good agreement between the calculated and measured Hugoniots

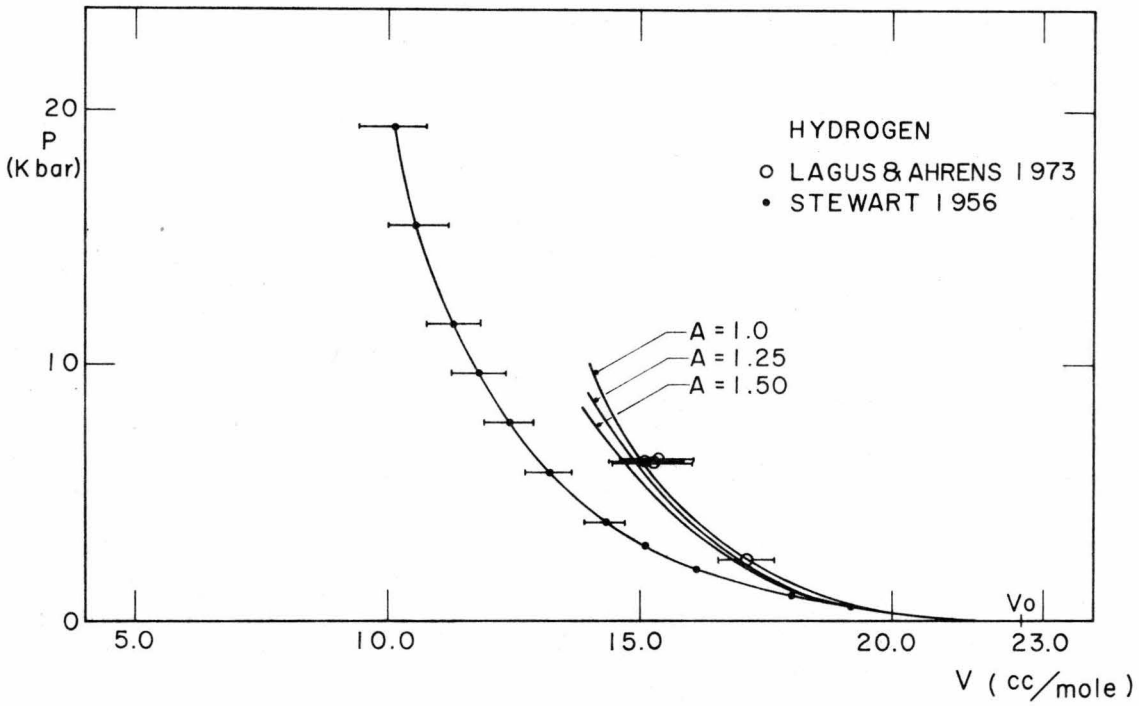

Figure 5. Solid hydrogen Hugoniot data. Also plotted are the experimentally determined 4°K isotherm, and theoretical Hugoniots calculated from the isotherm (see text).

was found for the case $A = 1.0$. This corresponds to the assumption that γ/V is constant.

A linear fit to the solid hydrogen data in the U_s-U_p plane yields

$$U_s = (1.79 \pm 0.07) + (1.89 \pm 0.08)U_p$$

The zero particle velocity intercept of 1.79 km/sec agrees well with the bulk sound speed of 1.72 km/sec measured by Bezuglyi and Minyafaev (1967).

Temperatures along the hydrogen Hugoniot were calculated by the method of Ahrens et al. (1969, see Appendix II). The variation of specific heat was taken from Ahlers (1963) up to 15°K. A Debye model was used to extrapolate to higher temperatures. The melting line of hydrogen has been measured by Mills and Grilly (1956) to 3500 kg/cm^2. Kennedy and Vaidya (1970) conclude that for substances such as solid helium and hydrogen the melting line is well represented by a Simon equation. Extrapolation to 6.3 kbar using their melting line parameters gives a melting point of 86°K, leading to the conclusion that the hydrogen was still solid, but just barely (see Fig. 6).

It might be argued that the agreement between the zero particle velocity intercept and the measured bulk sound speed for the solid augers well for the present data to correspond to the solid phase. However, in shock wave experiments on alkali metals, Rice (1965) has shown that extrapolation of U_s-U_p data from a region in which shock melting has definitely occurred, results in agreement with bulk sound speeds measured for the solid phase.

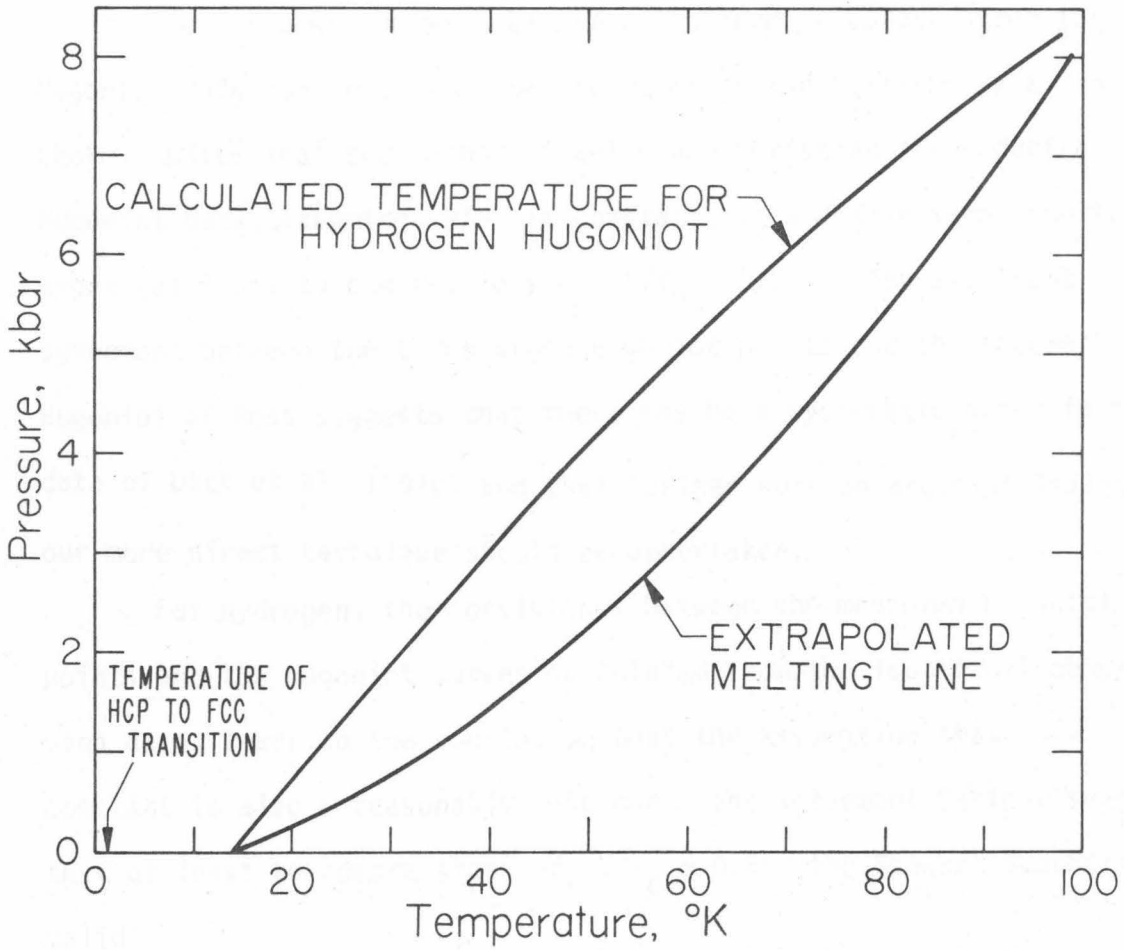

Figure 6. Temperature on hydrogen Hugoniot. Also shown is the melting line of Mills and Grilly (1956) extrapolated using $P = -279.63 + 2.749\ T^{1.744}$.

D. Conclusions

The agreement between the $77^{o}K$ isotherm calculated from the Hugoniot data for argon and the experimentally determined $77^{o}K$ isotherm implies that the method of Walsh and Christian for reducing Hugoniot data, assuming γ/V is constant, is a viable technique for argon (at least to compressions of $V/V_0 \simeq 0.6$) . The excellent agreement between the three argon Hugoniot points and the theoretical Hugoniot of Ross suggests that there may be a systematic error in the data of Dick et al. (1970) and that further work on argon utilizing our more direct technique should be undertaken.

For hydrogen, the consistency between the measured Hugoniot points and the Hugoniot curves calculated from the isothermal compression data, leads to the conclusion that the assumption that γ/V is constant is also a reasonably good one. The agreement further suggests that at least to compressions of $V/V_0 \simeq 0.65$ the Stewart isotherm is valid.

Due to the moderate uncertainties ($\sim$5-6%) extant in the shock wave measurements presented, these data cannot be used to differentiate between various proposed forms of the equation of state. Reduction of the uncertainties by a factor of 2 or 3 should allow such data, when used in conjunction with isothermal compression data, to provide quantitative information on the thermal contribution to the equation of state.

E. Chapter II, Appendix I

In shock wave studies at cryogenic temperatures, a Hugoniot for the standard material centered at a lower-than-room-temperature density is required. Hugoniot data on metals at reduced temperatures are not generally available, and thus a low temperature Hugoniot must be calculated on the basis of available principal Hugoniot and thermodynamic data. The problem can be simply stated (see Fig. 1). To find the dashed Hugoniot centered at V_0' given the Hugoniot centered at V_0:

Applying the Rankine-Hugoniot energy equation to each Hugoniot

$$E_H = P_H/2\,(V_0 - V) \tag{1}$$

$$E = P/2\,(V_0' - V) \tag{2}$$

Then, assuming that the Gruneisen parameter is a function of volume only,

$$\Delta E + E + \int_P^{P_H} \frac{V}{\gamma(V)}\,dP = E_H \tag{3}$$

where ΔE is the internal energy difference between V_0 and V_0' at P = 1 bar.

Also:

$$\Delta E + \int_0^{P_H'} \frac{V_0'}{\gamma(V_0')}\,dP = P_H'/2\,(V_0 - V_0') \tag{4}$$

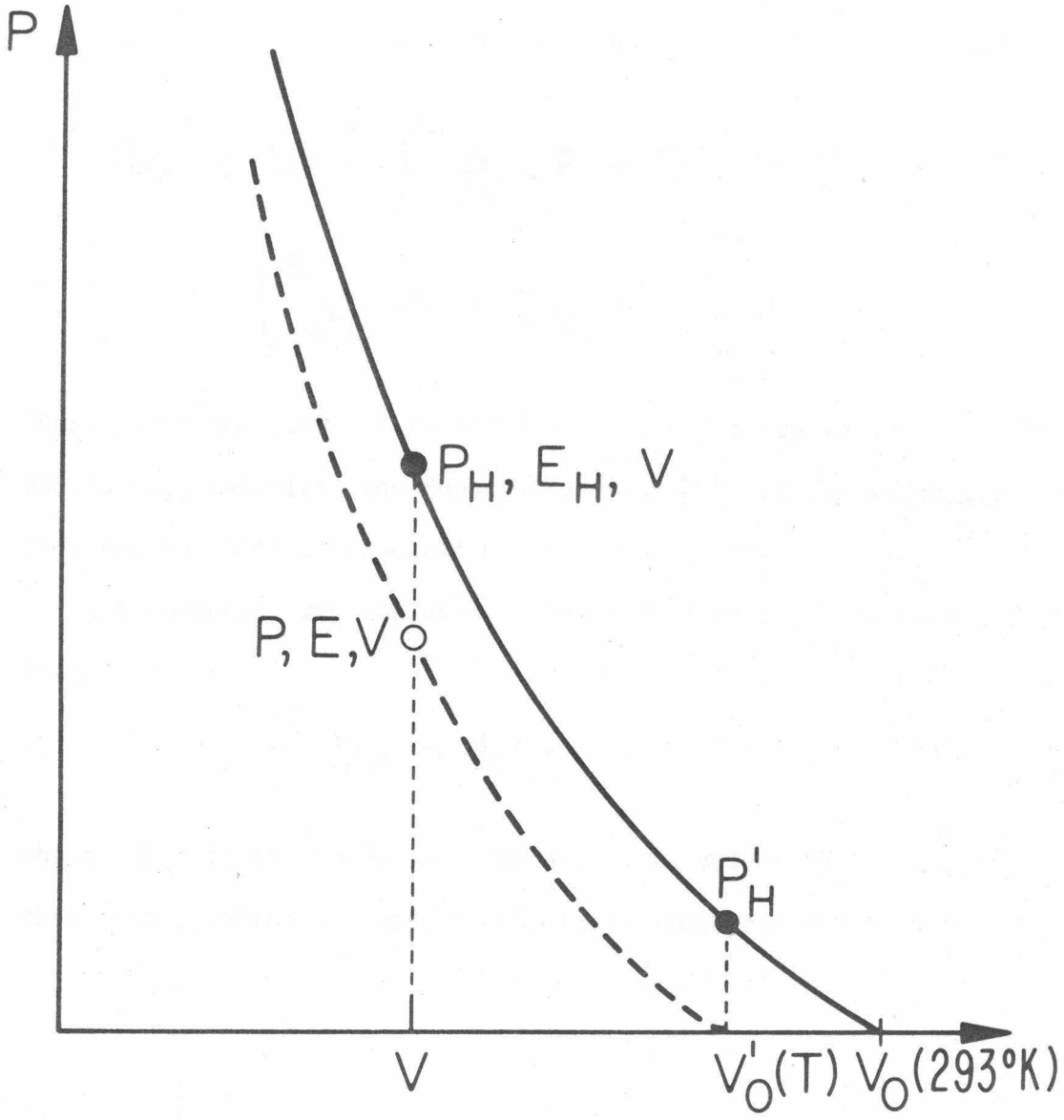

Figure 1. Hugoniot curve centered at room temperature and one centered at a lower temperature.

where in (3) and (4) we use the fact that energy is a state function.

Combining (1)-(4), an integral equation for P is obtained:

$$P_H'/2\,(V_o - V_o') - \int_o^{P_H'} \frac{V_o'}{\gamma(V_o')}\,dP + P/2\,(V_o' - V)$$

$$+ \int_P^{P_H} \frac{V}{\gamma(V)}\,dP = P_H/2\,(V_o - V) \qquad (5)$$

Thus, given the Hugoniot centered at V_0, and a new volume V_0', it is possible to calculate the Hugoniot pressure P at any volume V on this new Hugoniot using equation (5).

A common assumption used in the reduction of shock wave data is that

$$\gamma/V = \gamma_o/V_o \qquad (6)$$

where γ_0 is the Gruneisen parameter at a volume V_0. Substituting this into equation (5) reduces (5) to an algebraic equation for P:

$$P = \frac{1}{G}\left\{P_H'\left[V_o\left(\frac{1}{2} - \frac{1}{\gamma_o}\right) - \frac{V_o'}{2}\right] - P_H\left[V_o\left(\frac{1}{2} - \frac{1}{\gamma_o}\right) - \frac{V}{2}\right]\right\} \qquad (7)$$

where $$G = \left(\frac{V_o}{\gamma_o} - \frac{V_o'}{2} + \frac{V}{2}\right)$$

For the experiments previously described, the Hugoniot data for Type 304 stainless steel (McQueen et al. 1970) at 293°K were corrected to 77°K and 5°K utilizing the thermal expansion data of Corruccini and

Gniewek (1961), to calculate the volume $V_o'(T)$.

Figures 2 and 3 show the Hugoniot for Type 304 stainless steel plotted in the P-U_p and U_s-U_p plane. Table I provides U_s-U_p Hugoniots along with the corresponding initial densities and temperatures. The U_s-U_p Hugoniot at 293°K is a linear fit to experimental data (McQueen et al. 1970).

TABLE I

Hugoniots Centered at Various Temperatures

$T = 293^oK$ $\rho_o = 7.8960$

$U_s = 4.569 + 1.490\ U_p$

$T = 77^oK$ $\rho_o = 7.9607$

$U_s = 4.599 + 1.092\ U_p$

$T = 5^oK$ $\rho_o = 7.9634$

$U_s = 4.601 + 1.091\ U_p$

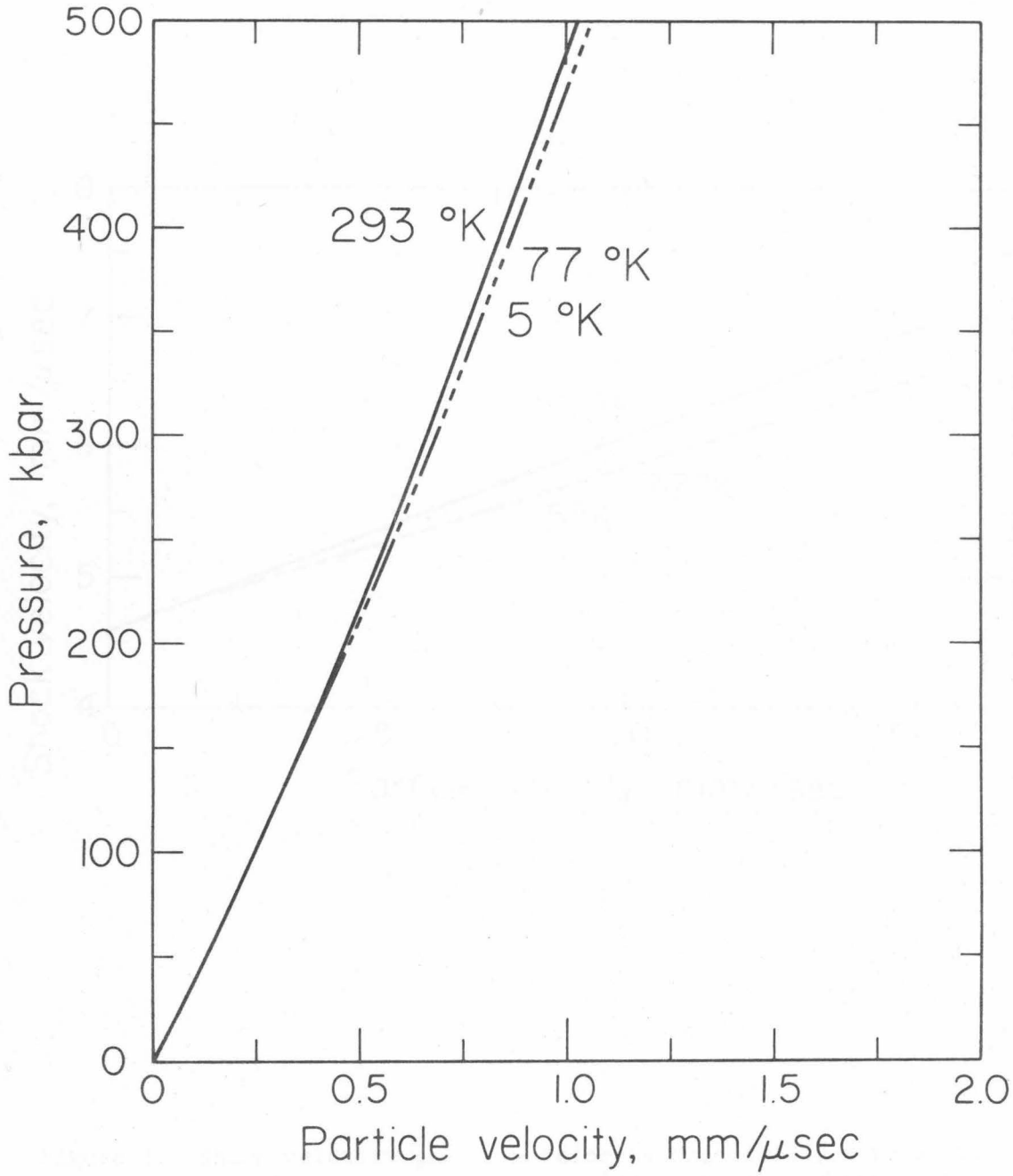

Figure 2. Pressure-particle velocity Hugoniots for type 304 stainless steel centered at 293°K, 77°K and 50°K.

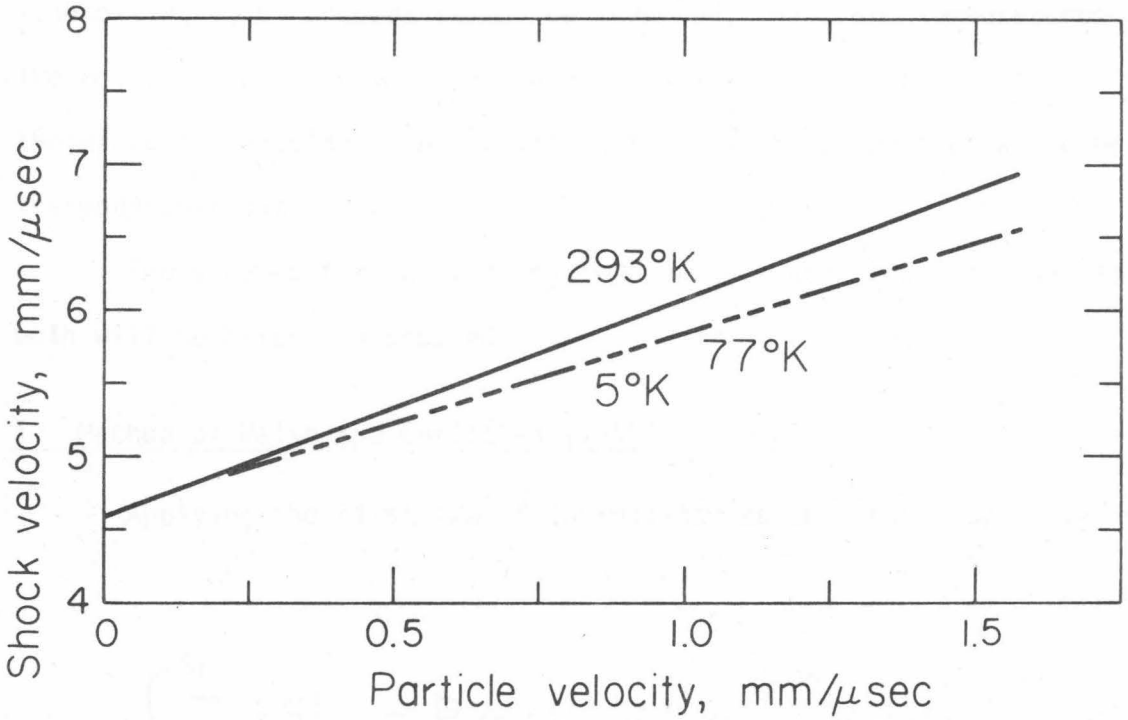

Figure 3. Shock velocity-particle velocity Hugoniots for type 304 stainless steel centered at 293°K, 77°K, and 50°K.

E. Chapter II, Appendix II

From measurements of shock wave velocities in a variety of substances, P, V, E properties may be inferred. However, temperatures are not yet routinely measured in a shock wave experiment and must therefore be calculated on the basis of P, V, E properties and other thermodynamic data.

Two schemes for calculating temperatures are generally used and both will be briefly discussed.

1. Method of Walsh and Christian (1955)

Applying the first law of thermodynamics to a Hugoniot curve

$$\int_{S_0}^{S_1} T\,dS\Big|_{HUG} = P_1/2\,(V_0 - V_1) + \int_{V_0}^{V_1} P\,dV\Big|_{HUG} \qquad (1)$$

differentiate with respect to V_1 :

$$\frac{d}{dV_1}\left\{\int_{S_0}^{S_1} T\,dS\Big|_{HUG}\right\} = \frac{dP_1}{dV_1}\,\frac{(V_0 - V_1)}{2} + \frac{P_1}{2} \qquad (2)$$

Using the thermodynamic identity

$$T\,dS = C_v\,dT + \left(\frac{\partial P}{\partial T}\right)_v T\,dV \qquad (3)$$

$$\frac{d}{dV_1}\left\{\int_{S_0}^{S_1} T\,dS\Big|_{HUG}\right\} = C_v\,\frac{dT_1}{dV_1} + \left(\frac{\partial P}{\partial T}\right)_v T_1 \qquad (4a)$$

$$= \frac{dP_1}{dV_1}\frac{(V_0 - V_1)}{2} + \frac{P_1}{2} \tag{4b}$$

The right-hand side of equation (4b) is a function of volume only. A solution of

$$C_v \frac{dT_1}{dV_1} + \left(\frac{\partial P}{\partial T}\right)_V T_1 = \frac{dP_1}{dV_1}\frac{(V_0 - V_1)}{2} + \frac{P_1}{2} \tag{5}$$

is

$$T_1(V_1) = T_0 e^{b(V_0 - V_1)} + e^{-bV_1}\int_{V_0}^{V_1}\left[\frac{f(V)}{C_v} e^{bV}\right] dV \tag{6}$$

if b and C_V are constant. In (6) the definitions

$$b = \left(\frac{\partial P}{\partial T}\right)_V / C_v \tag{7a}$$

$$f(V) = \frac{dP}{dV}\frac{(V_0 - V)}{2} + \frac{P}{2} \tag{7b}$$

and the condition

$$T = T_0 \quad \text{at} \quad V = V_0$$

were used.

Expression (6) can be easily integrated numerically to yield temperatures on the Hugoniot as a function of volume.

Note that assuming b = constant, (7a) is equivalent to the assumption that γ/V is a constant.

$$\gamma = V\left(\frac{\partial P}{\partial E}\right)_V = \frac{V}{C_V}\left(\frac{\partial P}{\partial T}\right)_V \tag{8}$$

from which

$$\gamma/V = \left(\frac{\partial P}{\partial T}\right)_V / C_V \quad = b \tag{9}$$

This method appears to work well in solid argon shocked to pressures $\sim$ 140 kb (Lagus and Ahrens, 1973). It has the advantage of calculational simplicity; however, the assumptions of constant C_V and γ/V may not always be viable.

2. Method of Ahrens et al. (1969)

A disadvantage to the method of Walsh and Christian is the need to assume a constant value of C_V. Figure 1 shows a Hugoniot and an adiabat centered at the same initial volume, and appropriately labeled. It is possible to calculate temperatures using the following scheme, given a Hugoniot curve.

Along an adiabat, centered at V_o

$$E_A - E_o = -\int_{V_o}^{V} P\,dV \tag{1}$$

The energy to go from E_A to E_H is

$$E_H - E_A = \int_{P_A}^{P_H}\left(\frac{\partial E}{\partial P}\right)_V dP = \int_{P_A}^{P_H}\frac{V}{\gamma}\,dP \tag{2}$$

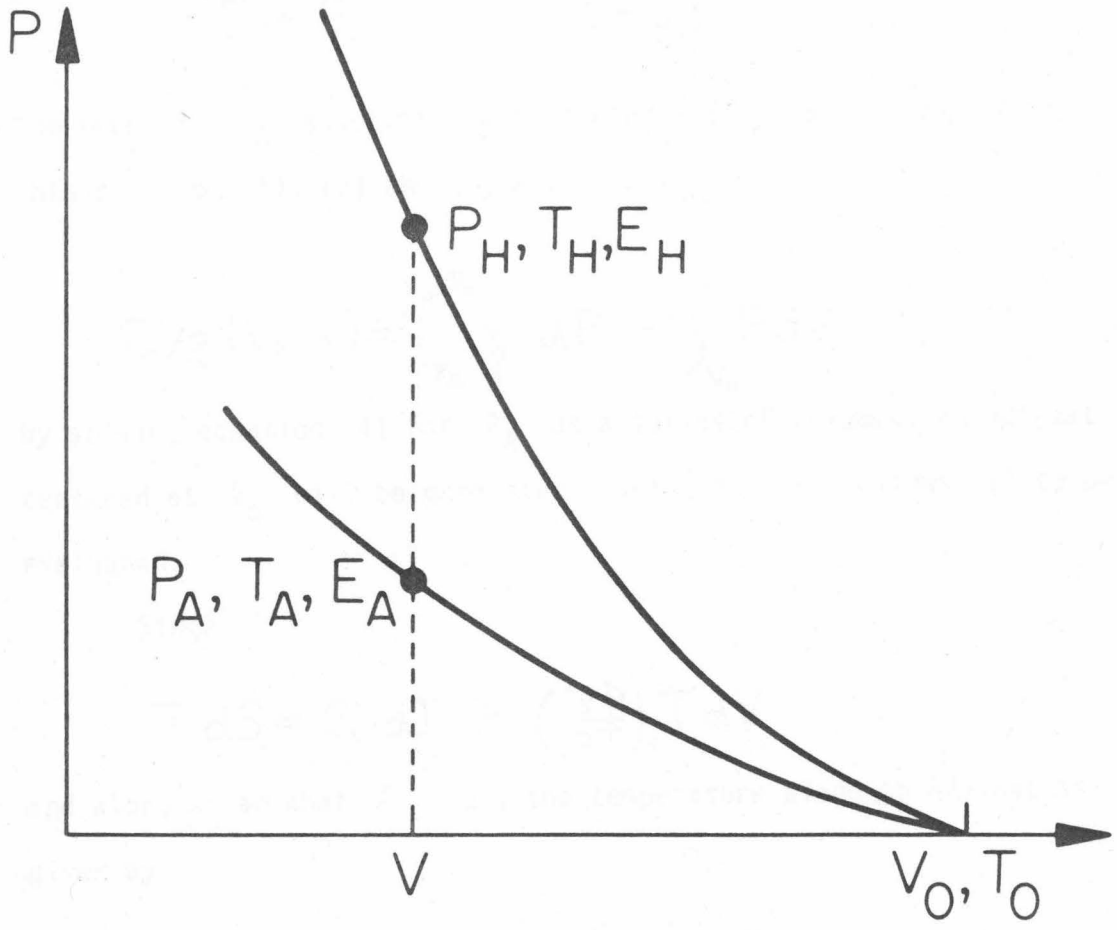

Figure 1. Hugoniot and adiabat centered at a volume V_o.

Along the Hugoniot curve

$$E_H - E_o = P_H/2\,(V_o - V) \tag{3}$$

The pressure P_A associated with the adiabat at any volume V is obtained from (1), (2) and (3) as:

$$P_H/2\,(V_o - V) = \int_{P_A}^{P_H} \frac{V}{\gamma}\, dP - \int_{V_o}^{V} P\,dV \tag{4}$$

By solving equation (4) for P_A at a series of volumes, an adiabat centered at V_o will be generated. This, in turn, allows (1) to be evaluated.

Since

$$T\,dS = C_v\,dT + \left(\frac{\partial P}{\partial T}\right)_v T\,dV \tag{5}$$

and along an adiabat $dS = 0$, the temperature along an adiabat is given by

$$T = T_o \exp\left[\int_V^{V_o} \frac{\gamma}{V}\, dV\right] \tag{6}$$

which allows a calculation of T_A at volume V.

Then

$$E_H - E_A = \int_{T_A}^{T_H} C_V\,dT \tag{7}$$

which can be solved for the temperature T_H on the Hugoniot at a series of volumes.

Equations (1)-(7) have the advantage over the Walsh and Christian formulation, that neither C_v nor γ/V need be assumed constant. In

the case where sufficient data on the volume (and temperature) dependence exists, these data may be directly incorporated into the calculation of temperature.

G. References to Chapter II

1. Ahlers, G., "Some Properties of Solid Hydrogen at Small Molar Volumes", UCRL Report 10757 (1963).
2. Ahrens, T. J., D. L. Anderson, and A. E. Ringwood, Rev. Geophys. 7, 667 (1969).
3. Ahrens, T. J., P. L. Lagus, J. H. Lower, H. L. Richardson, J. L. Blayney, and D. C. Johnson, to be published (1973).
4. Ahrens, T. J. and M. H. Ruderman, J. Appl. Phys. 37, 4758 (1966).
5. Bezuglyi, P. A. and R. K. Minyafaev, Sov. Phys. Sol. St. 9, 480 (1967).
6. Bruce, T. A., Phys. Rev. B5, 4170 (1972).
7. Corruccini, R. J. and J. J. Gniewek, "Thermal Expansion of Technical Solids at Low Temperatures", NBS Monograph 29 (1961).
8. Dick, R. D., R. H. Warnes, and J. Skalyo, J. Chem. Phys. 53, 1648 (1970).
9. Ebner, C. and C. C. Sung, Sol. St. Comm. 8, 1903 (1970).
10. Ebner, C. and C. C. Sung, Phys. Rev. B4, 2638 (1971).
11. Ebner, C. and C. C. Sung, Sol. St. Comm. 11, 489 (1972).
12. Keeler, N., in Phys. of High Energy Density, edited by H. Knoepfel (Adison Wesley, New York, 1973) pp. 1-88.
13. Keeler, R. N., M. van Thiel, and B. J. Adler, Physica 31, 1437 (1965).
14. Kennedy, G. C. and S. N. Vaidya, JGR 75, 1019 (1970).
15. Krumhansl, J. A. and S. Wu, Phys. Rev. B5, 4155 (1972).
16. Lagus, P. L. and T. J. Ahrens, J. Chem. Phys. 59, 3517 (1973).
17. Lawrence, D. J. and F. E. Neale, Proc. Phys. Soc. 85, 1251 (1965).

18. McQueen, R. G., S. P. Marsh, J. W. Taylor, J. N. Fritz, and W. J. Carter, in High Velocity Impact Phenomena, edited by R. Kinslow (Academic Press, New York, 1970), pp. 515-568.

19. Megaw, H., Phil. Mag. 28, 129 (1939).

20. Mills, R. L. and E. R. Grilly, Phys. Rev. 101, 1246 (1956).

21. Pollack, E. L., T. A. Bruce, G. V. Chester, J. A. Krumhansl, Phys. Rev. B5, 4180 (1972).

22. Pollack, G. L. and E. N. Farabaugh, J. Appl. Phys. 36, 313 (1963).

23. Rice, M. H., J. Phys. Chem. Solids 26, 483 (1965).

24. Rice, M. H., R. G. McQueen, and J. N. Walsh, in Solid State Physics, edited by F. Seitz and D. Turnbull (Academic Press, New York, 1958), Vol. 6, pp. 1-63.

25. Ross, M., "Shock Compression and the Melting Curve for Argon", UCRL Preprint 74478 (1973).

26. Ross, M. (private communication).

27. Stewart, J. W., J. Phys. Chem. Solids 1, 146 (1956).

28. Stewart, J. W., J. Phys. Chem. Solids 29, 641 (1968).

29. Tribitsyn, U. P., Sov. Phys. Sol. St. 7, 1708 (1966).

30. Urvas, A. O., D. L. Losee, and R. P. Simmons, J. Phys. Chem. Solids 28, 2269 (1967).

31. van Thiel, M. and B. J. Alder, J. Chem. Phys. 44, 1056 (1966a).

32. van Thiel, M. and B. J. Alder, Mol. Phys. 10, 427 (1966b).

33. Walsh, J. M. and R. H. Christian, Phys. Rev. 97, 1544 (1955).

34. Wu, S., "A Quantum Theory of Equation of State for Solid Hydrogen", Ph.D. Dissertation, Cornell University (1967).

35. Zubarev, V. N. and G. S. Telegin, Sov. Phys. Dok. 7, 34 (1962).

CHAPTER III

EQUATION OF STATE FOR MOLECULAR HYDROGEN

A. Introduction

Exact calculation of the equation of state for solid molecular hydrogen represents a challenging theoretical problem. Early calculations (Kronig et al. 1946, DeBoer and Blaisse 1948) attempted to construct a P-V relation at $0^{o}K$ utilizing an intermolecular potential of the Lennard-Jones 6-12 type. The validity of such a potential to calculate a P-V equation of state is questionable, since it is known that an inverse twelfth power repulsion is too "stiff" at large compressions in solidified or liquified gases (van Thiel and Alder 1966, Zubarev and Telegin 1962). A more fundamental objection to such calculations (at least in the case of Kronig et al.) is their omission of the contribution of zero point energy to the calculated pressures. Due to their small masses and weak interaction potentials, substances such as hydrogen and helium have a large zero point energy.

The success of the quantum crystal formulation in explaining the properties of solid helium (see, for example, Bernardes 1958,1960, Nosanow 1964,1966, Guyer 1969) has led various investigators to attempt a similar approach in calculating a pressure volume equation of state for molecular hydrogen (Wu 1967, Krumhansl and Wu 1968,1972, Ebner and Sung 1970,1971,1972, Pollack et al. 1972, Bruce 1972). All of these calculations assume some form for the intermolecular potential (often including nonspherical terms) in an attempt to produce a pressure-volume curve which will agree with the measured $4^{o}K$ isotherm for solid hydrogen (Stewart 1956). The agreement between theory and experiment

is generally quite good below about 4 kbar. However, as can be seen in Fig. 1, the agreement worsens as pressure increases, until at pressures of 10 kbar (corresponding to a molar volume of ∿12 cc/mole) all the calculations so far published yield pressures which are more than 30% higher than the experimentally determined pressure. Discrepancies of this magnitude appear to cast doubt on the usefulness of the quantum crystal formulation in predicting the pressure-volume properties of solid hydrogen.

This failure is particularly unfortunate in the case of hydrogen since experimentally it is quite difficult to obtain reliable pressure volume data for pressures between 200 kbar and several megabars. In this range molecular hydrogen is conjectured to transform to a metallic phase, which phase is thought to have important physical (Ashcroft 1968, Ginzberg 1969) and astrophysical (De Marcus 1958, Peebles 1964, Hubbard 1968,1969,1970) implications.

Under a variety of assumptions, the equation of state for metallic hydrogen is thought to be well known (Neece et al. 1971, Trubitsyn 1966b, De Marcus 1958, Wigner and Huntington 1935, Dynin 1972). Uncertainty in the equation of state of molecular hydrogen is such, however, that transition pressures ranging from 250 kbar to 20 mbar have been proposed.

Guyer (1969) alludes to the possibility that the full quantum crystal formulation may not be necessary to deduce an acceptable equation of state for molecular hydrogen. Even though the mass of the hydrogen molecule is less than that of the helium atom, the depth of the energy well is roughly three times greater. Guyer notes that

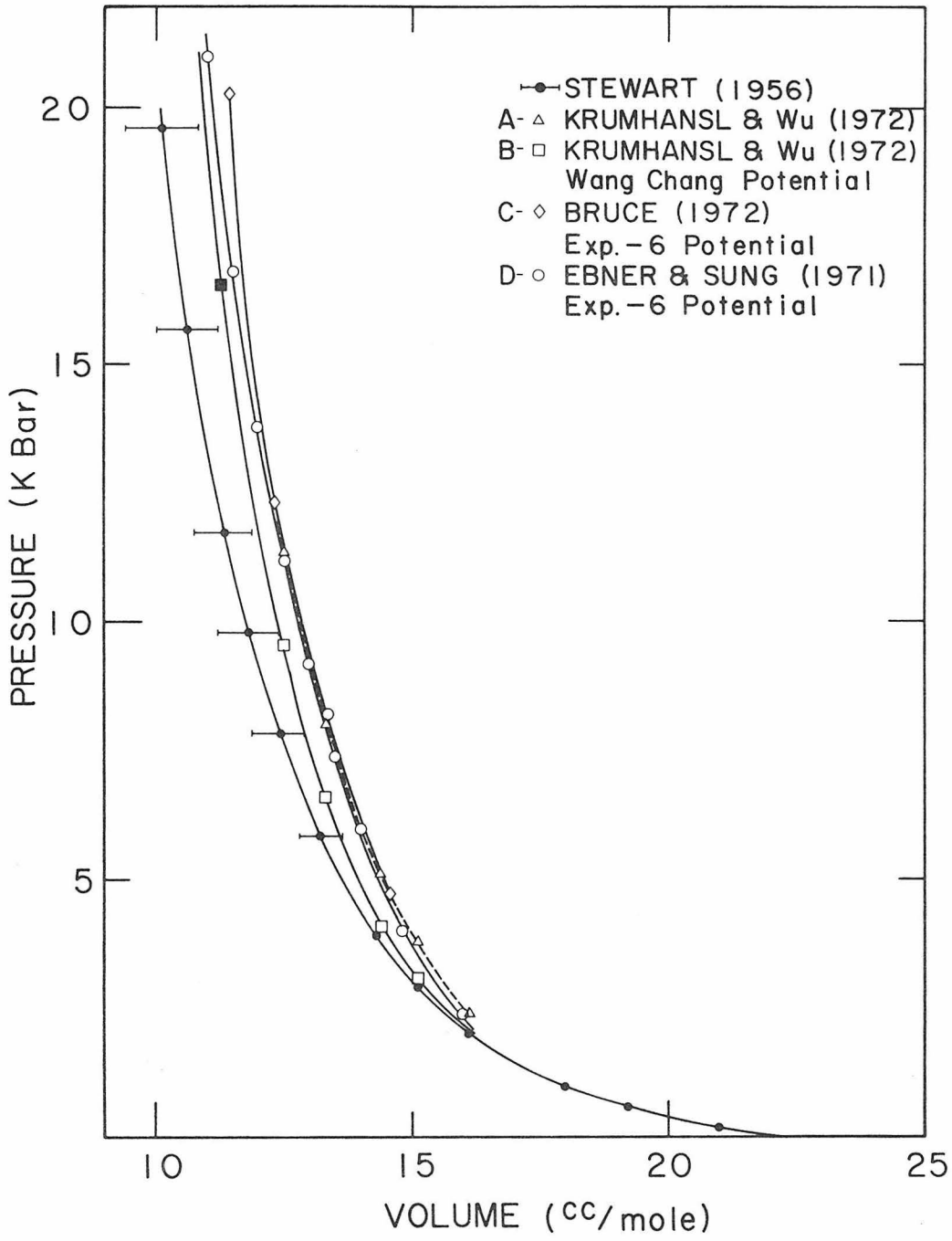

Figure 1. Stewart 4°K isotherm for solid hydrogen and several theoretical 0°K isotherms calculated by quantum crystal methods.

"quantum corrections" (presumably inclusion of a zero point form) are needed for equation of state calculations on hydrogen. Ebner and Sung (1970) claim that a rigid lattice model would be a good approximation. These suggestions led to a re-examination of previous semi-classical calculations of the equation of state for hydrogen. By explicitly including various forms for the volume variation of the zero point contribution to the total internal energy, it is possible to calculate an improved pressure volume equation of state for molecular hydrogen.

B. Potential Interaction Energy

At $0^{o}K$ the total internal energy of a crystal of solid hydrogen can be written as

$$\epsilon_p(v) = \epsilon_1(v) + \epsilon_{z.p.}(v) \tag{1}$$

where $\epsilon_1(v)$ is the contribution to the total internal energy of the repulsive and attractive terms in the interaction potential, and

$\epsilon_{z.p.}(v)$ is the contribution to the total internal energy due to zero point motion.

$\epsilon_{zp}(v)$ will be discussed in part C.

The energy of interaction of two hydrogen molecules can be expressed as

$$\Phi_{TOT} = \Phi_{REP} + \Phi_{QQ} + \Phi_6 + \Phi_8 \tag{2}$$

where Φ_{REP} is the repulsive interaction energy due to the overlapping of wave functions;

Φ_{QQ} is the electrostatic quadrupole-quadrupole interaction energy;

Φ_6 is the inverse sixth power term in the dispersion energy, semi-classically called the dipole-dipole interaction;

Φ_8 is the inverse eighth power term in the dispersion energy, semi-classically called the dipole-quadrupole interaction.

In all the calculations undertaken in this paper e, $\hbar$, m, and c have been set equal to unity, resulting in so-called "atomic" or "natural" units. The atomic units of distance, energy, and pressure are then, respectively, 0.529×10^{-8} cm, 27.2 eV, and 294 mbar.

Many calculations of the repulsive interaction energy between two hydrogen molecules have been undertaken. De Boer (1942) used a first order perturbation technique to calculate this energy. He used Wang-type atomic orbitals, and set all multiple exchange and intramolecular electron exchange integrals equal to zero. The interaction energy he obtained agreed well with that deduced from the values of the second virial coefficient. Evett and Margenau (1953a,1953b) and Mason and Hirschfelder (1957) undertook more extensive calculations utilizing a high speed computer to evaluate many of the integrals which De Boer neglected. Surprisingly, the more sophisticated calculations do not significantly improve the agreement with experimental data over that

obtained by De Boer. Mason and Hirschfelder (1957) probed this point and concluded that the exchange integrals which De Boer neglected are large, but apparently there is a fortuitous cancellation of these terms. DeBoer's original calculations may, therefore, represent the actual physical situation in a reasonable manner.

If the atoms in each of two interacting H_z molecules are labeled as a-b and c-d respectively, De Boer found that (z) may be written as:

$$\mathcal{I}_{REP} = 2.78\left[e^{-1.87\, r_{ac}} + e^{-1.87\, r_{ad}} + e^{-1.87\, r_{bc}} + e^{-1.87\, r_{bd}} \right] \qquad (3)$$

where r_{ij} = distance from atom i of one molecule to atom j of the second molecule.

In this form, however, $\mathcal{I}_{REP}$ is cumbersome to use due to the implicit angular dependence of the r_{ij}.

For a diatomic molecule in a crystal, Pauling (1930) showed that the motion of a molecule in its dependence on the polar angles Θ and ϕ, may approach one of two limiting cases, oscillation or rotation. If the intermolecular forces are strong and the moment of inertia is large (e.g., I_2) the eigenfunctions and the energy levels approach those corresponding to oscillation about equilibrium positions. If, on the other hand, the intermolecular forces are weak and the moment of inertia is small (e.g., H_2), the eigenfunctions and energy levels

approximate those of a freely rotating molecule, even in the lowest energy state. Hydrogen molecules, then, can be considered to be freely rotating with the intermolecular forces producing only small perturbations from uniform rotation. This suggests that the form of (3) represents the intermolecular repulsion if suitably averaged over the rotation angles implicit in the r_{ij}.

Following a suggestion of Trubitsyn (1966a) this may be accomplished by averaging the interactions of hydrogen atoms over the spherical surfaces defined by the free rotation of the hydrogen molecule. The spheres are centered a distance R (corresponding to intermolecular separation) apart, and their radii are taken to be half the experimental intramolecular separation (H-H distance), denoted by ℓ. A typical term in equation (3), after averaging, appears as

$$\langle \Phi_{TERM} \rangle \sim A\eta(R)e^{-BR} \tag{4}$$

with A = 2.78, B = 1.87

$$\eta(R) = \left(\frac{\sinh x}{x}\right)^2\left[1 - \frac{2}{BR}(x\coth x - 1)\right] \tag{5}$$

where $x = B\ell$

The total interaction potential is the sum of four such terms.

To check the validity of averaging in this way, a plot of Φ_{AV} is shown in Fig. 2, along with a plot of an approximation (labeled A) which De Boer claimed to be a valid representation of (3) in the range R = 6

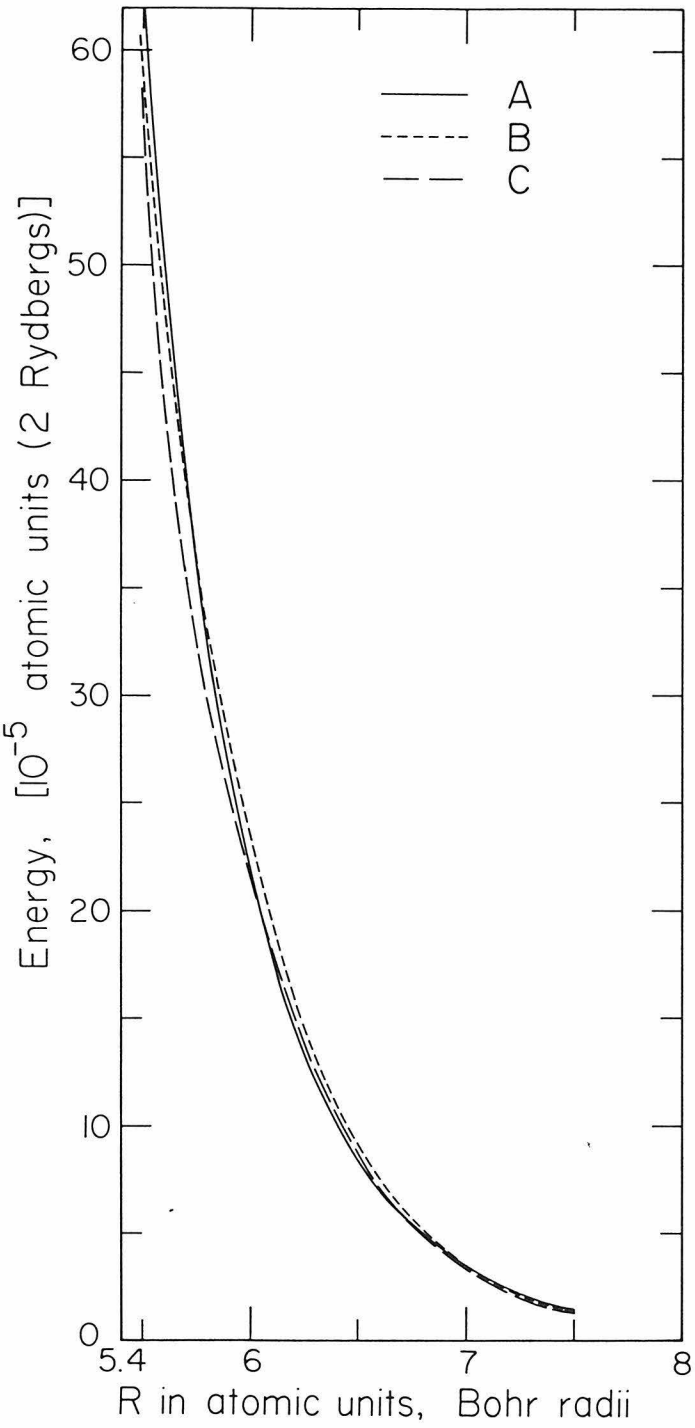

Figure 2. Averaged repulsive potential compared with experimentally verified repulsive potential. Curve A is DeBoer repulsive interaction. Curve B is averaged repulsive potential with η a variable. Curve C is averaged repulsive with η constant.

to $R = 8$. The agreement is good, and suggests that averaging in this manner is valid. The curve labeled B demonstrates the case of η (R) (equation 5) a variable, whereas the curve labeled C holds η (R) equal to a suitably averaged constant value (see discussion which follows equation 10).

Intuitively one would expect rotational motion to be increasingly hindered upon compression of the solid. At present there appears to be no quantitative way to assign a threshold value after which the assumption of rotation, and hence the rationale for the averaging scheme, is questionable. Neece et al. (1971) assert that somewhere between 3 and 7 cc/mole the assumption of rotation becomes untenable. Since, however, this corresponds to pressures between $\sim$ 1 Mbar and 100 kbar, this calculation is of little value other than to indicate that caution should be exercised in accepting the averaging above 100 kbar. Raich and Etters (1972) have investigated the rotational to oscillational transition in para-hydrogen and find that it occurs above $\sim$100 kbar (compression $V/V_0 \simeq 0.30$). However, they assert that this transition will lead to only small changes in the calculated p-V curve. In Section C, experimental evidence is presented which implies that the method of averaging the repulsive potential is valid to $\sim$400 kbar.

The quadrupole-quadrupole interaction is not important in this calculation, since averaging the Φ_{QQ} term over all orientations leads to a value of zero (see, for instance, Hirschfelder et al. (1954) or Margenau and Kestner (1971)).

The inverse sixth power and inverse eighth power dispersion interaction energies have been given by Margenau (1943). He used published data on the index of refraction to obtain:

$$\Phi_6 = -C R^{-6}$$
$$C = 10.9 \qquad (6)$$

and

$$\Phi_8 = -D R^{-8}$$
$$D = 116.0 \qquad (7)$$

Equations (4), (6) and (7) form the basis for calculating $\epsilon_1(\upsilon)$.

The contribution to the internal energy of equations (4), (6), and (7) is the sum of the energies of pair interactions of molecules.

Between $14^{o}K$ and $1.3^{o}K$, solid molecular hydrogen exists in a hexagonal closest packed (hcp) crystal structure, while below $1.3^{o}K$ it undergoes a transition to a face-centered cubic (fcc) structure (Meyer 1969, Mills and Schuch 1965). All calculations in this paper have been made assuming a fcc structure for the hydrogen molecules. Comparison is then made with experimental data at $4^{o}K$ (Stewart 1956) which is presumably hexagonally closest packed. The difference in energy between these two lattice types is small, since both lattices contain the same number of lattice points out to second nearest neighbors. Thus, within the precision of these calculations the various lattice sums are equal. In addition, Seitz (1940) and Tosi and Arai (1966) point out that calculations of internal energy in most cases do not possess sufficient precision to discriminate between a hexagonal and a face-centered close packed structure.

Assuming an fcc lattice, the interaction energy E_1 is

$$E_1 = \frac{1}{2} \sum \left(\Phi_{REP} + \Phi_6 + \Phi_8 \right)$$

$$= \frac{1}{2} N \left[12 \cdot 4 \cdot A \eta(R) e^{-BR} - 14.45 C R^{-6} - 12.80 D R^{-8} \right] \quad (8)$$

where R = nearest neighbor distance;

N = number of molecules in xtal.

For an fcc lattice, the volume per atom is $v = \frac{\sqrt{2}}{4} R^3$. The interaction energy per atom $\epsilon_1 = E_1/2N$, as a function of volume is then

$$\epsilon_1(v) = 33.36\, \eta_v(v) \exp(-2.644\, v^{1/3}) - 4.921\, v^{-3} - 23.20\, v^{-8/3} \quad (9)$$

where

$$\eta_v(v) = 1.7189 - \frac{0.6696}{v^{1/3}} \quad (10)$$

In the calculation of the P-V EOS for molecular hydrogen, $\eta_v(v)$ was incorporated into the numerical computations in two ways. In one version $\eta_v(v)$ was allowed to vary from $\eta \sim 1.58$ (corresponding to $\eta \sim 1.42$ (corresponding to v at ~2 mbar). In the other, $\eta_v(v)$ was replaced by its average value over this volume range.

Plots of the various calculations indicate (see Fig. 3) that there is little difference in the pressures predicted by the two versions, so that the form with $\eta_v(v) = \text{const}$ could be used for the

sake of analytical convenience, although in the calculation of molecular-metallic transition pressure, both forms were used.

At $0^{o}K$,

$$P_1 = - \frac{d\epsilon_1(v)}{dv}$$

so that

$$P_1 = -33.36 \frac{d\eta_v(v)}{dv} \exp(-2.644 v^{1/3}) + 1/3 \cdot 33.36 \eta_v(v) v^{-2/3} \exp(-2.644 v^{1/3}) - 2 \cdot 4.92 v^{-3} - 8/3 \cdot 23.20 v^{-11/3} \quad (11)$$

Equations (9) and (11) are, respectively, the volume dependent interaction energy per atom and the potential contribution to the pressure of a crystal of solid molecular hydrogen, interacting via a De Boer-type repulsive and an inverse sixth and eighth power attractive potential.

C. Zero Point Interaction Energy

Experimental heat capacity determinations suggest that solid molecular hydrogen behaves as a Debye solid down to $4^{o}K$ (Ahlers 1963, Hill and Lounasmaa 1959). In the Debye approximation it is known that the contribution to the total internal energy due to zero point motion is (see, for instance, Fowler 1936)

$$\epsilon_{zp} = \frac{9}{8} k \Theta_D \quad (12)$$

where ϵ_{zp} = zero point energy per molecule

k = Boltzmann constant

Θ_D = Debye temperature.

The zero point contribution to the pressure then follows from

$$P_{zp} = - \frac{d\epsilon_{zp}(v)}{dv}$$

If one can derive a suitable expression for the volume dependence of Θ_D, then in principle the volume dependence of the zero point energy contribution should be calculable directly. Practically speaking there are several ways to arrive at the volume dependence of the Debye temperature. One method notes the fact that, in the Debye model, it can be shown that (Fowler 1936)

$$\Theta_D = C^* V^{1/6} K^{1/2} \tag{13}$$

where V = volume

K = adiabatic bulk modulus at volume V

C^* = constant.

By using experimental data, C^* can be evaluated. Having calculated a C^*, the volume dependence of Θ_D at any volume (and hence the zero point energy) can be calculated. The volume dependence of K can be calculated by taking the appropriate derivatives of equation (11). Thus, in atomic units, the zero point contribution to internal energy can be written

$$\epsilon_{zp}(v) = q\, v^{1/6} K^{1/2} \tag{14}$$

where $q = 0.0302$.

Then

$$P_{zp}(v) = -\tfrac{1}{6} q v^{-5/6} K^{1/2} - \tfrac{1}{2} q v^{1/6} K^{-1/2} \frac{dK}{dv} \tag{15}$$

A second approach to the evaluation of the zero point contribution is to use the Debye approximation for the Gruneisen parameter

$$\gamma = - \frac{d \ln \Theta_D}{d \ln V} \tag{15a}$$

where γ = Gruneisen parameter. Traditionally researchers in the field of high pressure phenomena utilize a simple form for the volume variation of the Gruneisen parameter:

$$\gamma = M V \tag{16}$$

where M is a constant. Integrating (15a) in conjunction with (16) gives

$$\Theta_D = \Theta_D^* \exp[M(V^* - V)] \tag{16a}$$

where Θ_D^* is the experimentally determined Debye temperature at volume V^*.

The experimental data of Ahlers (1963) allow an evaluation of M. Thus, in atomic units, equation (12) becomes

$$\epsilon_{zp}(v) = N \exp[M(v^* - v)] \tag{16b}$$

where $M = 0.01798$;

$N = 2.640 \times 10^{-4}$.

From which it follows that

$$P_{zp}(v) = N \cdot M \exp\left[M(v^* - v)\right] \tag{16c}$$

Using this assumption, shock data may be reduced to isothermal data (see, for instance, Walsh and Christian 1955, Alder 1963, Lagus and Ahrens 1973). Comparison of the resulting isotherms, with isothermal compression data, usually reveals excellent agreement. Hence, equation (16) is generally accepted as a useful and correct relation. However, the original work which established the usefulness of (16) was carried out on materials in which high pressures were achieved with only moderate compressions. Holt and Ross (1970) point out that for extreme compression (16) does <u>not</u> have the proper limiting form. They suggest that for such compression a more physically appropriate form would be

$$\gamma = W V + \gamma_0 \tag{17}$$

where γ_0 is the proper γ at $V = 0$.

An appropriate choice at γ_0 is $\gamma_0 = 1/2$ (Latter 1956, Kopyshev 1965). Equation (17) should be more valid than (16) in representing volume behavior of γ for a highly compressible substance such as solid hydrogen.

Integrating (15) in the light of (17),

$$\Theta_D = \Theta_D^* \exp\left[W(V^*-V) + \tfrac{1}{2}\ln\left(\tfrac{V^*}{V}\right)\right] \qquad (18)$$

where Θ_D^* = Debye Θ_D at volume V^*.

Utilizing the experimental data of Ahlers (1963) it is possible to evaluate W.

Converting to atomic units, the expression for $\epsilon_{zp}(v)$ becomes

$$\epsilon_{zp}(v) = H \exp\left[W(v^*-v) + \tfrac{1}{2}\ln\left(\tfrac{v^*}{v}\right)\right] \qquad (19)$$

where Ahlers' data for γ, Θ_D, and V has been used to evaluate W and H:

$$W = 0.01837$$

$$H = 3.015 \times 10^{-4}$$

From (19) it follows that

$$P_{zp}(v) = H\left(W + \tfrac{1}{2}v\right) \exp\left[W(v^*-v) + \tfrac{1}{2}\ln\left(\tfrac{v^*}{v}\right)\right] \qquad (20)$$

A less empirical technique to infer the volume variation at the Debye temperature is to relate the Debye temperature directly to the elastic constants of the crystal. Since an interaction potential has been assumed, it is straightforward, although tedious, to calculate the elastic constants and their volume dependence, and thus to arrive at the volume dependence of the Debye temperature.

Following Fowler (1936), the Debye temperature is given as

$$\Theta_D = \left(\frac{3N}{4\pi V}\right)^{1/3} \frac{h\bar{c}}{k} \qquad (21)$$

where h = Planck constant;

k = Boltzmann constant;

$\bar{c}$ = average velocity of sound defined by averaging sound velocity over all directions of the wave vector in the xtal

Herzfeld and Mayer (1934) have shown that an appropriate choice for $\bar{c}$ is

$$F = \rho^3 \bar{c}^6 = C_{11} C_{44}^2 + \tfrac{1}{5} C_{44} \left[(C_{11} - C_{44})^2 - 4 C_{12}^2 \right] + \tfrac{1}{105} \left[(C_{11} - C_{44})^3 - 12 (C_{11} - C_{44}) C_{12}^2 + 16 C_{12}^3 \right] \qquad (22)$$

where ρ is the density, and

C_{11}, C_{12}, C_{44} are the three elastic constants of a cubic lattice.

The elastic constants may be calculated from the prescription (Born and Huang 1954, Sammis 1971):

$$C_{11} = \frac{1}{2V} \sum \left\{ P x^2 + Q x^4 \right\}$$

$$C_{12} = \frac{1}{2V} \sum \left\{ -P x^2 + Q x^2 y^2 \right\}$$

$$C_{44} = \frac{1}{2V} \sum \left\{ P x^2 + Q x^2 y^2 \right\} \qquad (23)$$

where $$P = \frac{1}{R} \frac{\partial \Phi(R)}{\partial R}$$

and $$Q = \frac{1}{R} \frac{\partial}{\partial R} \left(\frac{1}{R} \frac{\partial \Phi(R)}{\partial R} \right)$$

$\Phi(R)$ = interaction potential as a function of nearest neighbor distance.

Using (22) in (21), in light of (12),

$$\epsilon_{zp}(v) = Q^* v^{1/6} F^{1/6} \tag{24}$$

where $Q^* = 4.86 \times 10^{-2}$,

from which it follows that

$$P_{zp}(v) = -\tfrac{1}{6} Q^* v^{-5/6} F^{1/6} - \tfrac{1}{6} Q^* v^{1/6} F^{-5/6} \frac{dF}{dv} \tag{25}$$

Numerical evaluation of the four forms for the zero point contribution indicates (see Fig. 3 and discussion in Section D) that the fourth method (elastic constant zero point) when combined with the interaction contribution to the pressure, yields the best agreement with Stewart's $4^{o}K$ isotherm. However, the Holt-Ross Gruneisen approximation to the zero point energy gives results only slightly worse than the elastic constant method, and may be preferred for calculations due to its greater simplicity.

D. Calculation of P-V Relation for Solid Molecular Hydrogen: The Metallic Transition

Combining the expressions from parts B and C, the internal energy and pressure as a function of volume can be written as

$$\epsilon(v) = \epsilon_1(v) + \epsilon_{zp}(v)$$

$$P(v) = P_1(v) + P_{zp}(v) \qquad (26)$$

These equations (26), utilizing the various zero point forms of part A, can be compared directly with experimental data.

Isothermal compression data for solid hydrogen is scarce. Megaw (1939) measured the compressibility of solid hydrogen to 100 kg/cm^2, and Stewart (1956) measured the same quantity to approximately 20 kbar. Stewart's 20 kbar, 4^{o}K isotherm has been the main datum which various theoreticians have attempted to reproduce. The surprising inability of the quantum crystal formulation to reproduce his isotherm has led some workers to conjecture that Stewart's data may be significantly in error at high compressions (Pollack et al. 1972, Krumhansl and Wu 1972). While this possibility cannot be ruled out, recent shock wave studies in solid hydrogen (Lagus and Ahrens 1973) are in substantial agreement with the Stewart isotherm (to compressions of $V/V_0 \pm 0.65$). Furthermore, the quoted errors attendant upon Stewart's data are more than generous, yet the theoretical models to date do not even approach the error bars.

In Fig. 3 Stewart's 4^{o}K isotherm is plotted, along with various 0^{o}K isotherms calculated as per the formulations in parts A and B. Curve A represents the isotherm calculated using the compressibility zero point term. Curve B is calculated according to the Holt-Ross Gruneisen

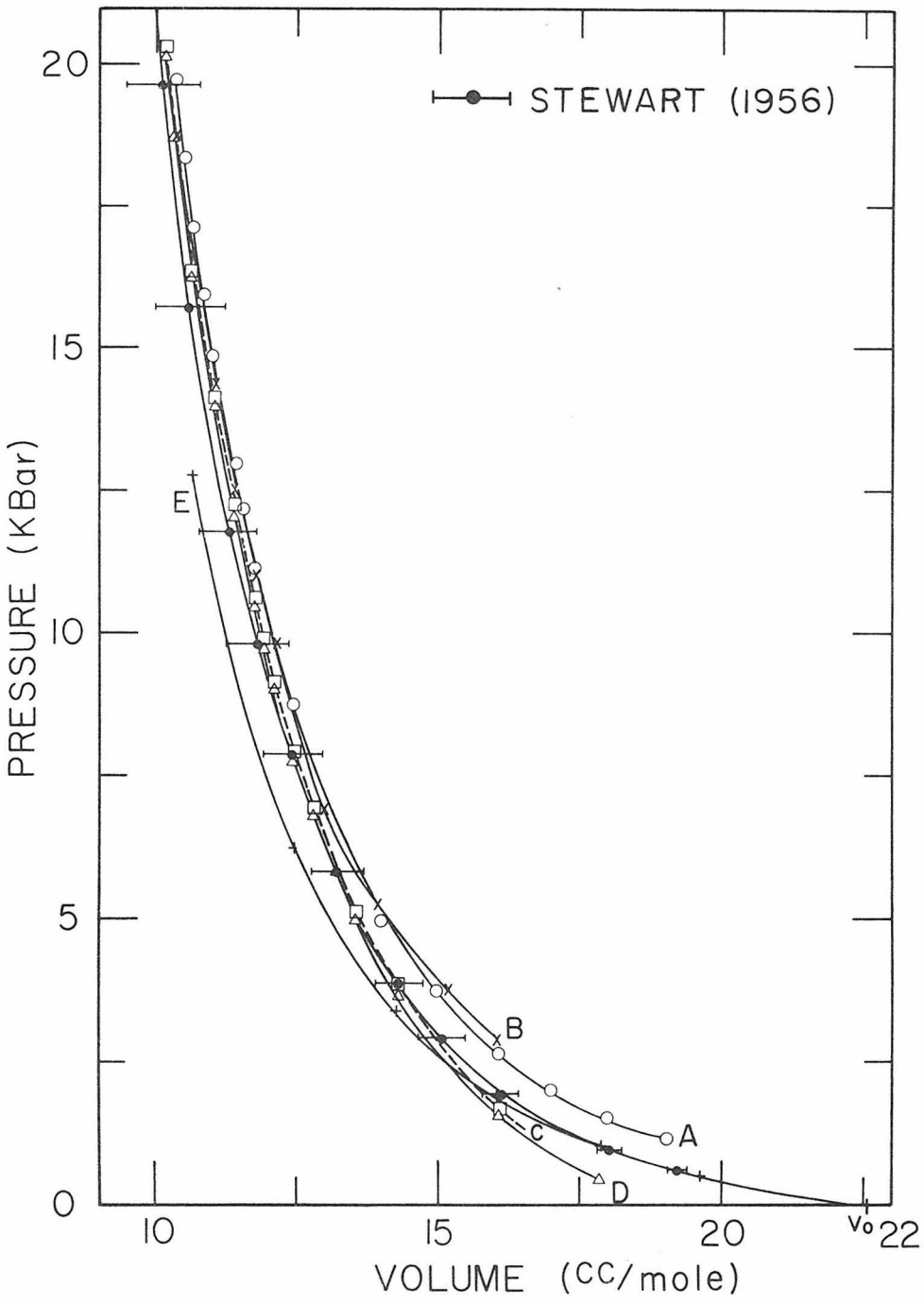

Figure 3. Stewart 4°K isotherm and calculated 0°K isotherms. Curve A represents isotherm calculated using compressibility zero point term. Curve B, calculated using Holt-Ross Gruneisen relation. Curves C and D, calculated utilizing elastic constant zero point term: Curve C assumes a variable η while D takes it to be constant (see text). Curve E is obtained using simple Gruneisen relation to find the zero point term.

relation. Curves C and D are calculated utilizing the elastic constant zero point term: Curve C assumes a variable $\eta(R)$, while D uses an η representative of the pressure range 0 to 2 mbar. (This is the range in which it is thought the molecular to metallic phase transition occurs).

Curve C is in slightly better agreement with the Stewart data than curve D. This is due to the slightly lower mean value of η over the larger pressure range (since η decreases uniformly with increasing pressure).

Curve E is calculated on the basis of a Gruneisen parameter which varies as $\gamma = MV$. Note on Curve E that for compressions to volumes less than ∿15 cc/mole the calculated pressure is too low for a given volume. Lagus and Ahrens (1973) report that on the basis of experimental shock wave data for solid hydrogen the choice of $\gamma = MV$ renders the shock data consistent with the isothermal data to a molar volume of ∿15 cc/mole ($V/V_0 \simeq 0.65$). There is little doubt, however, that at large compressions the Holt-Ross form of the volume variation of the Gruneisen parameter is to be preferred. The theoretical need for such a form calls the results of Lagus and Ahrens into question. However, reference to curve E indicates that a simple Gruneisen zero point plus interaction energy equation of state gives an excellent fit to the $4^{o}K$ isotherm down to volumes of ∿15 cc/mole. Apparently, then, for volumes greater than ∿15 cc/mole the form (16) is valid. For volumes less than this value a form for the volume variation of the Gruneisen parameter similar to (17) gives better agreement with experiment.

All of the models investigated either crossed the pressure axis before the equilibrium volume (22.56 cc/mole at 1 bar) was reached, or failed to cross the pressure axis at all. Thus, although the bulk modulus for solid hydrogen is known from ultrasonic measurements (Bezuglyi and Minyafaev 1967) at atmospheric pressure, it was not possible to compare this value with one calculated from the models.

In light of the crude approximations made in the model, the agreement between the various calculated P-V curves and the Stewart data (see Fig. 3) is gratifying. Most surprising is the correspondence of the equation of state which incorporates the Holt-Ross Gruneisen zero-point energy and the equation of state which utilizes calculated elastic constants to predict the volume variation of the zero-point energy.

Below $\sim$3-5 kbar, the fit between experiment and the present theory is poor for all models except the simple Gruneisen zero-point model. However, at high compressions and pressures the agreement is quite good. Since interest in the P-V relation of molecular hydrogen as it relates to the molecular-metallic phase transition is at pressures higher than are attainable with moderate precision, it appears to be reasonable to use one or more of the forms presented to extrapolate to high pressures. In the remainder of this section, the Holt-Ross Gruneisen zero-point form of the equation of state is used for analytical convenience.

In Fig. 4, various proposed 0^{o}K equations of state for molecular hydrogen are plotted, along with the result derived in this paper. The

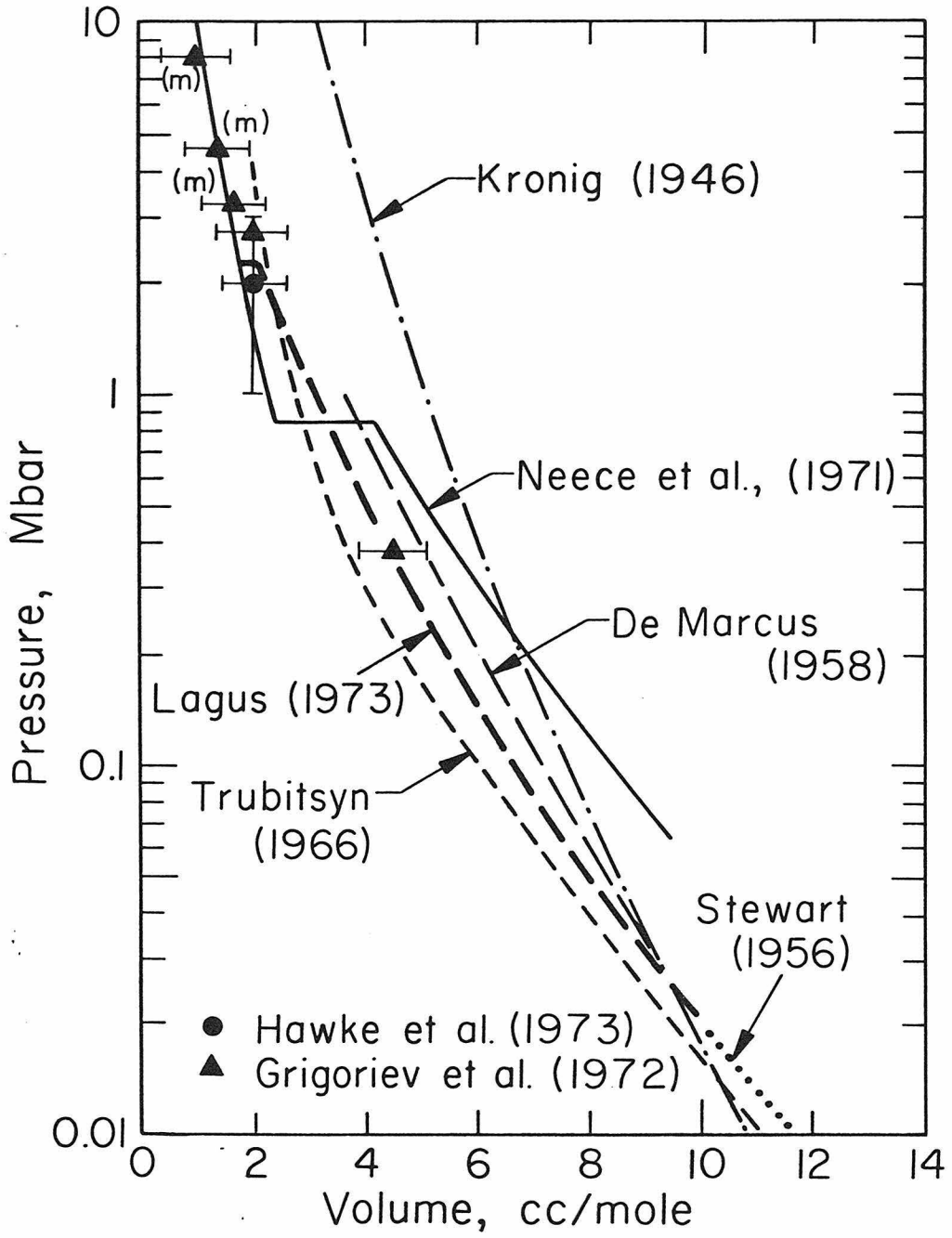

Figure 4. Proposed 0°K isotherms of solid molecular hydrogen (not calculated by quantum crystal formalism) and 0°K isotherm of metallic hydrogen proposed by Neece et al. (1971). Also plotted are: 4°K isotherm of Stewart (1956), and isentropic compression data centered at 4°K due to Grigoriev et al. (1972), and an isentropic compression datum due to Hawke et al. (1973) in liquid molecular hydrogen at an unspecified initial temperature. Grigoriev et al. data conjectured by them to be in metallic phase labeled with (m).

metallic equation of state (at $0^{o}K$) is that of Neece et al. (1971). The high pressure data are those of Hawke et al. (1973) who experimented on liquid hydrogen and Grigoriev et al. (1972) who started with initially solid hydrogen. Both of these groups utilized magnetic flux compression techniques to achieve high pressures. Note that the lowest pressure point of Grigoriev et al. and the theoretical P-V curve agree well at 370 kbar. The pressure offset between the Grigoriev isentrope and the $0^{o}K$ theoretical curve is calculated to be less than 10 kbar at this compression. This agreement suggests that the spherical averaging of the repulsion potential appears valid to volumes of $\sim$4 cc/mole. The ϵ and P relations which generated curve B can be used to calculate a Gibbs energy as a function of pressure for the molecular phase of hydrogen.

Three recently proposed $0^{o}K$ equations of state for metallic hydrogen have been utilized to calculate the Gibbs energy for the metallic phase.

Neece et al. (1971):

$$P = -0.08/v + 0.143/v^2$$

$$\epsilon = -0.0904 + 0.08 \ln v + 0.143/v \qquad (28)$$

Trubitsyn (1966):

$$P = \tfrac{2}{3} \cdot 2.871\, v^{-5/3} - \tfrac{1}{3} \cdot 2.183\, v^{-8/3} + \tfrac{1}{3} \cdot 0.00527\, v^{-2/3}$$
$$- 0.008\, v^{-1} + \tfrac{1}{2} \cdot 0.08\, v^{-3/2}$$

$$\epsilon = 2.871\, v^{-2/3} - 2.183\, v^{-1/3} + 0.4606$$
$$- 0.00527\, v^{1/3} + 0.008 \ln v + 0.08\, v^{-1/2} \qquad (29)$$

Dynin (1972):

$$P = \tfrac{2}{3} \cdot 2.817\, v^{-5/3} - \tfrac{1}{3} \cdot 2.1825\, v^{-4/3}$$
$$- \tfrac{1}{3} \cdot 0.00065\, v^{-2/3} - 0.005/v + \tfrac{1}{2} \cdot 0.08\, v^{-1/2}$$

$$\epsilon = 2.817\, v^{-2/3} - 2.1825\, v^{-1/3} + 0.00065\, v^{1/3}$$
$$+ 0.005 \ln v + 0.08\, v^{-1/2} + 0.4721 \qquad (30)$$

Equations (28), (29) and (30) are in atomic units. The P-V relations are plotted in Fig. 5. Note that to pressures of 30 mbar, there is less than a 10% spread in predicted pressures at a given volume. Experiments such as those of Hawke et al. (1973) and Grigoriev et al. (1972) need to improve their precision by an order of magnitude before it will be experimentally possible to distinguish between the various theoretical formulations of the metallic equation of state. Error bars are not plotted ($\sim \pm 0.5$ cc/gm in volume and $\sim \pm 1$ mbar in pressure). The trend apparent in the data of Grigoriev et al., if real, appears to imply a "softer" metallic equation of state. Due to the extreme difficulty of performing such experiments, it is unclear at this point

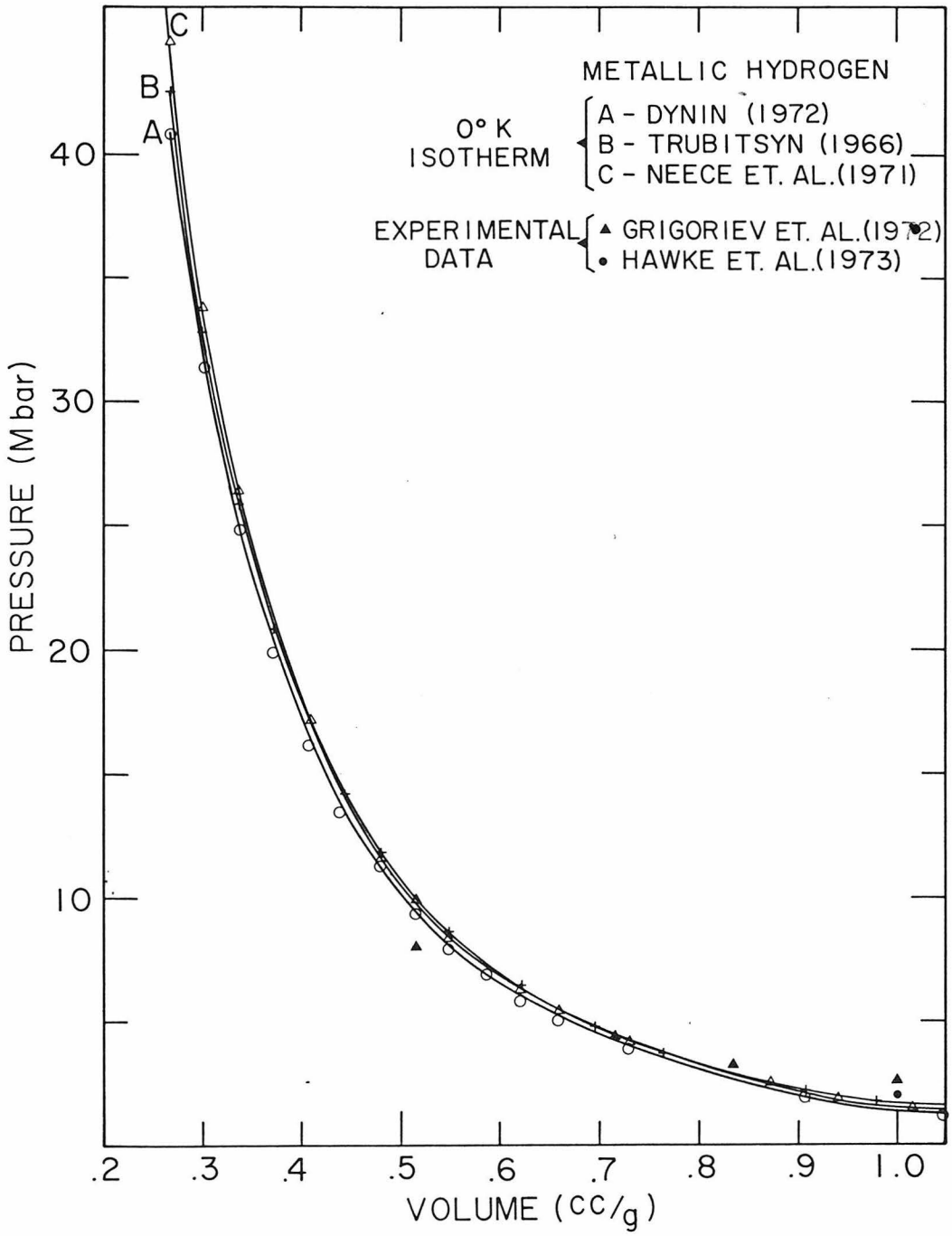

Figure 5. 0°K isotherms for metallic hydrogen proposed by Neece et al. (1971), Dynin (1972), and Trubitsyn (1966b). Also plotted are experimental data of Grigoriev et al. (1972) and Hawk et al. (1973).

whether theory or experiment needs to be improved. However, the method used to calculate the metallic equation of state by Neece et al. (1971) has been used to calculate the pressure volume properties of lithium and sodium with great success. This, and the general agreement between the various theoretical formulations of the metallic equation of state suggests that the Grigoriev et al. (1972) data should be taken with caution until independently checked.

The Gibbs free energy as a function of pressure for each metallic equation of state (EOS) is plotted in Fig.6abc along with the Gibbs free energies for the molecular phase as calculated for each form of the molecular EOS. In all cases, the curves intersect at a small angle so that the exact transition pressure is uncertain by perhaps ±0.2 mbar. For the three metallic EOS considered, the transition pressures under the assumption of each of the four forms proposed for the molecular EOS are tabulated in Table I.

In spite of the variety of forms for both the molecular and metallic equations of state, the predicted transition pressures cluster in a small range. It is tempting to assign a value of 1.9 ± 0.4 mbar for the pressure of the molecular to metallic phase transition in hydrogen at $0^{o}K$.

E. Discussion

In light of the crude assumptions inherent in the model for molecular hydrogen, the agreement with the Stewart isotherm and the convergence of the various transition pressure estimates is gratifying.

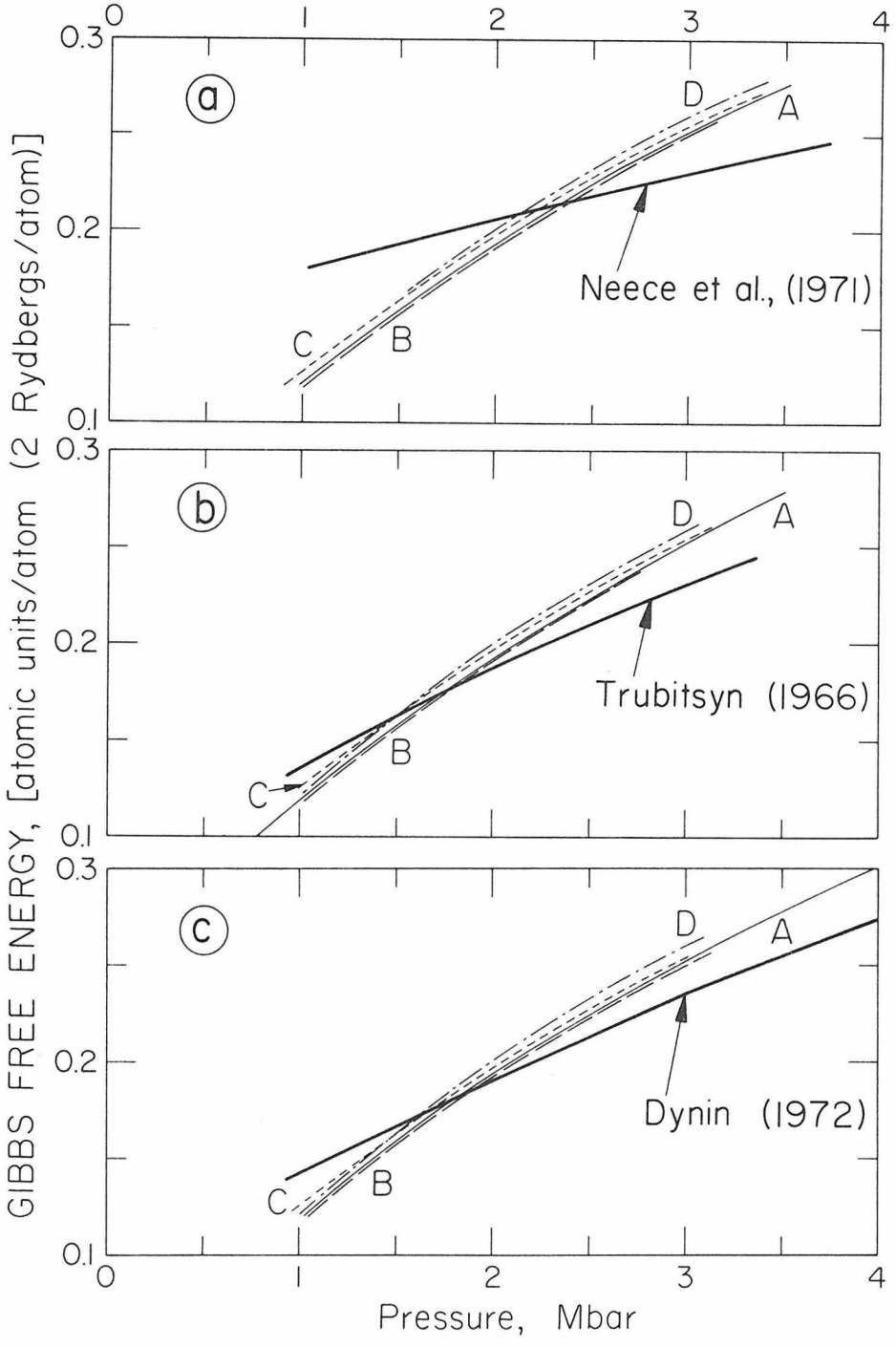

Figure 6. Gibbs free energy of the calculated molecular equations of state (labeled as in Figure 3) versus pressure plotted with Gibbs free energy for metallic hydrogen equations of state, a) Neece et al. (1971), b) Trubitsyn (1966), c) Dynin (1972).

Table I

PREDICTED TRANSITION PRESSURES (IN MBAR)

METAL	η variable: elastic constant zero point	η constant: elastic constant zero point	η constant: compressibility zero point	η constant: Holt-Ross Gruneisen zero point
Neece et al. (1971)	2.20	2.0	2.25	2.30
Trubitsyn (1966)	1.60	1.55	1.65	1.70
Dynin (1972)	1.77	1.65	1.70	1.80

In all cases (except for the simple Gruneisen case which fails to fit the experimental $4^{o}K$ isotherm above $\sim$5 kbar) the proposed model for molecular hydrogen appears to fail below $\sim$4 kbar. The quantum crystal calculations, on the other hand, are uniformly in agreement with the Stewart data in this range, indicating that below $\sim$4 kbar, short range correlation effects are important. However, the success of the model suggests that above $\sim$4 kbar short-range correlation effects play an unimportant role in determining the pressure-volume properties of molecular hydrogen. Pollack et al. (1972) concluded that above a few kbar pressure a semi-classical model such as the one presented may in fact be valid. However, they failed to reproduce the Stewart isotherm, because of their attempts to utilize a quantum crystal approach for the entire pressure range.

On the basis of the calculations presented here, it appears that at present there is little hope for producing a single EOS which reproduces the measured P-V properties over the entire pressure range. The semi-classical model fails at low pressure due to its neglect of short range correlations. The quantum crystal formulation yields satisfactory agreement at low pressure, but fails as pressures increase. Such behavior is characteristic of an inadequate representation of the interaction potential. However, the various investigators have attempted to incorporate some physically realistic potentials (e.g., Wu 1967) with little or no improvement in the agreement with experiment. Resolution of the discrepancy awaits further developments in the theory of quantum crystals. In the interim, calculations such as the one presented here can be used to calculate the pressure volume

properties of solid molecular hydrogen at pressures greater than a few kilobars.

F. Chapter III, Appendix I

A physical explanation of zero point energy follows from an application of the Heisenberg uncertainty principle to a particle confined in a simple harmonic potential well. It is well known that localization of a particle within a spatial uncertainty of Δx immediately implies that the momentum of this particle is uncertain by

$$\Delta p \approx \hbar/\Delta x \tag{1}$$

Consider now a particle in a parabolic well:

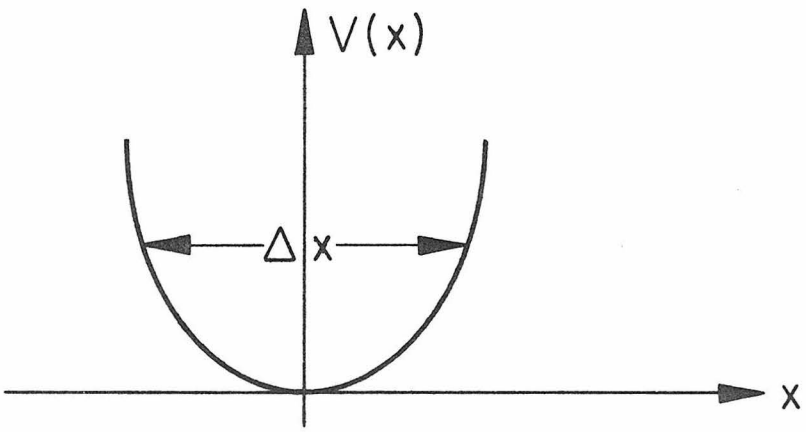

The energy of the particle in this well is given by

$$E \approx \frac{p^2}{2m} + \frac{m\omega^2 x^2}{2} \tag{2}$$

Since localizing the particle in this well implies an uncertainty of Δx, from (1) it follows that

$$E = \frac{\hbar^2}{(\Delta x)^2 2m} + \frac{m\omega^2 (\Delta x)^2}{2} \tag{3}$$

To find the lowest possible energy of this system, minimize with respect to Δx

$$\frac{\partial E}{\partial(\Delta x)} = 0 = -\frac{2\hbar^2}{2m(\Delta x)^3} + m\omega^2(\Delta x) \tag{4}$$

Thus,

$$(\Delta x)^2 = \hbar/m\omega \tag{5}$$

substituting into (3)

$$E_{LOWEST} = \hbar\omega \tag{6}$$

Thus the act of localizing the particle causes an uncertainty in momentum such that the minimum energy of the particle is on the order of $\hbar\omega$. Equation (5) also indicates those systems in which the uncertainty in position (displacement from equilibrium) will be large. Classically ω is a measure of the force constant, hence the weaker the interaction, the larger will be Δx. Similarly, for a smaller value of m, the value of Δx will be greater. This is the physical reason for the assertion that quantum effects are important only in crystals of low mass and small binding energy.

In Table I parameters which describe the rare gas solids and hydrogen are given using a 6-12 potential. Figure 1 illustrates the parameters which characterize the potential. Note that for all crystals <u>except</u> helium the distance to the potential minimum is approximately equal to the nearest neighbor separation. The large motion in column (f) suggests that zero point effects would be appreciable in solid

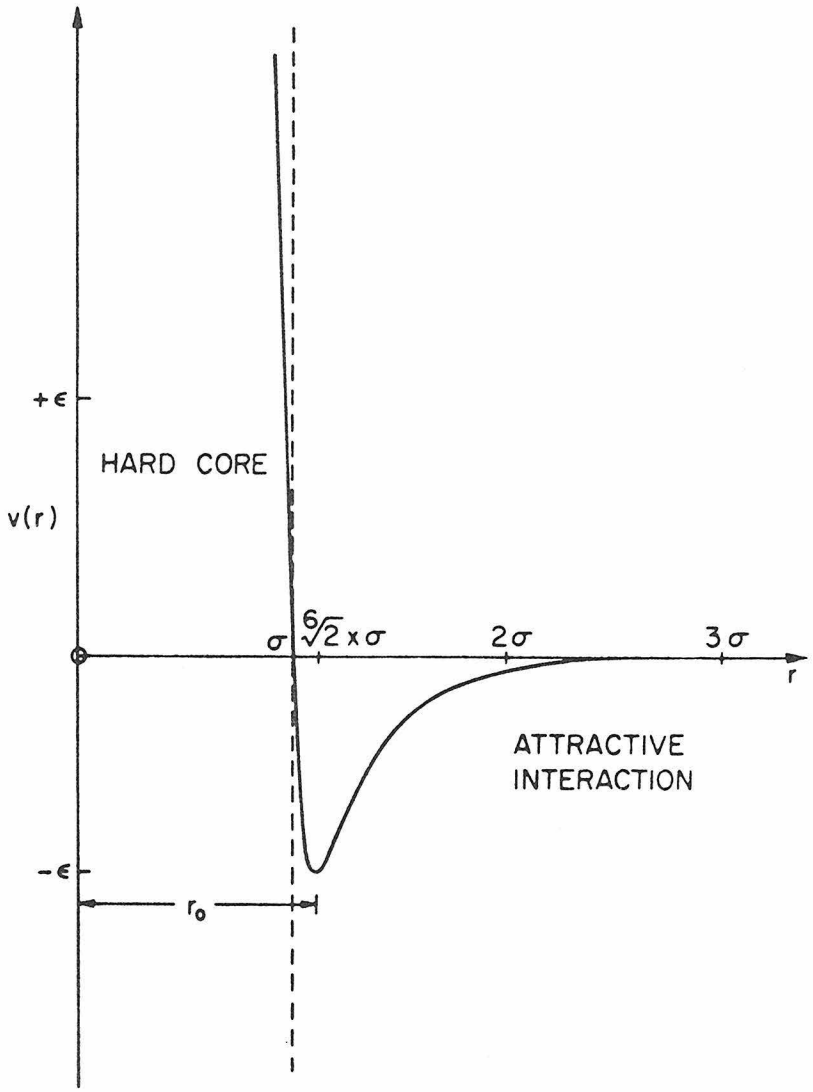

Figure 1. Lennard Jones 6-12 potential plotted as a function of interparticle distance. Note that the hard core is defined by the separation at which the 6-12 potential becomes zero.

hydrogen, but the agreement between (d) and (e) implies that the degree of "quantumness" is not as great as for helium.

Another criterion for the onset of quantumness is the quantum parameter of De Boer (De Boer 1948, De Boer and Michels 1938)

$$\Lambda = \frac{h}{\sigma(m\epsilon)^{1/2}} \tag{7}$$

For $\Lambda << 1$ quantum effects are negligible, i.e., m is large and/or the interaction is not weak. For $\Lambda > 1$ quantum effects play a dominant role (Krumhansl and Wu 1972, Wu 1967). Figure 2 shows a plot of the rare gas solids plus hydrogen which delineates the quantum and nonquantum regions. Hydrogen lies inside the quantum envelope, but not nearly so far as helium, i.e., its properties are more classical than those of helium. As a substance is compressed, the criterion (7) no longer applies and ϵ must be interpreted to be the kinetic energy of relative motion (De Boer and Michels 1938). This will increase upon compression of the solid and should lead to a region of nonquantum behavior in solid hydrogen. The calculations in Chapter III suggest that this region is attained rather quickly for solid hydrogen, since the calculations agree well with experiment above pressures of 3-5 kbar.

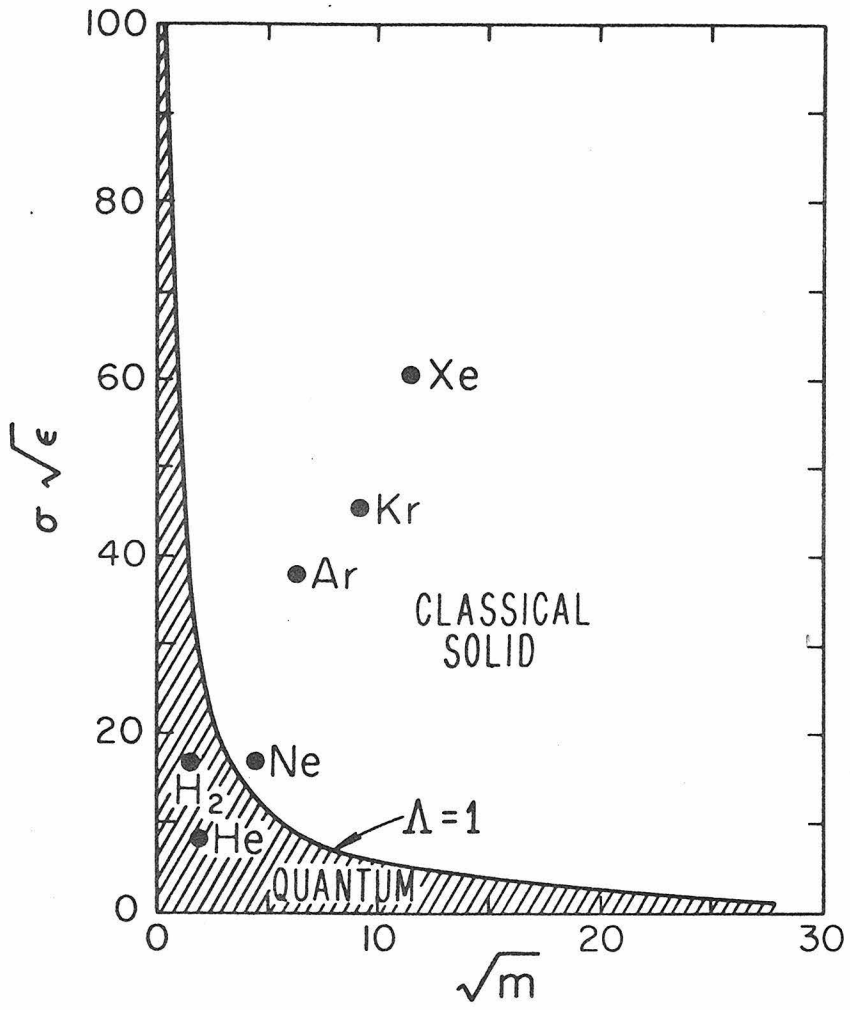

Figure 2. The quantum parameter. The cross hatched region corresponds to values of the quantum parameter > 1. Solids which plot in this region exhibit quantum behavior (modified from Guyer, 1969).

TABLE I

Parameters for Solid Gas Crystals[†]

Element	(a) m, mass (amu)	(b) ε (^{o}K)	(c) σ (Å)	(d) r_o (Å)	(e) Δ (Å)	(f) $\langle u^2 \rangle_D^{1/2}$ (Å)	(g) Θ_D (^{o}K)
Helium	4	10.2	2.59	2.86	3.77	0.82	18
Hydrogen	2	37.0	2.93	3.29	3.17	0.46	128
Neon	20	36.3	2.82	3.16	3.16	0.27	65
Argon	40	119.3	3.45	3.87	3.76	0.16	93
Krypton	84	159.0	3.60	4.46	3.87	0.11	55
Xenon	131	228.0	397	4.04	3.99	0.13	72

1) Data on rare gases from Guyer (1969)

2) Data on hydrogen from Hirschfelder et al. (1954)

[†]Column (a) mass; (b) strength of potential, well depth; (c) hard core or interaction length; (d) distance to potential minimum; (e) experimental nearest neighbor distance; (f) rms displacement calculated from Θ_D; (g) Debye temperature (for hydrogen Θ_D is from Ahlers 1963).

G. Chapter III, Appendix II

In a quantum crystal the zero point motion of an atom or molecule about its equilibrium position is a large fraction of the nearest neighbor distance. Alternatively, a quantum crystal can be defined as one in which the zero point energy comprises a substantial fraction of the total internal energy. The failure of liquid helium to solidify under its own vapor pressure at any temperature is the best known example of a material whose properties are determined by a large zero point energy.

At 4^{o}K helium requires a pressure of 143 bars to solidify. To describe the properties of such a solid, the conventional lattice dynamic approach (Born and Huang 1954, Liebfreid and Ludwig 1961) does not work since these theories assume <u>small</u> displacements from equilibrium. A different theoretical approach had to be discovered which would allow large departures from the equilibrium separation of constituent atoms in the solid. Such a framework has been developing since the publication of Bernardes' (1958,1960) and Nosanow's (1966) theories of quantum crystals.

For a system of particles interacting with two body forces, the Hamiltonian is

$$\hat{H} = -\frac{\hbar^2}{2m} \sum_i \nabla_i^2 + \sum_{i<j} v(r_{ij}) \qquad (1)$$

where $\underline{r}_i$ denotes position of i^{th} particle

$r_{ij} = |\underline{r}_i - \underline{r}_j|$ is the distance between particles i and j

$v(r_{ij})$ = interaction potential between particles i and j .

Denote by Ψ the unsymmetrized ground state wave function describing the N particles in the system, which satisfies

$$\hat{H}\Psi = E_o\Psi \tag{2}$$

Then an upper bound for E_0 is

$$E_o = \frac{\int \Psi^* \hat{H} \Psi \, d\tau}{\int \Psi^* \Psi \, d\tau} \tag{3}$$

Since particles in the system being described must be at least a distance equal to their hard core away from each other, the motion of a particle and its neighbor is correlated. Such correlations are essential to the correct description of a quantum solid.

In a non-quantum crystal, it is possible to write a wave function which describes the system as the product of one-particle wave functions ϕ .

$$\Psi_{\substack{\text{NON} \\ \text{QUANTUM}}} = \prod_i \phi(r_i) \tag{4}$$

Such a wave function works well as long as the particles in the system being considered are well localized. However, for a quantum crystal, the particles are not well localized, and an effort must be made to explicitly keep the particles apart at small separations, which is the same as requiring the total wavefunction to explicitly include correlated motions.

This is generally accomplished by multiplying $\psi_{nonquantum}$ by a function (f) which will become very small (vanish) when one particle lies inside another's hard core, and which leaves the wave function unaffected for large separations. Additionally the function f should not give ψ the property that particles have a larger probability of being far apart than of being at the interaction potential minimum.

Under the assumption that two particles in a quantum crystal interact via a Lennard-Jones 6-12 type potential, these conditions may be written as

$$f(r) \sim \exp(-\text{CONSTANT}/r^5) \qquad r \ll \sigma \tag{5a}$$

$$f(r) \sim \text{Constant} \qquad r \gtrsim r_{\text{NEAREST NEIGHBOR}} \tag{5b}$$

$$f(r_{MIN}) \geq f(\infty) \tag{5c}$$

Nosanow (1966) proposed the following function to satisfy the conditions 5a,b,c:

$$f(r) = \exp[-K\eta(r)] \tag{6}$$

where K can be used as a variational parameter

$$\eta(r) = (\sigma/r)^{12} - (\sigma/r)^6$$

σ = van der Waals hard core.

Actually, equation (6) does not satisfy all the above conditions on the

function f from $r = 0$ to $r = \infty$. It obviously does not satisfy (5a), however in the region near $r \simeq r_{\substack{\text{nearest} \\ \text{neighbor}}}$, (5a) does not apply. Since there is no simple analytic form which has all the correct properties, Nosanow chose (6) as a good compromise, and proposed that a suitable wave function for solid helium would be written as (Jastrow 1955):

$$\Psi = \prod_i \phi_i(|\underline{r}_i - \underline{R}_i|) \prod_{i<j} f(r_{ij}) \tag{7}$$

where ϕ_i is a single particle wave function centered on the i^{th} lattice site,

$|\underline{r}_i - \underline{R}_i|$ is the distance from the i^{th} particle to the i^{th} lattice site at $\underline{R}_i$, and

$f(r_{ij})$ is a pair correlation function which describes the effects of correlation between two particles, i and j.

Correlations between closely approaching particles are referred to as short range correlations. They play an essential role in determining the properties of all hard core systems, e.g., liquid helium, nuclear matter, quantum solids, etc. (Bruckner 1959). Substitution of (7) into (3) yields a ground state energy:

$$E_o = \frac{\left\{ \sum_i (\Psi, P_i \Psi) + \sum_{i<j} (\Psi, V_{ij} \Psi) \right\}}{(\Psi, \Psi)} \tag{8}$$

where

$$P_i = -\frac{\hbar^2}{2m\phi_i^2} \left(\phi_i \nabla_i^2 \phi_i - \nabla_i \phi_i \cdot \nabla_i \phi_i \right) \tag{9a}$$

$$V_{ij} = v_{ij} - \frac{\hbar^2}{2m f_{ij}^2} \left(f_{ij} \nabla_i^2 f_{ij} - \nabla_i f_{ij} \cdot \nabla_i f_{ij} \right) \tag{9b}$$

Where V_{ij} and f_{ij} are the matrix elements between ϕ_i and ϕ_j.

The second term in (9b) is due to the effects of correlation

Expanding equation (8)

$$E_0 = \left\{ \sum_i \langle P_i \rangle + \tfrac{1}{2} \sum_{i<j} \left(\langle V_{ij} f_{ij}^2 \rangle / \langle f_{ij}^2 \rangle \right) \right\}$$

$$+ \left\{ \sum_{ij} \left[\langle P_i f_{ij}^2 \rangle / \langle f_{ij}^2 \rangle - \langle P_i \rangle \right] \right.$$

$$+ \tfrac{1}{2} \sum_{ijk} \left[\langle V_{ij} f_{ij}^2 f_{ik}^2 f_{jk}^2 \rangle / \langle f_{ij}^2 f_{ik}^2 f_{jk}^2 \rangle \right.$$

$$\left. \left. - \langle V_{ij} f_{ij}^2 \rangle / \langle f_{ij}^2 \rangle \right] \right\}$$

$$+ \ldots \tag{10}$$

where

$$\langle A(\underline{r}_1, \ldots, \underline{r}_N) \rangle = \int d\underline{r}_1 \, \phi_1^2 \int d\underline{r}_2 \, \phi_2^2 \cdots \int d\underline{r}_N \, \phi_N^2 A(\underline{r}_1, \ldots \underline{r}_N) \tag{11}$$

In practice only the first term in (10) is kept and the assumption is made that all other terms are negligible (Krumhansl and Wu 1972)

$$E_o = \sum_i \langle P_i \rangle + \tfrac{1}{2} \sum_{ij}{}' \langle V_{ij} f_{ij}^2 \rangle / \langle f_{ij}^2 \rangle$$

$$= -\frac{\hbar^2}{2m} \sum_i \int d\underline{r}_i \, \phi_i \nabla_i^2 \phi_i$$

$$+ \tfrac{1}{2} \sum_{ij}{}' \left(\frac{\int d\underline{r}_i \int d\underline{r}_j \, \phi_i^2 \phi_j^2 f_{ij}^2 V_{ij}}{\left(\int d\underline{r}_i \int d\underline{r}_j \, \phi_i^2 \phi_j^2 f_{ij}^2 \right)} \right) \qquad (12)$$

Nosanow (1964) found that for solid helium, the single particle wave functions could be well approximated by a Gaussian

$$\phi(r) \sim \exp(-B r^2) \qquad (13)$$

where B = a constant.

Wu (1967) and Krumhansl and Wu (1972) used the forms (13) and (6) in an effort to apply this formalism to solid hydrogen. They found that the method failed at high densities due to the presence of a constant σ in the form of the correlation function. These authors next allowed σ to become a variable in an effort to improve agreement of a series of volumes at their theoretically calculated pressures with the measured isothermal pressures of Stewart (1956). Below volumes of $\sim$14 cc/mole their methods give consistently higher isothermal pressures than those measured by Stewart.

Other investigators (Bruce 1972, Pollack et al. 1972, Ebner and Sung 1970,1971,1972) have attempted to solve (1) using wave functions (6) under differing assumptions about the interaction potential and the form of the correlation function.

No calculated pressure versus volume relation for solid hydrogen yet published is in agreement with the Stewart isotherm.

H. References for Chapter III

1. Ahlers, G., "Some Properties of Solid Hydrogen at Small Molar Volumes", UCRL Report 10757 (1963).
2. Alder, B. J., in Progress in Very High Pressure Research, edited by F. P. Bundy, W. R. Hibbard, H. M. Strong (Wiley & Sons, New) York, 1961).
3. Ashcroft, N. W., Phys. Rev. Lett. 21, 1748 (1968).
4. Bernardes, N., Phys. Rev. 112, 1534 (1958).
5. Bernardes, N., Phys. Rev. 120, 807 (1960).
6. Bezuglyi, P. A. and R. K. Minyafaev, Sov. Phys. Sol. St. 9, 480 (1967).
7. Born, M. and K. Huang, Dynamical Theory of Crystal Lattices (Oxford University Press, 1954).
8. Bruce, T. A., Phys. Rev. B5, 4170 (1972).
9. Bruckner, K. A., Many Body Problems (Wiley & Sons, N.Y., 1959).
10. De Boer, J., Physica 9, 363 (1942).
11. De Boer, J., Physica 14, 139 (1948).
12. De Boer, J. and B. S. Blaisse, Physica 14, 149 (1948).
13. De Boer, J. and A. Michels, Physica 5, 945 (1938).
14. De Marcus, W. C., A.J. 63, 1255 (1958).
15. Dynin, E. A., Sov. Phys. Sol. St. 13, 2089 (1972).
16. Ebner, C. and C. C. Sung, Sol. St. Comm. 8, 1903 (1970).
17. Ebner, C. and C. C. Sung, Phys. Rev. B4, 2638 (1971).
18. Ebner, C. and C. C. Sung, Sol. St. Comm. 11, 489 (1972).

19. Evett, A. A. and H. Margenau, J. Chem. Phys. 21, 958 (1953a).

20. Evett, A. A. and H. Margenau, Phys. Rev. 90, 1021 (1953).

21. Fowler, R. H., Statistical Mechanics, second edition (Cambridge Press, 1936).

22. Ginzberg, V. L., Sov. Phys. Usp. 12, 241 (1969).

23. Grigoriev, F. V., S. B. Kormer, O. L. Mikhailova, A. P. Tolochko, V. D. Urlin, JETP 5, 288 (1972).

24. Guyer, R. A., Sol. St. Phys. 23, 413 (1969).

25. Hawke, R. S., D. E. Duerre, J. G. Huebel, R. N. Keeler, H. Klapper, PEPI 6, 44 (1973).

26. Herzfeld, K. F. and M. G. Mayer, Phys. Rev. 46, 995 (1934).

27. Hill, R. W. and O. V. Lounasmaa, Phil. Mag. 4, 785 (1959).

28. Hirschfelder, J. O., C. F. Curtiss, R. B. Bird, Molecular Theory of Gases and Liquids (Wiley & Sons, N.Y., 1954).

29. Holt, A. C. and M. Ross, Phys. Rev. B1, 2700 (1970).

30. Hubbard, W. B., Ap. J. 152, 745 (1968).

31. Hubbard, W. B., Ap. J. 155, 333 (1969).

32. Hubbard, W. B., Ap. J. 162, 687 (1970).

33. Jastrow, R., Phys. Rev. 98, 1479 (1955).

34. Kronig, R., J. De Boer, J. Korringa, Physica 12, 245 (1946).

35. Krumhansl, J. A. and S. Wu, Phys. Lett. 28A, 263 (1968).

36. Krumhansl, J. A. and S. Wu, Phys. Rev. B5, 4155 (1972).

37. Kopyshev, V. P., Dok. Sov. Phys. 10, 338 (1965).

38. Lagus, P. L. and T. J. Ahrens, in press (1973).

39. Latter, R., J. Chem. Phys. 24, 280 (1956).

40. Liebfreid, G. and W. Ludwig, Sol. St. Phys. 12, 275 (1961).

41. Margenau, H., Phys. Rev. 64, 131 (1943).

42. Margenau, H. and N. R. Kestner, Theory of Intermolecular Forces (Pergamon Press, Elmsford, N.Y., 1971)

43. Mason, E. A., J. O. Hirschfelder, J. Chem. Phys. 26, 756 (1957).

44. Megaw, H., Phil. Mag. 28, 129 (1939).

45. Meyer, L., Adv. in Chem. Phys. 16, 343 (1969).

46. Mills, R. L. and A. F. Schuch, Phys. Rev. Lett. 15, 722 (1965).

47. Neece, G. A., F. J. Rogers, W. G. Hoover, J. Comp. Phys. 7, 621 (1971).

48. Nosanow, L. H., Phys. Rev. Lett. 13, 270 (1964).

49. Nosanow, L. H., Phys. Rev. 146, 120 (1966).

50. Pauling, L., Phys. Rev. 36, 430 (1930).

51. Peebles, P.J.E., Ap. J. 140, 328 (1964).

52. Pollack, E. L., T. A. Bruce, G. V. Chester, J. A. Krumhansl, Phys. Rev. B5, 4180 (1972).

53. Raich, J. C., R. D. Etters, J. Low Temp. Phys. 6, 229 (1972).

54. Sammis, C. G., "Seismological Applications of Lattice Theory", Ph.D. dissertation, California Institute of Technology, 1971.

55. Seitz, T., Modern Theory of Solids (McGraw-Hill Book Co., New York, 1940).

56. Stewart, J. W., J. Phys. Chem. Solids 1, 146 (1956).

57. Stewart, J. W., J. Phys. Chem. Solids 29, 641 (1968).

58. Trubitsyn, V. P., Sov. Phys. Sol. St. 7, 2708 (1966a).

59. Trubitsyn, V. P., Sov. Phys. Sol. St. 8, 688 (1966b).

60. Tosi, M., T. Arai, Adv. in High Pressure Res. 1, 265 (1966).

61. van Thiel, M. and B. J. Alder, J. Chem. Phys. 44, 1056 (1966).

62. Walsh, J. M. and R. H. Christian, Phys. Rev. 97, 1544 (1955).

63. Wigner, E. and H. B. Huntington, J. Chem. Phys. 3, 764 (1935).

64. Wu, S., "A Quantum Theory of Equation of State for Solid Hydrogen", Ph.D. Dissertation, Cornell University, 1967.

65. Zubarev, V. N. and G. S. Telegin, Sov. Phys. Dok. 7, 34 (1962).

CHAPTER IV

THERMALLY EXPANDED MODELS OF THE JOVIAN INTERIOR

A. Introduction

One method available for inferring gross internal structure of a planetary-sized body is through the construction of model planets. Generally, a suite of elements and phases are chosen on the basis of cosmic or terrestrial elemental abundances. The appropriate equations of state or their combination give a relation between density, pressure and temperature. In describing planetary-sized objects, usually it is first assumed that the temperature is $0^{o}K$ so that density is a function of pressure only. The assumption of hydrostaticity is made, and the equations of hydrostatic equilibrium are integrated. A suitable model is obtained when the calculated mass and radius match the known mass and radius of the planet. Should some of the moments in the expansion of the planet's gravitational field be known (from direct observations of ellipticity and/or the motion of satellites around the planet) these may be used to differentiate amongst a larger class of models which match the mass and radius. Later on, corrections for a temperature gradient can be introduced. Such corrections, for the largely fluid planets, require a knowledge of the surface, or atmosphere temperature, and some information about the mechanism of internal heat transport and heat sources within the planet.

Countless models for the interior of Jupiter have been proposed. The models are simplified by the observation that Jupiter is probably of solar composition and thus primary constituents are the elements hydrogen and helium. Since it is possible to calculate theoretical equations of state for these elements more reliably than for

more complex elements and compounds (Neece et al. 1971, Trubitsyn 1962, 1966a,b, Dynin 1972, Lagus 1973), this offsets somewhat the lack of direct knowledge about internal properties. A minor complication is the existence of a phase change in hydrogen from the molecular to the metallic phase at a pressure whose exact value is unknown, but is thought to be on the order of 2 Mbar. (A similar phase change in He is thought to occur at pressures greater than those present in Jupiter.)

Previous studies (DeMarcus 1958, Peebles 1964, Hubbard 1968, 1969, 1970) have shown that temperature effects are important in Jupiter, and have focused on the hydrogen abundance implied by various proposed equations of state for the metallic phase.

This section is an attempt to construct a model of the interior of Jupiter incorporating recently improved theoretical equations of state for metallic and molecular hydrogen, a realistic equation for helium and a Van der Waals atmosphere.

B. Theory of Model Planet Calculations

Following Peebles (1964), a surface of constant density can be represented by

$$r = s\left[1 + \epsilon_2(s) P_2(\cos\theta) + \epsilon_4(s) P_4(\cos\theta)\right] \qquad (1)$$

where s labels the surfaces of constant density. The "jovipotential" (gravitational plus centrifugal) can be expressed in terms of $\epsilon_2(s)$, $\epsilon_4(s)$ and the density $\rho(s)$ (Jeffries 1962) (see Appendix I). By requiring this total potential to be constant on surfaces of the form (1), integral equations for $\epsilon_2(s)$ and $\epsilon_4(s)$ are then obtained.

Integration of the equation of hydrostatic equilibrium determines the density necessary to evaluate $\varepsilon_2(s)$ and $\varepsilon_4(s)$ (see Table I).

Note that in formula (IV) the first derivative under the integral sign is given incorrectly as $d/da\,[a^7\varepsilon_2(a)]$ in Peebles' paper.

The gravitational moments J and K are defined by the multipole expansion of the gravitational field outside the planet and are determined by the condition that the sum of the gravitational potential and the centrifugal potential be constant on the surface of the planet. (see Table II). These coefficients are sensitive to the near surface density distribution of the planet. The moment K may be considered to be a measure of the density at more shallow levels than is the case for J. This can be seen by examining the expressions for ε_2 and ε_4. A given mass, distributed uniformly over a surface characterized by given values of ε_2 and ε_4 can contribute more effectively to the asymmetric part of the gravitational field, the further the shell is from the center of the planet. If the density of the planet were constant, ε_2 would be equal to -0.07 (Peebles 1964), independent of radius. If most of the mass of the planet were concentrated near the center, ε_2 would be equal to -0.028 at the surface and would decrease as the cube of the distance to the center of the planet.

Upon integration of the hydrostatic equations an assumption must be made concerning the manner in which the constituent elements (equations of state) mix. Commonly ideal mixing is assumed:

Table I

Formulae For Determining ϵ_2 and ϵ_4

$$M(s) = 4\pi \int_0^s \rho(a)\, a^2\, da \qquad (I)$$

$$\frac{dP}{ds} = -\frac{G\rho(s)M(s)}{s^2} + \frac{2}{3}\omega^2 s\rho(s) \qquad (II)$$

$$\epsilon_2(s) = -\frac{\omega^2 s^3}{3GM(s)}\left[1 - \frac{10}{7}\epsilon_2(s)\right] + \frac{2}{7}\epsilon_2^2(s) +$$

$$\frac{4\pi}{5M(s)s^2}\left[1 - \frac{6}{7}\epsilon_2(s)\right]\int_0^s \rho(a)\frac{d}{da}\left\{a^5\left[\epsilon_2(a) + \frac{4}{7}\epsilon_2^2(a)\right]\right\}da$$

$$+\frac{4\pi s^3}{5M(s)}\left[1 + \frac{4}{7}\epsilon_2(s)\right]\int_s^{\bar{s}} \rho(a)\frac{d}{da}\left[\epsilon_2(a) - \frac{1}{7}\epsilon_2^2(a)\right]da \qquad (III)$$

$$\epsilon_4(s) = \epsilon_4^{(0)}(s) + \frac{4\pi}{9M(s)}\left\{\frac{1}{s^4}\int_0^s \rho(a)\frac{d}{da}\left[a^7\epsilon_4(a)\right]da\right.$$

$$\left. + s^5\int_s^{\bar{s}} \rho(a)\frac{d}{da}\left[\frac{\epsilon_4(a)}{a^2}\right]da\right\} \qquad (IV)$$

$$\epsilon_4^{(0)}(s) = \frac{54}{35}\epsilon_2^2(s) - \frac{72\pi\epsilon_2(s)}{35M(s)s^2}\int_0^s \rho(a)\frac{d}{da}\left[a^5\epsilon_2(a)\right]da$$

$$+\frac{24\pi}{35M(s)s^4}\int_0^s \rho(a)\frac{d}{da}\left[a^7\epsilon_2^2(a)\right]da \qquad (V)$$

$$-\frac{12\pi s^5}{35M(s)}\int_s^{\bar{s}} \rho(a)\frac{d}{da}\left[\frac{\epsilon_2^2(a)}{a^2}\right]da$$

G	is the gravitational constant
M(s)	is the mass out to radius s
ω	is the rotational velocity
$\bar{s}$	is the value of s at the surface

Table II
Expressions for J and K

$$\phi(r,\theta) = -\frac{GM}{r}\left[1 - \frac{2}{3}J\left(\frac{Re}{r}\right)^2 P_2(\cos\theta) + \frac{4}{15}K\left(\frac{Re}{r}\right)^4 P_4(\cos\theta)\right]$$

$$J = -3/2\left\{\epsilon_2(\bar{s}) + \frac{\omega^2\bar{s}^3}{3GM}\left[1 - \frac{10}{7}\epsilon_2(\bar{s})\right] - \frac{2}{7}\epsilon_2^2(\bar{s})\right\}\left[1 + \frac{13}{7}\epsilon_2(\bar{s})\right]$$

$$K = \frac{5\pi}{3M\bar{s}^4}\int_0^{\bar{s}} \rho(a)\frac{d}{da}\left[a^7\left(\epsilon_4(a) + \frac{54}{35}\epsilon_2^2(a)\right]da\right.$$

R_e=equatorial radius
M=total mass
s =value of s at surface

$$\frac{1}{\rho} = \frac{x}{\rho_H} + \frac{y}{\rho_{He}} \qquad (2a)$$

$$x + y = 1 \qquad (2b)$$

where ρ_H = density of hydrogen

ρ_{He} = density of helium, and

x and y are the mass abundances of hydrogen and helium.

This equation is valid for immiscible fluids and also for mixtures of ideal gases. Recently, Hubbard (1973) has undertaken calculations which indicate that equation (2a) is obeyed under Jupiter-like conditions to within 10%.

A model of Jupiter with roughly solar composition ($x \sim 0.6$, $y \sim 0.4$, Aller 1961) implies that $x \sim 2y$. Since helium is at least three times as dense as hydrogen, the helium term in (2a) is $\sim$15% of the hydrogen term. Thus, uncertainty in the hydrogen equation of state reflects itself as the dominant uncertainty in the model.

In model planet calculations, the equation of hydrostatic equilibrium is integrated utilizing (2a) to incorporate the forms for the various equations of state. The relative abundance of hydrogen to helium is varied until the mass and radius are matched. It is possible to obtain a large variety of models in this manner (depending on equations of state used, atmosphere, and assumptions about homogeneity or non-homogeneity). Calculation of J and K allows a further differentiation between models (see Table III). Care must be exercised, however, in interpretation of the resultant fit to the observational data, due to the fact that the two operations (1) matching mass and

TABLE III

Physical Characteristics of Jupiter

(Brouwer and Clemence 1961)

Mass	1.902×10^{30} gm
Equatorial Radius	7.14×10^{4} km
Oblateness	0.065
J	0.02206 ± 0.00022
K	0.0025 ± 0.0014

Note that J determined from Galilean Satellites (De Sitter 1931)
K determined from Jupiter V

radius, (2) matching gravitational moments) are sensitive to somewhat different regions within Jupiter. The abundance of hydrogen (and hence the mass and radius) in Jupiter is determined primarily by the equation of state of the metallic phase of hydrogen. J and K, on the other hand, are affected by the outer layers comprised of molecular hydrogen and the atmosphere. Thus, model planet calculations must pay close attention to all three regions.

C. Previous Work

An exhaustive study of the structure of a cold ($T = 0^{o}K$) Jupiter was published by De Marcus in 1958. He calculated the equation of state for metallic hydrogen using the methods of Wigner and Huntington (1935) and obtained an equation of state for molecular hydrogen and helium by extrapolating extant isothermal compression data (in an arbitrary "eyeball" manner). Helium abundance was taken to be zero in the isothermal atmosphere (extending to $\sim$1% below the surface) gradually increasing to 27% near the center. To match the mass and radius a small helium core ($\sim$ 2% the mass of Jupiter)was added. Satisfactory agreement with the gravitational J and K could only be obtained, however, by assuming that the isothermal compression data overestimated the density by $\sim$2% at the highest pressure ($\sim$20 kbar). De Marcus found a hydrogen abundance of $x \sim 0.78$ and was able to demonstrate that the hydrogen abundance was quite stable with respect to small changes in the model.

Peebles (1969) developed the De Marcus models further by investigating the effects of an adiabatic atmosphere on the J and K

moments and found that satisfactory agreement with the observed J and K could be obtained if ideal mixing of hydrogen and helium in the entire planet (outside a small core) and a deep adiabatic atmosphere were assumed. He explicitly demonstrated the effect of the atmosphere on the calculated values of J and K and fixed the base of the Jovian atmosphere at $\sim$6% of the radius of Jupiter below the visible surface (corresponding to a pressure of 2×10^5 atmospheres). On the basis of an adiabatic atmosphere, assuming a constant ratio of specific heats, he found a temperature of 2000^{o}K at the base of the atmosphere. The calculated hydrogen abundance was in substantial agreement with the De Marcus value ($x \sim 0.76$).

Motivated by observations that Jupiter emits about 2.7 times more radiation than it receives from the sun (Low 1966, Aumann et al. 1969), Hubbard undertook a series of model planet calculations (Hubbard 1968,1969,1970) which explicitly included thermal effects in the molecular and metallic parts of the planet. Initially he adopted the De Marcus (1958) cold metallic hydrogen equation of state for his model, but discarded this in later papers for more sophisticated forms. Hubbard points out that raising the internal temperature of Jupiter has the effect of increasing the amount of helium in the planet. This causes the high density central core of De Marcus and Peebles to disappear. Complete mixing is assumed throughout the interior. Properties of the Hubbard models are given in Table IV.

The trend apparent in model planet calculations for Jupiter has been in the increasing awareness of the importance of temperature in the calculation of models of the Jovian interior. However, in the region

TABLE IV

Characteristics of Hubbard Jupiter Models

Equation of State	Jupiter (1968)	J7 (1969)	J8 (1970)
Helium	De Marcus (1958)	Salpeter & Zapolski (1967)	Salpeter & Zapolski (1967)
Metallic Hydrogen	De Marcus (1958)	Salpeter & Zapolski (1967)	Salpeter & Zapolski (1967)
Molecular Hydrogen	De Marcus (1958)	De Marcus (1958)	De Marcus (1958)
X	0.76	0.56	0.66
Central Temperature (^{o}K)	9350	14,000	7300

where thermal effects are largest (molecular phase of hydrogen and the atmosphere) the form of the equation of state used is the least precise. The models proposed all cite agreement with observed J and K values, but these cannot be too convincing in light of the essentially ad hoc treatment of the outer layers.

D. The Equations of State: The Model

Neece et al. (1971) have proposed a very complete equation of state for metallic hydrogen. They solve the Schrödinger equation by a Hartree-Fock method and include a term to account for lattice structure. Comparison of their calculational technique with experimental data for Li and Na yields excellent agreement. Such a comparison has not been attempted by authors of other EOS for metallic hydrogen.

Trubitsyn (1966a) and Dynin (1972) have also proposed metallic equations of state. Initially cold ($0^{o}K$) models were calculated and indicated little difference in models obtained with any of the three proposed metals. Since the Neece et al. (1971) technique has been compared with experiment, it was adopted in the remainder of the calculations (see Fig. 1).

Lagus (1973) has proposed an equation of state for molecular hydrogen based on the spherically averaged de Boer interaction potential of Trubitsyn (1966a). The equation has, in contrast to earlier proposed theoretical equations of state, successfully reproduced the $4^{o}K$ isotherm of solid hydrogen to 20 kbar (Stewart 1956). (See Fig. 2; the De Marcus equation of state is shown for comparison). The Neece et al. metallic equation of state and the Lagus molecular

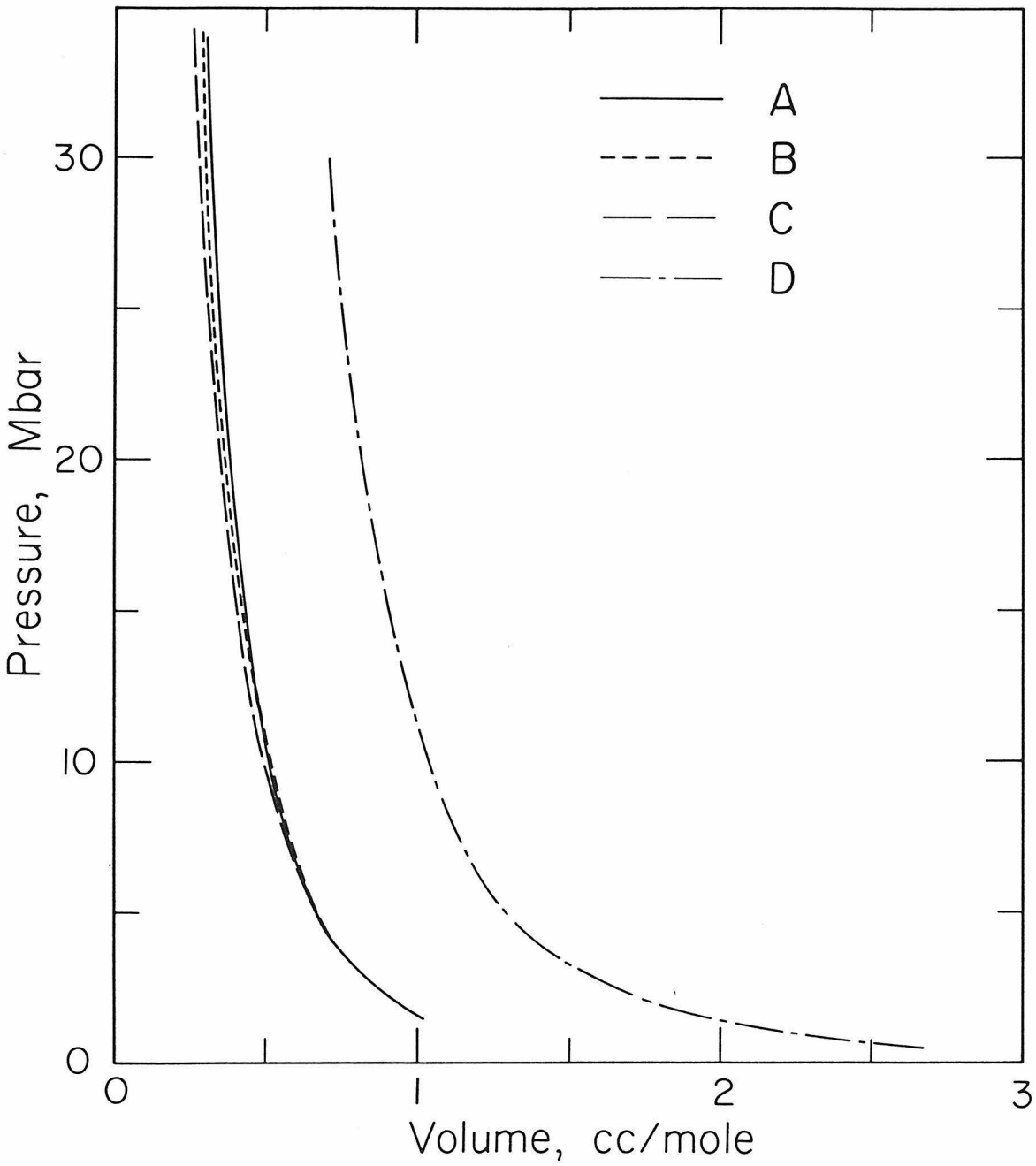

Figure 1. 0°K isentropes for metallic hydrogen (Curve A; Neece et al. (1971), Curve B; Trubitsyn (1966a), Curve C; Dynin (1972) and helium (Curve D; Trubitsyn, 1971).

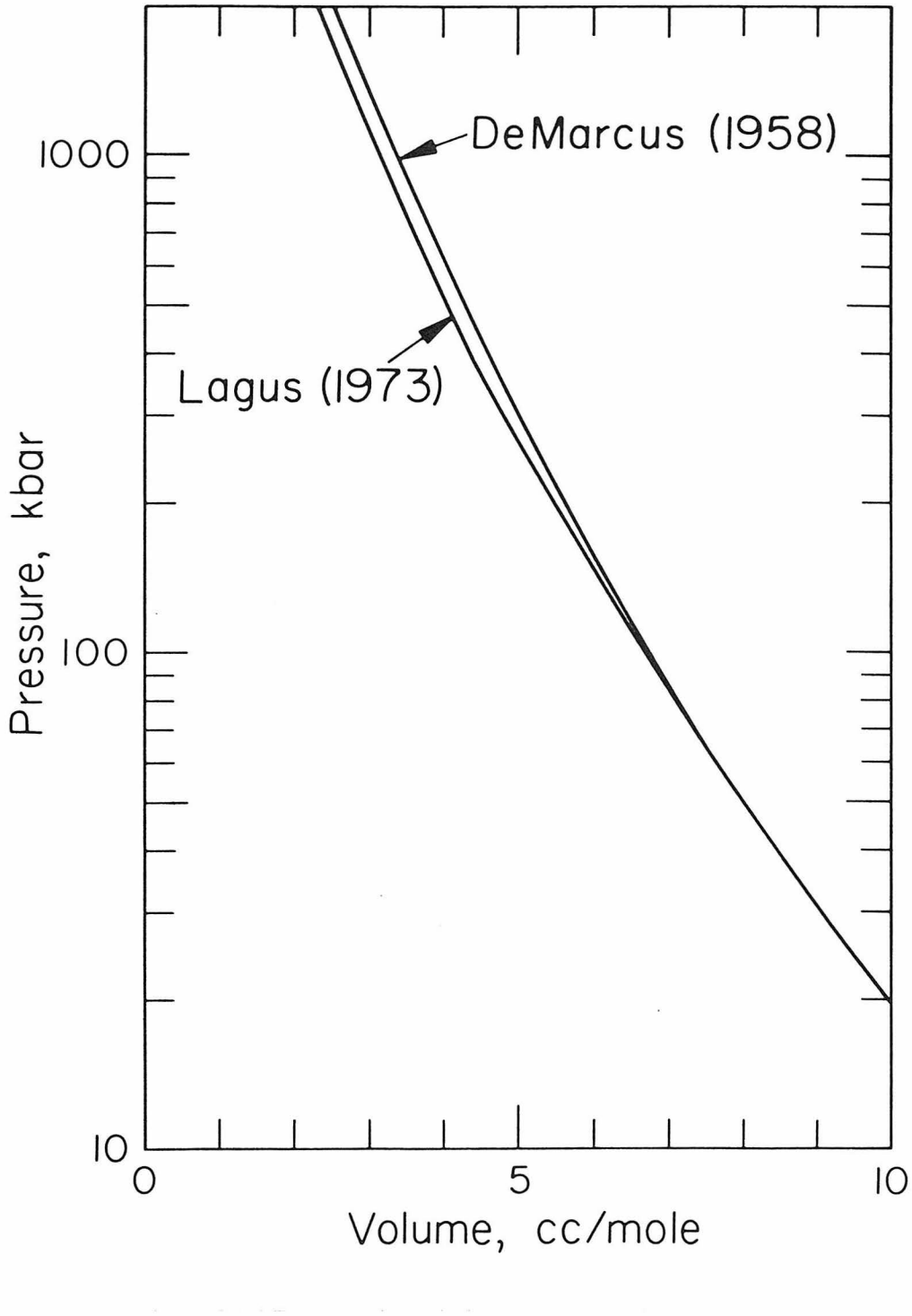

Figure 2. Extrapolation of 0°K isotherm of molecular hydrogen. Present extrapolation utilizes Lagus analytical form for the equation of state; DeMarcus' extrapolation was more arbitrary.

equation of state, taken together imply a transition pressure of 2.3 Mbar. This is the value adopted in the model calculations.

An equation of state for helium has been proposed by Trubitsyn (1971) which reproduces the Stewart (1956) isothermal compression measurements (see Fig. 1). Helium is conjectured to undergo a phase transition to the metallic state at a pressure of 90 Mbar. Since the central pressure of Jupiter is $\sim$30 Mbar, this transition is ignored.

The equations of state proposed are cold (0^{o}K) compression curves. Since the object is to calculate thermally expanded Jupiter models, a technique for doing this is required.

Solid molecular hydrogen appears to behave as a Debye solid at low temperatures and pressures (Ahlers 1963). Nothing is known about the thermal properties of the metallic phase of hydrogen, but since a Debye model describes the thermal properties of metals reasonably well, it is adopted here to provide the thermal contribution to the total pressure.

It is easily shown that

$$P_{TOT}(V) = P(V) + 3N\mathcal{D}kT\frac{\gamma}{V}D\left(\frac{\Theta_D}{T}\right) \qquad (3)$$

where $P(V)$ = cold compression curve

N = number of molecules

$\mathcal{D}$ = number of atoms in molecule

Θ_D = Debye temperature

γ = Gruneisen parameter

V = volume

$D(\frac{\Theta_D}{T})$ = Debye function

Hubbard makes the apparently valid assumption that throughout the metallic phase this relation is at its high pressure- high temperature limit. In the molecular phase, however, he abandons this relationship entirely due to a lack of an acceptable equation of state for the molecular phase.

For molecular hydrogen, the Gruneisen parameter γ was taken to vary as (Holt and Ross 1970)

$$\gamma = CV + \tfrac{1}{2} \tag{4}$$

Then, using the definition

$$\gamma = -\frac{d \ln \Theta_D}{d \ln V} \tag{5}$$

it is possible to derive an expression for the volume variation of the Debye temperature

$$\Theta_D = \Theta_D^* \exp\left[C(V^*-V) + \tfrac{1}{2} \ln\left(\frac{V^*}{V}\right)\right] \tag{6}$$

where Θ_D^* is evaluated at V^* (Ahlers 1963). In the metallic phase of hydrogen γ was taken to be 1/2 (Kopyshev 1965) so that

$$\Theta_D = \Theta_D^* \left(\frac{V^*}{V}\right)^{1/2} \tag{7}$$

where Θ_D^* is evaluated using the van Horn (1967) equation for a Coulomb lattice.

For helium, Trubitsyn (1967) has proposed the following forms for γ and Θ_D.

$$\gamma = 7/3$$

$$\Theta_D = 7.5 \times 10^6 \upsilon^{-7/3} \qquad (8)$$

For $p \lesssim 10^4$ bar

$$\gamma = 0.033\upsilon + 0.15\upsilon \exp[-0.1\upsilon]$$

$$\Theta_D = 3.1 \times 10^3 \exp\left[-0.033\upsilon + 1.5\exp(-0.1\upsilon)\right] \qquad (9)$$

10^4 bar $< p \lesssim 10^8$ bar

For the present these estimates for helium are accepted uncritically, as the influence of the exact form of these corrections is small.

As previously discussed, Peebles (1964) attempted to include an explicit atmosphere in his calculations. In an attempt to remove some of the arbitrariness in the treatment of the atmosphere, a van der Waals type equation of state was assumed for a mixture of hydrogen and helium. Ideally the efficacy of such an equation of state could be demonstrated by calculating an isotherm and comparing it with experimental data. Unfortunately, with the sole exception of a 30°C and a 65°C isotherm to 13 kbar (Bridgman 1924), isothermal compression data are limited to pressures of less than 2000 atmospheres (Landolt-Börnstein 1971). The Bridgman data would be extremely valuable if they were trustworthy. However, De Marcus points out that these data are in

serious conflict with other, lower pressure data which have been obtained (Michels and Goudeket 1941, Michels et al. 1959). It is not possible by any smooth extrapolation to match the high pressure Bridgman data with the lower pressure data. Thus, the only recourse is to note that the van der Waals equation is in good agreement with isothermal compression data for gases such as argon and CO_2 to specific volumes on the order of twice that of the corresponding solid phase (Hirschfelder et al. 1954).

The van der Waals equation is

$$\left(P + \frac{a}{\tilde{V}^2}\right)\left(\tilde{V} - b\right) = RT \tag{10}$$

where P = pressure

$\tilde{V}$ = molar volume

T = temperature

R = gas constant

a = constant which describes cohesion between molecules

b = measures volume of molecules.

For a mixture of van der Waals gases, Hirschfelder et al. (1954) note that

$$a = a_{11} x_1^2 + 2 a_{12} x_1 x_2 + a_{22} x_2^2$$

$$b = b_{11} x_1^2 + 2 b_{12} x_1 x_2 + b_{22} x_2^2 \tag{11}$$

where x_i = mole fraction of component i

a_{ii} = a for component i

b_{ii} = b for component i

$$a_{12} = \sqrt{a_{11} a_{22}}$$

$$\sqrt[3]{b_{12}} = \tfrac{1}{2}\left[\sqrt[3]{b_{11}} + \sqrt[3]{b_{22}}\right] \tag{12}$$

Also from Hirschfelder et al. the following properties are found:

For hydrogen

$a = 1.623 \times 10^5 \text{atm(cc/mole)}^2$

$b = 21.67$ cc/mole

For helium

$a = 2.266 \times 10^4 \text{atm(cc/mole)}^2$

$b = 19.27$ cc/mole

These allow calculation of

$b_{12} = 20.45$

$a_{12} = 6.064 \times 10^4 \text{atm(cc/mole)}^2$

Substitution of these values into equations (11) allows a value of a and b for a mixture of hydrogen and helium to be calculated.

A van der Waals adiabat can be calculated from the first law of thermodynamics.

$$T\,dS = dU + P\,dV \tag{13}$$

On an adiabat $dS = 0$, and for a van der Waals equation of state

$$dU = C_v\,dT + \frac{a}{\tilde{V}^2}\,d\tilde{V} \tag{14}$$

Then, on an adiabat

$$\frac{d\tilde{V}}{\tilde{V}-b} = -\frac{C_v}{R}\frac{dT}{T} \tag{15}$$

Since

$$C_p - C_v = -T\frac{\left(\frac{\partial P}{\partial T}\right)_v \left(\frac{\partial P}{\partial T}\right)_v}{\left(\frac{\partial P}{\partial v}\right)_T} \tag{16}$$

for a van der Waals gas

$$C_p - C_v = \frac{R}{1-Q}$$

$$Q = \frac{2a}{\tilde{V}^3}\frac{(\tilde{V}-b)^2}{RT} \tag{17}$$

In the volume and temperature range ($\tilde{V} \sim 10^5$ to 10^2cc/mole, $T \sim$ few thousand ^oK) of interest $Q \ll 1$ and hence

$$C_p - C_v \approx R \tag{18}$$

From which it follows, defining $\Gamma = C_p/C_v$, from (15)

$$T(\tilde{V}-b)^{\Gamma-1} = \text{constant} \tag{19}$$

on a van der Waals adiabat.

It was found that this equation of state could be extrapolated to pressures of $\sim 2\times 10^5$atm without being affected by the mathematical singularity in the equation. Temperatures along the van der Waals adiabat were calculated and found to be $\sim 4000^oK$ at a pressure of

2×10^5 atm. The equation of state for the atmosphere was smoothly fit to the equation of state for the molecular layer beneath it. In all cases studied, the densities of the van der Waals atmosphere and the molecular layer were comparable in order of magnitude so that the extrapolation was performed over a small range in density (see Fig. 3).

On the basis of his equation of state for metallic hydrogen, Hubbard (1970) has recently calculated an adiabatic gradient $(\frac{\partial \ln T}{\partial \ln P})_s$ throughout the entire metallic phase of ~ 0.3.

In the molecular layer, the gradient is somewhat more uncertain. Hubbard assumed a value $T = C\rho^n$ where C is a constant. He found his best model to fit $n = 0.4$, although there was little difference between $n = 0.4$ and $n = 0.5$. In his 1969 paper Hubbard assumes that $T = C\rho^{1/2}$ throughout the entire planet. This is valid in the metallic region where $\frac{\partial \ln T}{\partial \ln \rho})_s = 1/2$, but in the molecular region this assumption is poor. In fact, since $\frac{\partial \ln T}{\partial \ln \rho} = \gamma$ the assumption $T = C\rho^{1/2}$ is approached only at the highest densities (~ 0.8 gm/cm^3) achieved in the molecular layer.

The adiabatic gradient is defined as

$$\left(\frac{\partial \ln T}{\partial \ln P}\right)_s \tag{20}$$

which by identity is equal to

$$\left(\frac{\partial \ln T}{\partial \ln \rho}\right)_s \left(\frac{\partial \ln \rho}{\partial \ln P}\right)_s \tag{21}$$

Consider the following thermodynamic identity

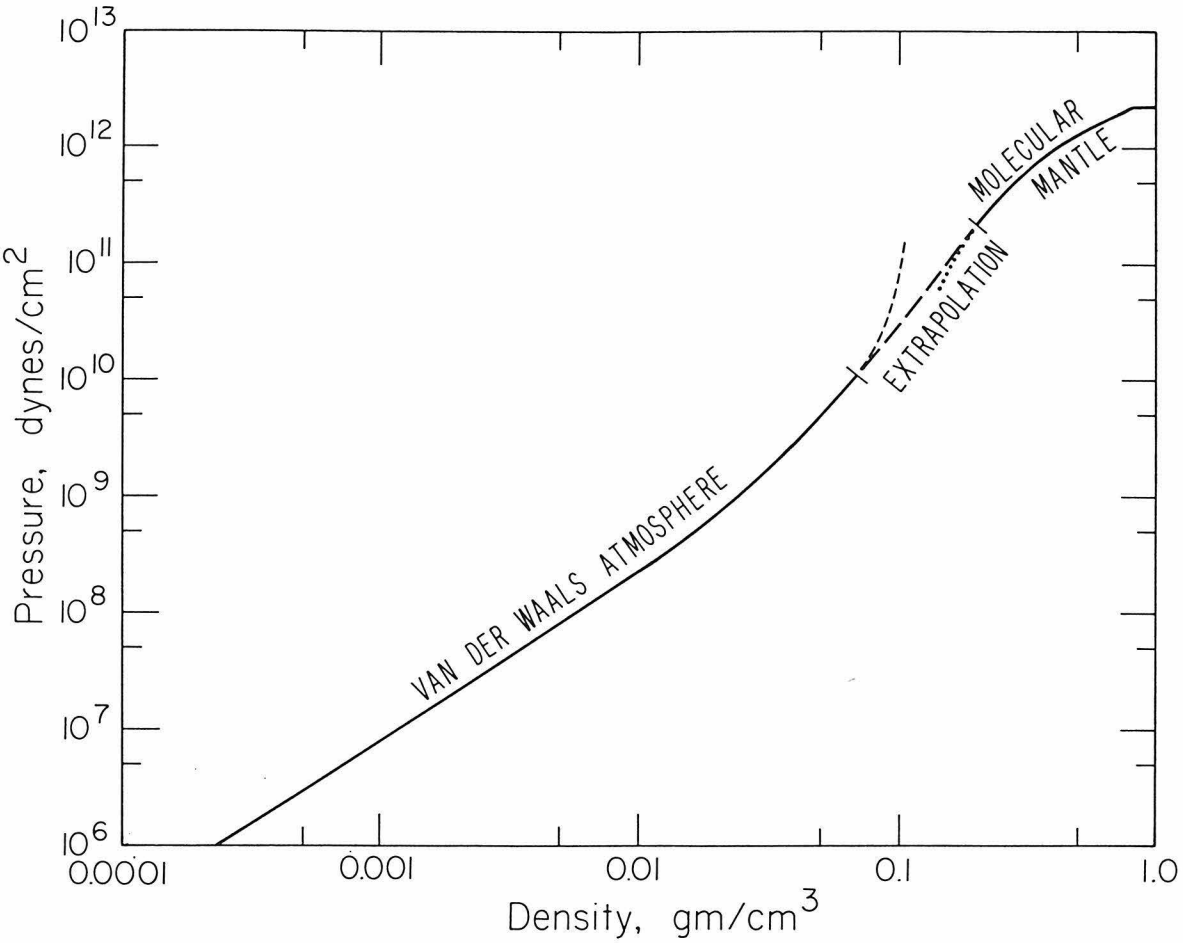

Figure 3. Pressure-density relation for adiabatic van der Waals atmosphere with x = 0.57, y = 0.43. Also shown is extrapolation to Jovian mantle.

$$T dS = C_v dT + \left(\frac{\partial P}{\partial T}\right)_v T dV \tag{22}$$

On an adiabat $dS = 0$ so that

$$\frac{dT}{T} = - \frac{\left(\frac{\partial P}{\partial T}\right)_v}{C_v} dV \tag{23}$$

Using the definition of the Gruneisen parameter

$$\gamma = V \left.\frac{\partial P}{\partial E}\right)_v = V \left.\frac{\partial P}{C_v \partial T}\right)_v \tag{24}$$

in equation (23), it follows that

$$\left.\frac{\partial \ln T}{\partial \ln \rho}\right)_s = \gamma \tag{25}$$

To evaluate the second term in equation (21), the assumption is made that the temperature dependent parts of the internal energy and pressure represent small perturbations to the total internal energy and pressure. Performing the differentiation of the equations of state for both metallic and molecular phases provides values as shown in Table V In the molecular phase a variable Gruneisen parameter (Holt and Ross 1970)

$$\gamma = CV + 1/2 \tag{26}$$

was used, while in the metallic phase a constant value (Kopyshev 1965)

$$\gamma = 1/2 \tag{27}$$

was taken. These values allowed evaluation of $\left.\frac{\partial \ell n\, T}{\partial \ell n\, P}\right)_s$ as given in

TABLE V

$\left(\frac{\partial \ln \rho}{\partial \ln P}\right)_s$ and $\left(\frac{\partial \ln T}{\partial \ln P}\right)_s$ for Hydrogen

ρ	$\left(\frac{\partial \ln \rho}{\partial \ln P}\right)_s$	$\left(\frac{\partial \ln T}{\partial \ln P}\right)_s$	ρ	$\left(\frac{\partial \ln \rho}{\partial \ln P}\right)_s$	$\left(\frac{\partial \ln T}{\partial \ln P}\right)_s$
0.36	0.30	0.28	1.0	0.31	0.15
0.49	0.34	0.28	1.5	0.38	0.19
0.70	0.43	0.31	2.0	0.42	0.21
0.80	0.49	0.34	3.0	0.45	0.22
0.94	0.64	0.43	4.0	0.46	0.23

$\left(\frac{\partial \ln T}{\partial \ln P}\right)_s = 0.3$ in Molecular Phase

$\left(\frac{\partial \ln T}{\partial \ln P}\right)_s = 0.2$ in Metallic Phase

Table V.

Taking a representative value for each phase from Table V, adiabatic indices equal to 0.3 for the molecular phase and 0.2 for the metallic phase were adopted. However, the value in the molecular phase is of dubious value, since the thermal contribution to the total pressure is not small.

The model which best fit the mass radius and gravitational moments is presented in Table VI. For the "surface" condition a temperature of 130°K at a pressure of 1 atm was assumed. Note that a model with 1 atm and 150°K "surface" condition gave almost as good a fit (J = 0.0215 and K = 0.0023).

This model is warmer than Hubbard's 1968 or 1970 model and is cooler than his 1969 model (see Fig. 4). A major shortcoming of this model is that with the high interior temperatures, hydrogen and helium are everywhere above their melting points. Thus models based on solid equations of state are inappropriate. What is significant is that with a more realistic atmosphere than that of Peebles, temperatures in an adiabatic atmosphere are higher than for Peebles' model. This can only have the effect of raising the internal temperatures and causing models based on solid equations of state to be inappropriate.

In fact, a simple calculation of the internal temperatures of Jupiter during accretion (Hanksand Anderson 1969) leads to a temperature profile intermediate between the present model and the Hubbard (1969) model. Thus, if the present adiabatic gradient is maintained by gravitational contraction of the planet (Low 1966, Smoluchowski 1967), the thermal regime presently within Jupiter could reflect the initial

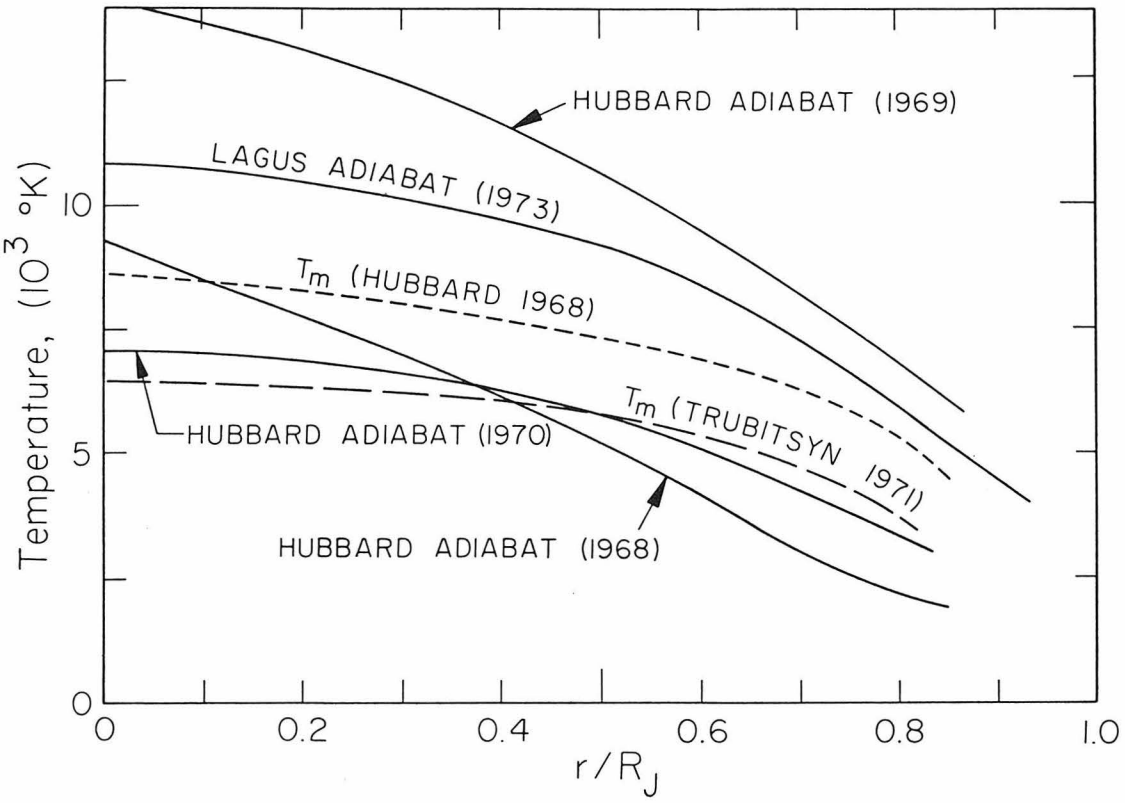

Figure 4. Proposed adiabatic temperature distributions in Jupiter. Also shown are melting curves for metallic hydrogen proposed by Hubbard (1968) and Trubitsyn (1971).

TABLE VI

Best Jupiter Model

r/R_J	T (^oK)	(g/cm^3)	P(Mbar)
0	10817	4.036	36.99
0.071	10784	4.009	36.43
.143	10685	3.928	34.80
.215	10521	3.795	32.20
.286	10288	3.611	28.80
.358	9987	3.380	24.81
.429	9610	3.109	20.47
.502	9152	2.798	16.04
.573	8606	2.456	11.79
.644	7948	2.085	7.92
.716	7142	1.685	4.64
.787	6200	1.1160	2.10
.858	5000	5.6977×10^{-1}	0.83
.93	4000	2.6654×10^{-1}	0.21
.945	3800	2.2184×10^{-1}	0.14
.960	3600	1.8375×10^{-1}	0.088
.973	3065	1.5683×10^{-1}	0.044
.987	2071	9.5296×10^{-2}	0.011
.990	1800	8.1845×10^{-2}	0.0069
.993	1400	6.2195×10^{-2}	0.0032
.997	950	3.2385×10^{-2}	0.0008
1.0	130	3.6974×10^{-4}	0.000001

x = 0.57 y = 0.43

van der Waals Atmosphere (T = 130^oK at P = 1 bar)

Lagus Molecular-Neece et al. Metallic

P_{trans} = 2.3 Mbar

Density at Transition: ρ_{mol} = 0.83, ρ_{met} = 1.01

J = 0.0222 K = 0.0027

thermal distribution present immediately after the planet's accretion.

E. Chapter IV, Appendix I

The origin of equations $_{III}$, $_{IV}$, and $_{V}$ is not obvious; thus in this appendix their derivation will be sketched.

Consider a homogeneous, nearly spherical, body whose surface is given as

$$r(\theta,\phi) = a\left[1 + \epsilon_2(a) P_2(\cos\theta) + \epsilon_4(a) P_4(\cos\theta)\right] \tag{1}$$

where $|a\epsilon_2(a)| \ll a$, and

$\epsilon_4(a)$ is of order $\epsilon_2^2(a)$.

All calculations will be done to second order in ϵ_2 and first order in ϵ_4 . The relations which are derived differ from those of De Marcus (1958) in form only and are equivalent to his relations to the above order.

External to this body the gravitational potential is given as

$$\Psi = G \int \frac{\rho \, dV'}{|r - r'|} \tag{2}$$

where the origin of coordinates is taken to be the center of the body (see Fig. 1)

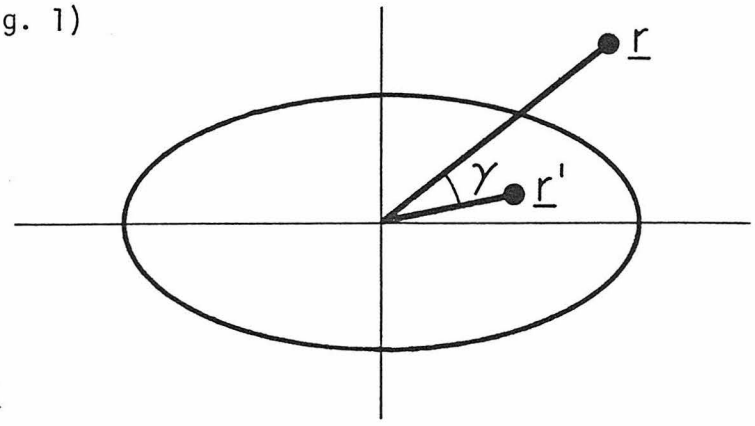

Fig. 1

where $r = r(\theta,\phi)$

$r' = r'(\theta',\phi')$

since

$$\frac{1}{|\underline{r}-\underline{r}'|} = \sum_{\ell} \frac{1}{r}\left(\frac{r'}{r}\right)^{\ell} P_{\ell}(\cos\gamma) \qquad r'<r \tag{3}$$

The external gravitational potential can be written as

$$\Psi = G\int_{0}^{a(1+\epsilon_2 P_2+\epsilon_4 P_4)} r'^2 dr' \int_{\theta',\phi'} d\Omega' \rho \sum_{\ell} \frac{1}{r}\left(\frac{r'}{r}\right)^{\ell} P_{\ell}(\cos\gamma) \tag{4a}$$

$$= \sum_{\ell} \frac{K_{\ell} P_{\ell}(\cos\gamma)}{r^{\ell+1}} \tag{4b}$$

To express $P_{\ell}(\cos\gamma)$ in terms of function of (θ,ϕ) and (θ',ϕ'), use the spherical harmonic addition theorem:

$$P_{\ell}(\cos\gamma) = \frac{4\pi}{2\ell+1} \sum_{m=-\ell}^{\ell} Y^{*}_{\ell m}(\theta',\phi') Y_{\ell m}(\theta,\phi) \tag{5}$$

where

$$Y_{\ell m}(\theta,\phi) = \sqrt{\frac{2\ell+1}{4\pi}\frac{(\ell-m)!}{(\ell+m)!}} P_{\ell}^{m}(\cos\theta) e^{im\phi} \tag{6}$$

and

$$P_{\ell}^{m}(\cos\theta) = (-1)^m (1-\cos^2\theta)^{m/2} \frac{d^m}{d^m(\cos\theta)} P_{\ell}(\cos\theta) \tag{7}$$

Multiply (4a) and (4b) by $P_k(\cos\theta)$ and integrate over θ and ϕ, using the fact that

$$P_k^0(\theta) = \sqrt{\frac{4\pi}{2l+1}}\, Y_{k0}(\theta,\phi) \tag{8}$$

and

$$\int d\Omega\, Y_{jk}^*(\theta,\phi)\, Y_{lm}(\theta,\phi) = \delta_{jl}\,\delta_{km} \tag{9}$$

Then, for ρ a constant

$$K_l = \rho \frac{a^{l+3}}{l+3} \int_{\theta',\phi'} d\Omega'\, P_l(\theta') \left(1 + (l+3)(\epsilon_2 P_2 + \epsilon_4 P_4) + \frac{(l+3)(l+2)}{2}\epsilon_2^2 P_2^2\right) \tag{10}$$

where terms to order ε_2^2 and ε_4 have been retained. A useful identity in what follows is

$$P_2^2(x) = \frac{18}{35} P_4(x) + \frac{2}{7} P_2(x) + \frac{1}{5} \tag{11}$$

Then the gravitational potential exterior to the body is (to terms of order ε_4):

$$\Psi_{EXT} = \frac{4\pi}{3} G \left[\frac{a^3}{r}\left(1 + \frac{3}{5}\epsilon_2^2\right) + \frac{3}{5}\frac{a^5}{r^3}\left(\epsilon_2 + \frac{4}{7}\epsilon_2^2\right) P_2 + \frac{1}{3}\frac{a^7}{r^5}\left(\epsilon_4 + \frac{54}{35}\epsilon_2^2\right) P_4\right] \tag{12}$$

To calculate the gravitational potential at a point inside the body, a slightly different expansion is used:

$$\Psi_{INT} = \int r'^2 dr' \int d\Omega' \rho \sum_{\ell} \frac{r^{\ell}}{(r')^{\ell+1}} P_{\ell}(\cos\gamma) + \Psi_0$$

(13)

where the geometry is now given by Fig. 2, and ψ_0 is the potential due to the material in a sphere of radius $|\underline{r}|$

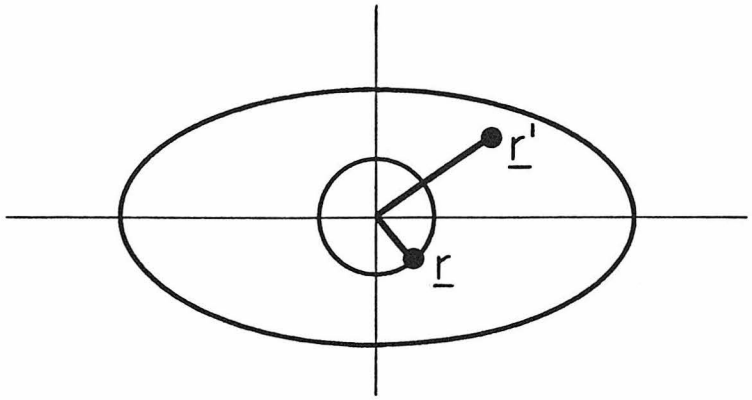

Fig. 2

For constant ρ the gravitational potential ψ_0 is

$$\Psi_0 = \frac{4\pi}{3} G \rho r^2$$

(14)

and using equations (8) and (9) in (13), the potential at a point within the body is given as

$$\Psi_{INT} = \frac{4\pi}{3} \rho a^3 G \left\{ -\tfrac{1}{2} \frac{r^2}{a^3} + \tfrac{3}{2} \frac{(1 + \epsilon_2^2/5)}{a} \right.$$

$$+ \frac{3}{5} \frac{r^2}{a^3} \left(\epsilon_2 - \tfrac{1}{7} \epsilon_2^2\right) P_2$$

$$\left. + \tfrac{1}{3} \frac{r^4}{a^5} \left(\epsilon_4 - \frac{27}{35} \epsilon_2^2\right) P_4 \right\}$$

(15)

For a heterogeneous body, the potential can be regarded as built up from shells corresponding to small increases in a in which ρ remains uniform. In the shell between a and $a + da$, the density varies from ρ to $\rho + d\rho$ and the contribution to ψ is found by taking the density to be uniform and equal to ρ and $\rho + d\rho$ respectively, over surfaces given by

$$r = s\left(1 + \epsilon_2(s) P_2 + \epsilon_4(s) P_4\right) \tag{16}$$

At internal points, the gravitational potential must be separated into two parts. Let s_1 be the value of s for the surface of constant density through the point considered. Then the contribution for $s < s_1$ is built up from equation (12) and that for $s > s_1$ from equation (15). Thus

$$\begin{aligned}
\frac{3}{4\pi G}\Psi = \int_0^{s_1} \rho(a) \frac{\partial}{\partial a} \Big[& \frac{a^3}{r}\left(1 + \tfrac{3}{5}\epsilon_2^2(a)\right) \\
& + \tfrac{3}{5}\frac{a^5}{r^3}\left(\epsilon_2(a) + \tfrac{4}{7}\epsilon_2^2(a)\right) P_2 \\
& + \frac{a^7}{r^5}\left(\frac{\epsilon_4(a)}{3} + \frac{18}{35}\epsilon_2^2(a)\right) P_4 \Big] da \\
+ \int_{s_1}^{\infty} \rho(a) \frac{\partial}{\partial a} \Big[& \tfrac{3}{2}a^2\left(1 + \frac{\epsilon_2^2(a)}{5}\right) \\
& + \tfrac{3}{5}r^2\left(\epsilon_2(a) - \tfrac{1}{7}\epsilon_2^2(a)\right) P_2 \\
& + \tfrac{1}{3}\frac{r^4}{a^2}\left(\epsilon_4(a) - \frac{27}{35}\epsilon_2^2(a)\right) P_4 \Big] da
\end{aligned} \tag{17}$$

To find the total potential on surfaces of constant density, a term for

the centrifugal potential $-\frac{1}{2}\omega^2 r^2 \sin^2\theta$ must first be added to (17), then substituting for (16) in (17)

$$\frac{3}{4\pi G}\Psi = \int_0^{s_1} \rho(a)\, d\left[\frac{a^3}{s}\left(1+\frac{3}{5}\epsilon_2^2(a) - \epsilon_2(s)P_2 - \epsilon_4(s)P_4 + \epsilon_2^2(s)P_2^2\right) + \frac{3}{5}\frac{a^5}{s^3}\left(\epsilon_2(a)P_2 + \frac{4}{7}\epsilon_2^2(a)P_2 - 3\epsilon_2(a)\epsilon_2(s)P_2^2\right) + \frac{a^7}{s^5}\left(\frac{\epsilon_4(a)}{3} + \frac{18}{35}\epsilon_2^2(a)P_4\right)\right]$$

$$+ \int_s^{\infty} \rho(a)\, d\left[\frac{3}{2}a^2\left(1+\frac{\epsilon_2^2(a)}{5}\right) + \frac{3}{5}s^2\left(\epsilon_2(a)P_2 - \frac{1}{7}\epsilon_2^2(a)P_2 + 2\epsilon_2(a)\epsilon_2(s)P_2^2\right) + \frac{1}{3}\frac{s^4}{a^3}\left(\epsilon_4(a) - \frac{27}{35}\epsilon_2^2(a)\right)P_4\right]$$

$$- \frac{3}{4\pi G}\frac{s^2\omega^2}{3}\left(P_2 - 1 + 2\epsilon_2(s)P_2^2 - 2\epsilon_2(s)P_2\right)$$

(18)

Equating coefficients of the Legendre polynomials to zero, and noting that $M(s) = 4\pi\int_0^s \rho(a)\, a^2\, da$, equations III, IV, and V in Table I of the preceding chapter (which is reproduced on the next page for convenience) $\bar{s}$ is the value of s at the surface of the planet.

Note, however, that to obtain equation V, use must be made of the identity

Table I

Formulae For Determining ϵ_2 and ϵ_4

$$M(s) = 4\pi \int_0^s \rho(a)\, a^2\, da \qquad (I)$$

$$\frac{dP}{ds} = -\frac{G\rho(s)M(s)}{s^2} + \frac{2}{3}\omega^2 s\rho(s) \qquad (II)$$

$$\epsilon_2(s) = -\frac{\omega^2 s^3}{3GM(s)}\left[1 - \frac{10}{7}\epsilon_2(s)\right] + \frac{2}{7}\epsilon_2^2(s) +$$

$$\frac{4\pi}{5M(s)s^2}\left[1 - \frac{6}{7}\epsilon_2(s)\right]\int_0^s \rho(a)\frac{d}{da}\left\{a^5\left[\epsilon_2(a) + \frac{4}{7}\epsilon_2^2(a)\right]\right\} da$$

$$+\frac{4\pi s^3}{5M(s)}\left[1 + \frac{4}{7}\epsilon_2(s)\right]\int_s^{\bar{s}} \rho(a)\frac{d}{da}\left[\epsilon_2(a) - \frac{1}{7}\epsilon_2^2(a)\right] da \qquad (III)$$

$$\epsilon_4(s) = \epsilon_4^{(0)}(s) + \frac{4\pi}{9M(s)}\left\{\frac{1}{s^4}\int_0^s \rho(a)\frac{d}{da}\left[a^7\epsilon_4(a)\right] da\right.$$

$$\left. + s^5\int_s^{\bar{s}} \rho(a)\frac{d}{da}\left[\frac{\epsilon_4(a)}{a^2}\right] da\right\} \qquad (IV)$$

$$\epsilon_4^{(0)}(s) = \frac{54}{35}\epsilon_2^2(s) - \frac{72\pi\epsilon_2(s)}{35M(s)s^2}\int_0^s \rho(a)\frac{d}{da}\left[a^5\epsilon_2(a)\right] da$$

$$+\frac{24\pi}{35M(s)s^4}\int_0^s \rho(a)\frac{d}{da}\left[a^7\epsilon_2^2(a)\right] da \qquad (V)$$

$$-\frac{12\pi s^5}{35M(s)}\int_s^{\bar{s}} \rho(a)\frac{d}{da}\left[\frac{\epsilon_2^2(a)}{a^2}\right] da$$

G	is the gravitational constant
M(s)	is the mass out to radius s
ω	is the rotational velocity
$\bar{s}$	is the value of s at the surface

$$\epsilon_2^2(s) = -\frac{\omega^2 s^3}{3GM(s)}\,\epsilon_2(s) + \frac{4\pi\,\epsilon_2(s)}{5M(s)s^2}\int_0^s \rho(a)\,d[a^5\epsilon_2(a)]$$

$$+\frac{4\pi s^3}{5M(s)}\,\epsilon_2(s)\int_s^{\bar{s}} \rho(a)\,d[\epsilon_2(a)] \qquad (19)$$

which is gotten from equation III.

The gravitational moments J and K are defined by the multipole expansion of the gravitational field outside the planet.

$$\phi(r,\theta) = -\frac{GM}{r}\left[1 - \tfrac{2}{3}J\left(\frac{R_e}{r}\right)^2 P_2 + \frac{4}{15}K\left(\frac{R_e}{r}\right)^4 P_4\right] \qquad (20)$$

where R_e = equatorial radius = $\bar{s}(1 - \frac{1}{2}\,\varepsilon_2(\bar{s}))$

M = mass of planet.

The shape of the surface of a planet is defined by the quantities $\varepsilon_2(\bar{s})$ and $\varepsilon_4(\bar{s})$. These quantities also determine the moments J and K according to the condition that the sum of the gravitational potential (20) and the centrifugal potential be constant on the surface of the planet.

Thus

$$J = -\tfrac{3}{2}\left\{\epsilon_2(\bar{s}) + \frac{\omega^2\bar{s}^3}{3GM}\left[1 - \tfrac{10}{7}\epsilon_2(\bar{s})\right] - \tfrac{2}{7}\epsilon_2^2(\bar{s})\right\}\left[1 + \tfrac{13}{7}\epsilon_2(\bar{s})\right] \qquad (21)$$

A more direct method to obtain both J and K is to equate like terms in equations (20) and (17) from which it immediately follows

that

$$J = -\frac{6\pi}{5}\frac{[1+\epsilon_2(\bar{s})]}{M\bar{s}^2}\int_0^{\bar{s}}\rho(a)\,d\left[a^5\left(\epsilon_2(a)+\frac{4}{7}\epsilon_2^2(a)\right)\right] \tag{22}$$

and

$$K = \frac{5\pi}{3M\bar{s}^4}\int_0^{\bar{s}}\rho(a)\,d\left[a^7\left(\epsilon_4(a)+\frac{54}{35}\epsilon_2^2(a)\right)\right] \tag{23}$$

F. References for Chapter IV

1. Ahlers, G., "Some Properties of Solid Hydrogen at Small Molar Volumes", UCRL Report 10757 (1963).
2. Aller, L. H., The Abundance of the Elements, Interscience, New York (1961).
3. Aumann, H. H., C. M. Gillespie, and F. J. Low, Ap. J. 157, L69 (1969).
4. Bridgman, P. W., Proc. Am. Acad. 59, 173 (1924).
5. Brouwer, D. and G. M. Clemence, "Orbits and Masses of Planets and Satellites", in Planets and Satellites, edited by G. Kuiper and B. Middlehurst, University of Chicago Press, Chicago (1961).
6. De Marcus, W. C., A. J. 63, 2 (1958).
7. De Sitter, W., M.N.R.A.S. 91, 706 (1931).
8. Dynin, E. A., Sov. Phys. Sol. St. 13, 2089 (1972).
9. Hanks, T. C. and D. L. Anderson, P.E.P.I. 2, 19 (1969).
10. Hirschfelder, J. O., C. F. Curtiss, and R. B. Bird, Molecular Theory of Liquids and Gases, John Wiley & Sons, New York (1954).
11. Holt, A. C. and M. Ross, Phys. Rev. B1, 2700 (1970).
12. Hubbard, W. B., Ap. J. 152, 745 (1968).
13. Hubbard, W. B., Ap. J. 155, 333 (1969).
14. Hubbard, W. B., Ap. J. 162, 687 (1970).
15. Hubbard, W. B., P.E.P.I. 6, 65 (1973).
16. Jeffries, H., The Earth (4th Ed.), Cambridge (1962).

17. Kopyshev, V. P., Dok Sov. Phys. 10, 338 (1965).

18. Lagus, P. L., to be published (1973).

19. Landolt-Börnstein, II. Band, 1. Teil, "Mechanisch-Thermische Zustandgrössen", Springer Verlag, Berlin (1971).

20. Low, F., A.J. 71, 391 (1966).

21. Michels, A. and M. Goudeket, Physica 8, 347 (1941).

22. Michels, A., W. de Graaf, T. Wassenaar, J.M.H. Levelt, and P. Louwerse, Physica 25, 25 (1959).

23. Neece, G. A., F. J. Rogers and W. G. Hoover, J. Comp. Phys. 7, 621 (1971).

24. Peebles, P.J.E., Ap. J. 140, 328 (1964).

25. Salpeter, E. E. and H. S. Zapolsky, Phys. Rev. 158, 876 (1967).

26. Smoluchowski, R., Nature 215, 691 (1967).

27. Stewart, J. W., J. Phys. Chem. Solids 1, 146 (1956).

28. Trubitsyn, V. P., Bok. Sov. Phys. 7, 45 (1962).

29. Trubitsyn, V. P., Sov. Phys. Sol. St. 7, 2708 (1966a)

30. Trubitsyn, V. P., Sov. Phys. Sol. St. 8, 688 (1966b).

31. Trubitsyn, V. P., Sov. Phys. Sol. St. 8, 2593 (1967).

32. Trubitsyn, W. P., Sov. Astronomy 15, 303 (1971).

33. van Horn,H. M., Phys. Rev. 157, 342 (1967).

34. Wigner, E. and H. B. Huntington, J. Chem. Phys. 3, 764 (1935).

V. CONCLUSIONS

The expendable vacuum chamber and cryogenic designs, as well as the immersed foil technique presented in this thesis appear capable of producing excellent shock wave data on solidified gases. In the case of argon the present data show less scatter and are in much better agreement with recent theoretical formulations than are the earlier data of Dick et al. (1970). The assumption that γ/V is a constant appears justified for solid argon, at least to compressions of $V/V_0 \simeq 0.6$. Thus, the method of Walsh and Christian, which has successfully been used to reduce Hugoniot data to isothermal and adiabatic data for metals, can be used (at least for a first approximation) for solid argon at low compressions.

The shock wave data for molecular hydrogen are consistent with the Stewart 4^oK isotherm (to compressions of $V/V_0 \simeq 0.65$) if the assumption that γ/V is constant is valid.

The speculation that for molecular hydrogen the relative contribution of the zero point energy to the total energy will become smaller at large compressions is explicitly demonstrated. Between 5 kbar and 370 kbar a non-quantum-crystal 0^oK equation of state reproduces experimental data very well. Below $\sim$5 kbar, the non-quantum crystal equation of state fails to predict the pressure-volume properties.

On the basis of the present molecular equation of state and several recently proposed metallic equations of state, a pressure for the molecular to metallic phase transition of 1.9 ± 0.4 mbar is

inferred at $0^{o}K$.

Incorporation of a van der Waals type atmosphere into a model of Jupiter leads to temperatures of $4000^{o}K$ at the base of the atmosphere. This temperature implies that the interior of Jupiter is probably everywhere above the melting temperature of metallic hydrogen.

A. Chapter V, Appendix I: Special Problems in Interpreting the Hydrogen Experiment Streak Camera Records

For reasons that remain not completely clear, the hydrogen streak records displayed some unexpected features which resulted in initial interpretation of the films, which I now know to be incorrect Since this anomalous effect caused so much difficulty, this problem is discussed below.

The streak camera record on the lower right-hand corner of page 11 explicitly demonstrates the nature of the difficulty. This picture represents the third experiment on solid hydrogen (in an initial series of four). It is also the only hydrogen shot of the initial series to show a sharp cut-off of the reflecting mirrors upon impingement by a shock. The true shock arrival at the base of the solid hydrogen is identified in the photograph. Note, however, the bright line halfway up the streak of the right-hand flat mirror. Careful examination of the other three records disclosed that similar lines could be found. The interval between the weak arrival and the sharp cut-off is roughly the same as that required for a shock to reflect from the unsilvered surface (top) of the mirror and return to the silvered surface. It was natural, then, to assume that the weak arrivals correspond to shock entrance into the solid hydrogen. This

assumption then leads to very low shock velocities and a very compressible Hugoniot curve. (The problem of picking shock entrance into solid argon was not so severe as argon becomes luminous when shocked.)

Although this initial interpretation of the data, implying much greater hydrogen compressibility than had previously been measured, was regarded with suspicion, the extant isothermal data were also meticulously scrutinized in an effort to uncover an unsuspected source of error in the work of Stewart. Simultaneously, a theoretical investigation was undertaken to determine if the Stewart isotherm was consistant with reasonable molecular interaction potentials. This theoretical investigation formed the basis for chapter III of this thesis.

Next a second series of four experiments in solid hydrogen were undertaken. The only significant experimental change was to severely abrade the surface immediately beneath the flat mirrors. Three usable records resulted from this series, two of which showed a weak arrival and a sharp cut-off as per the record on page 11. The third showed only the sharp cut-off.

The resolution of the problem came in recognizing that weak arrivals on the flat mirrors mounted on the base of the sample chamber could also result from the impact of the stainless steel foil shortly before the striker place (projectile) arrival. Because this foil is very thin, a rarefaction from its rear surface would rapidly attenuate a shock in the sample, and hence not appreciably affect the state in the sample, prior to arrival of the main shock. If only sharp cut-offs

are considered to represent bonafide shock arrivals, all the streak records with sharp cut-offs were found to be consistent with the isothermal compression data. Since only ~50% of the records showed clear arrivals some of the records, unfortunately, had to be discarded. Due to the complexity and expense of each shock experiment on solidified hydrogen, there is an overwhelming temptation to squeeze an interpretation from each streak record. The painful lesson learned from these experiments is that it is easy to go astray when attempting to extract meaningful information from a noisy background. Unappealing as it is, only those data which show unequivocal shock arrivals should be included in any subsequent interpretation of the raw data.